A STUDY OF ORDERING IN IRON-COBALT ALLOYS AND SPIN WAVE THEORY IN TRIANGULAR ANTIFERROMAGNETS

By

JAMES AKINDELE OYEDELE, B.Sc.,M.Sc.

A Thesis

Submitted to the Faculty of Graduate Studies

in Partial Fulfilment of the Requirements

for the Degree

Doctor of Philosophy

McMaster University

May 1978

A STUDY OF ORDERING IN IRON-COBALT ALLOYS

AND

SPIN WAVE THEORY IN TRIANGULAR ANTIFERROMAGNETS

DOCTOR OF PHILOSOPHY (1978) McMASTER UNIVERSITY
(Physics) Hamilton, Ontario

TITLE: A Study of Ordering in Iron-Cobalt Alloys and Spin Wave Theory in Triangular Antiferromagnets

AUTHOR: James Akindele Oyedele, B.Sc. (University of Ife)
M.Sc. (McMaster University)

SUPERVISOR: Professor M. F. Collins

NUMBER OF PAGES: xiv, 181

ABSTRACT

This thesis describes studies of ordering in binary alloys, and spin waves in triangular antiferromagnets.

The order-disorder phase transition in iron-cobalt alloys was studied by neutron-powder diffraction techniques. Twelve different compositions in the range from 30 to 70 atomic percent cobalt were investigated. All the specimens exhibited an order-disorder phase transition and the long range order parameter in each specimen was determined by measuring the intensity of superlattice reflections. The plot of the transition temperature against composition shows a peak at 47.9±0.3 atomic percent cobalt; this is surprising since simple theories predict a peak at the stoichiometric 50% composition. To within error, the critical index β of the order parameter is independent of composition; its weighted mean value is 0.303±0.004. This is comparable to the value 0.312±0.005 predicted for the Ising model.

Spin wave theory was developed for triangular antiferromagnets. In these systems at low temperatures, the spins have a simple antiferromagnetic coupling along the hexagonal c-axis but lie in the basal plane where they form a triangular structure. By using trial values of the exchange constants along directions parallel and perpendicular to the hexagonal c-axis, a numerical calculation of the spin wave dispersion

relations in the system was carried out. There are six branches, including degeneracies, in the dispersion relations along the symmetry directions ($\xi 00$) and (00ξ). Due to the fact that there is a much stronger coupling of magnetic moments along the c-axis compared with that in the basal plane, the energies of spin waves propagating along the c-axis (00ξ) are much larger than those of the waves propagating in the perpendicular direction ($\xi 00$). The effect of the dipole-dipole interactions was to remove some of the degeneracies in the dispersion relations. The spin wave theory developed is applicable to any hexagonal triangular antiferromagnet having exchange and dipole-dipole coupling; it is applied in this thesis to $CsMnBr_3$ which is known to have a triangular antiferromagnetic structure.

ACKNOWLEDGMENTS

My gratitude goes to Professor M. F. Collins for his guidance throughout the course of this work. He has contributed greatly to my interest and knowledge in the field of solid state physics and of the techniques of neutron spectroscopy.

I would like to thank Professor B. N. Brockhouse for the use of his neutron spectrometer at McMaster University Nuclear Reactor.

Most of the experimental work was done at the Chalk River Nuclear Laboratories and the cooperation of the Atomic Energy of Canada is sincerely acknowledged.

Many thanks to my colleagues at McMaster University: Dr. D. Khatamian (now at Iowa State University), and Messrs. J. Couper, D. McDonald and J. Garret for many instructive discussions and assistance during the course of this work.

The iron-cobalt samples were prepared by Mr. T. Bryner and Mr. D. Hodgson, and the chemical analysis of the samples was done with the cooperation of Dr. O. E. Hileman.

I am indebted to Professor D. A. Goodings for his encouragement that helped me make the decision to do my graduate work at McMaster University, and for the useful discussions I had with him during the latter part of the work on spin waves.

The financial assistance of the National Research Council and of McMaster University made this work possible.

I would like to thank my family for their patience and encouragement, particularly during the latter part of this work.

Finally, I wish to express my sincere thanks to Mrs. H. Kennelly who patiently and accurately typed this manuscript.

TABLE OF CONTENTS

LIST OF FIGURES

LIST OF TABLES

CHAPTER I

INTRODUCTION

This thesis is a report of two projects carried out to study the order-disorder phase transitions in the binary alloy FeCo, and to study spin waves in triangular antiferromagnets. The two projects are not closely related so the thesis is effectively divided up into two independent parts.

The first part concerns the study of the FeCo system and this is described in chapters I-V.

The second part is a study of the stability and of the spin wave dispersion laws in triangular antiferromagnets and this is described in chapters VI-IX. The original contributions in this project are of a theoretical nature, in contrast to the first project where the emphasis was primarily experimental in nature.

I-1. Phase Transitions

One of the most interesting phenomena in the macroscopic physical world is change of phase or phase transition. In many cases the various phases of matter are quite dissimilar and separate, and transitions between them are quite abrupt. But by varying the temperature or other thermodynamic parameters, two distinct phases can frequently be made more and more

similar in their properties until at a certain temperature or critical point, all differences vanish. Beyond this point, only one homogeneous equilibrium phase exists and all changes are continuous or smooth. The most prominent examples of phase transitions are those which occur in the condensation of gases, and the melting of crystals, and which therefore affect nearly every substance. There are other phase transitions which are peculiar to particular substances, some of which only become apparent on detailed investigation of thermodynamical and mechanical properties. Examples of these are the transitions which affect ferromagnetic substances at their Curie point, and the transition in binary alloy at the critical temperature, from a state in which the two species have no preference for one or the other crystal sublattice (disordered state) to a state in which one sublattice is predominantly occupied by one species (ordered state).

Phase transitions are classified according to the type of singularity that appears in the thermodynamic properties of the system. Transitions in which one or more first derivatives of the relevant thermodynamic potentials change discontinuously as a function of their variables are called "first order phase transitions". An example is the entropy $S = -(\partial G/\partial T)_p$ of a fluid having Gibbs free energy G at temperature T and pressure p, which is discontinuous at the boiling and melting points. Transitions in which the first derivatives of the thermodynamic potential remain continuous while the second derivatives, such

as the specific heat or the susceptibility, are divergent or change discontinuously at the transition point are called "second order phase transitions". Those in which the divergence or discontinuity occur in higher-order derivatives are identified by the degree of the derivative. Second and higher order phase transitions are usually referred to as critical phase transitions.

Experimental studies of the behaviour of systems near their critical point have shown that the divergences in the thermodynamic quantities are in powers of the deviation from the critical point. These divergences are described by critical indices which are exponents in power laws. The determination of these indices is central to the study of critical phase transition.

In recent years, many similarities between apparently very different phase transitions have been observed. This has led to the concept of universality, which says that broad classes of systems can exhibit the same behaviour in the neighbourhood of their critical points. If this concept is valid, then it should be possible to compare different phase transitions with each other and with existing theories. One such comparison could be made between the Ising model of ferromagnetism which has been studied theoretically in an extensive way, and the order-disorder transition in binary alloy because they both have one dimensional order parameters. Experimental results obtained in such alloys should therefore be suitable

for testing the validity of this model.

Iron-cobalt is one of the few alloy systems that undergo a critical phase transition from an ordered to a disordered state. This study of the order-disorder phenomena in the iron-cobalt system is to improve our knowledge of this particular phase transition and critical phenomena in general.

a. Order-disorder phase transition

Solid solutions of transition metals are usually of the substitutional type, where the atoms substituted replace the host atoms at some of their sites in the lattice. That is for a crystal containing a quantity of metal B added to metal A, it is found that such a crystal is very similar to those of the pure A metal except that some of the lattice sites are now occupied by B atoms rather than by A atoms. Experiments show that in a number of alloys at sufficiently low temperatures, the substituted B atoms occupy only a certain type of site in the crystal lattice. That is, the lattice sites can be grouped into two interpenetrating sublattices each of which is occupied predominantly by one kind of atom. An alloy in such a state is said to be ordered. Figure 1-1(a) shows such an ordered state in a b.c.c. lattice in which the B atoms occupy the cube centres (b sites) and the A atoms occupy the cube corners (a sites). As the temperature increases, there occurs a transition of some of the substituted atoms from their sites (b sites) to "foreign" a sites; such an alloy is called partially ordered. The concentration of atoms of a given type on

foreign sites increases with temperature, while the concentration on their own sites decreases. At some temperature, the average occupation of a lattice site becomes entirely random. This is the disordered state of the alloy (Figure 1-1(b)). The temperature at which the alloy transforms from the ordered to the disordered state is called the order-disorder transition temperature or the critical temperature.

The transition from an ordered to a disordered state occurs in one of two ways. The first is such that the probability of occupation of a site by the "right atom" at the transition point changes discontinuously (step-change); this is a first-order phase transition (Figure 1-2(a)). The second way involves continuous changes of the probability of site substitution; this is called a second-order phase transition (Figure 1-2(b)).

The degree of order, called the long range order parameter, is a measure of how many of the 'a' sites are occupied by A atoms, and how many of the 'b' sites are occupied by B atoms. It is determined by the arrangement of atoms over the entire crystal. A quantitative definition for the parameter may be obtained as follows. We consider a binary alloy composed of N_A atoms of A and N_B atoms of B, in which the crystal lattice containing N sites may be divided into two sublattices. These sublattices are formed from N_1 sites of the first type ('a' sites), applying to atoms A, and N_2 sites of the second type ('b' sites), applying to atoms B respectively. Then $\cdot = N_1/N$

denotes the relative concentration of sites of the first type, and $C_A = N_A/N$ is the relative concentration of atoms of the first type. ($N_A = N_1$, only for an alloy with stoichiometric composition.) If N_{A1}, N_{A2}, N_{B1}, N_{B2} denote the number of atoms A and B on sites of the first and second type respectively, then the probability of occupation of the first and second sites for atoms A and B are

$$P_{A1} = \frac{N_{A1}}{N_1} , \quad P_{A2} = \frac{N_{A2}}{N_2} , \quad P_{B1} = \frac{N_{B1}}{N_1} , \quad P_{B2} = \frac{N_{B2}}{N_2} .$$

The degree of long range order S is defined as

$$S = \frac{P_{A1} - C_A}{1 - \nu} . \qquad (I\text{-}1)$$

Using the above relationships, it could be shown that

$$P_{A2} = C_A - \nu S . \qquad (I\text{-}2)$$

In a disordered alloy (of any composition), S = 0 because in a disordered alloy $P_{A1} = C_A$. For a completely ordered alloy of stoichiometric composition, S = 1 because $P_{A1} = 1$, $C_A = \nu = \frac{1}{2}$. For a non-stoichiometric alloy in which $C_A > \nu$, the state with greatest possible ordering is one in which all sites of the first type are occupied by atoms A and therefore $P_{A1} = 1$. Hence the maximum degree of long range order is, $S_{max} = (1-C_A)/(1-\nu) < 1$. For an alloy with $C_A < \nu$ in a state with the maximum possible order, all atoms A are found at sites of the first type and therefore the probability $P_{A2} = 0$. Hence from eqn (I-2), $S_{max} = C_A/\nu < 1$. Thus the long range order

parameter s varies from zero for the disordered state to unity for the completely ordered state. Consequently the degree of long range order decreases with an increase in temperature and disappears at the critical temperature. Its maximum value varies with the composition of the alloy and has the largest value of 1 at the equiatomic composition.

There may also be some short range or local order in the alloy. The corresponding degree of order - called the degree of short range order - is defined with respect to atoms of the alloy and not with respect to the lattice sites. For a binary alloy with equiatomic composition, the degree of short range order σ may be defined as

$$\sigma = (2N_{AB} - N_T)/N_T$$

where N_{AB} is the number of pairs of neighbouring atoms A and B, and N_T is the total number of pairs of neighbouring atoms. The degree of short range order varies from unity (for complete ordering, when $N_{AB} = N_T$) to zero (for a completely random arrangement, when $N_{AB} = N_T/2$). The short range order parameter, σ, is therefore a measure of how well on the average the A atoms are surrounded by nearest neighbour B atoms.

B. The iron-cobalt system

Iron-cobalt alloys have a body-centred cubic lattice at low temperatures from pure iron to about 75 atomic percent cobalt. The alloy shows an order-disorder transition into the cesium chloride structure for compositions which are close to 50% [illegible] and

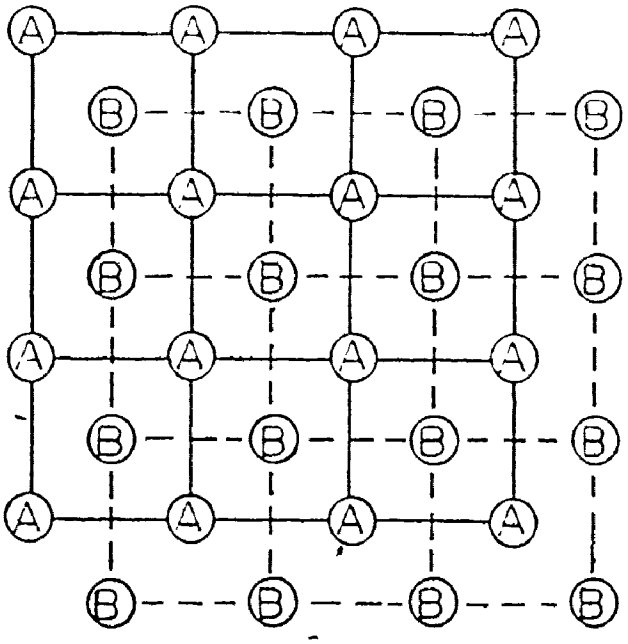

a(1)

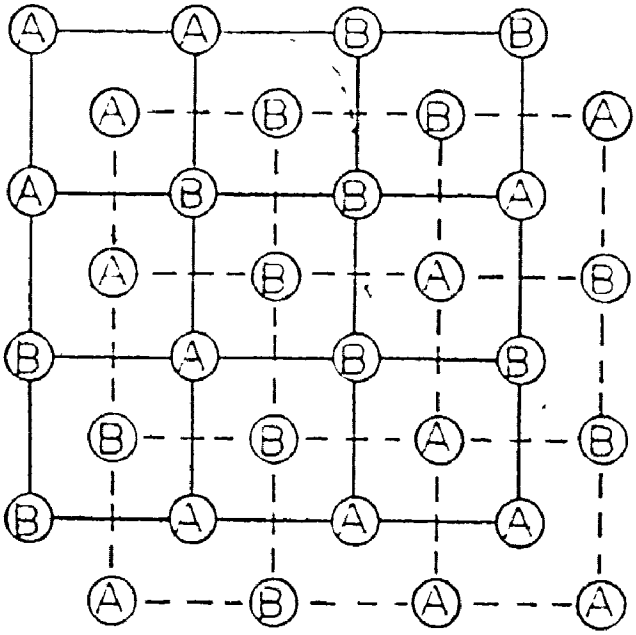

b(1)

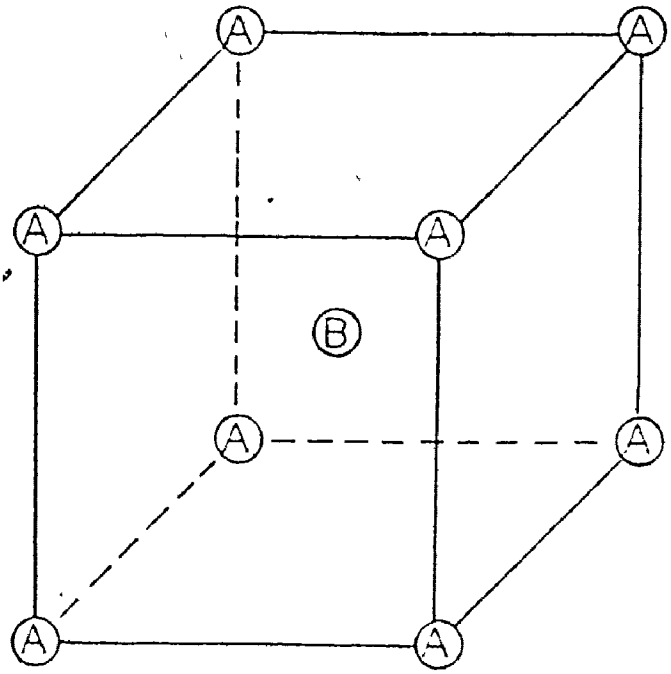

a(2)

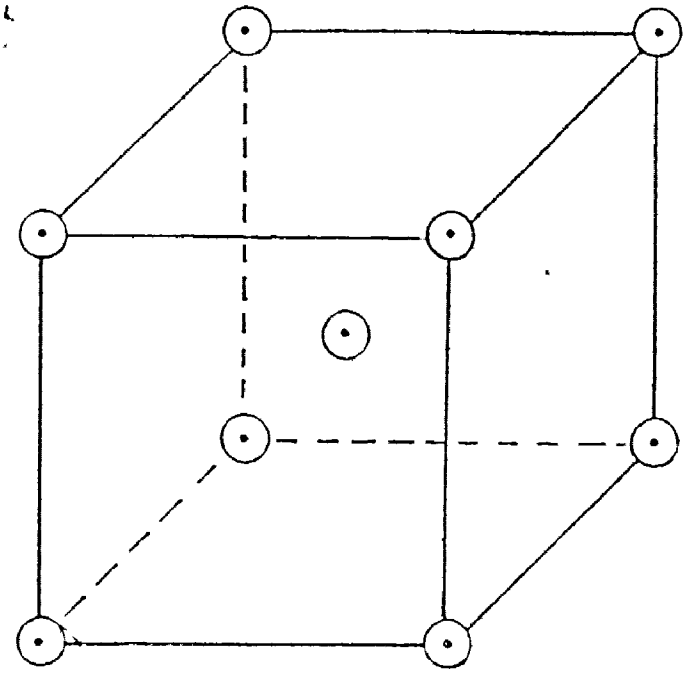

b(2)

⊙ A or B

Fig. I-1. Ordered ( ) and disordered (m : of

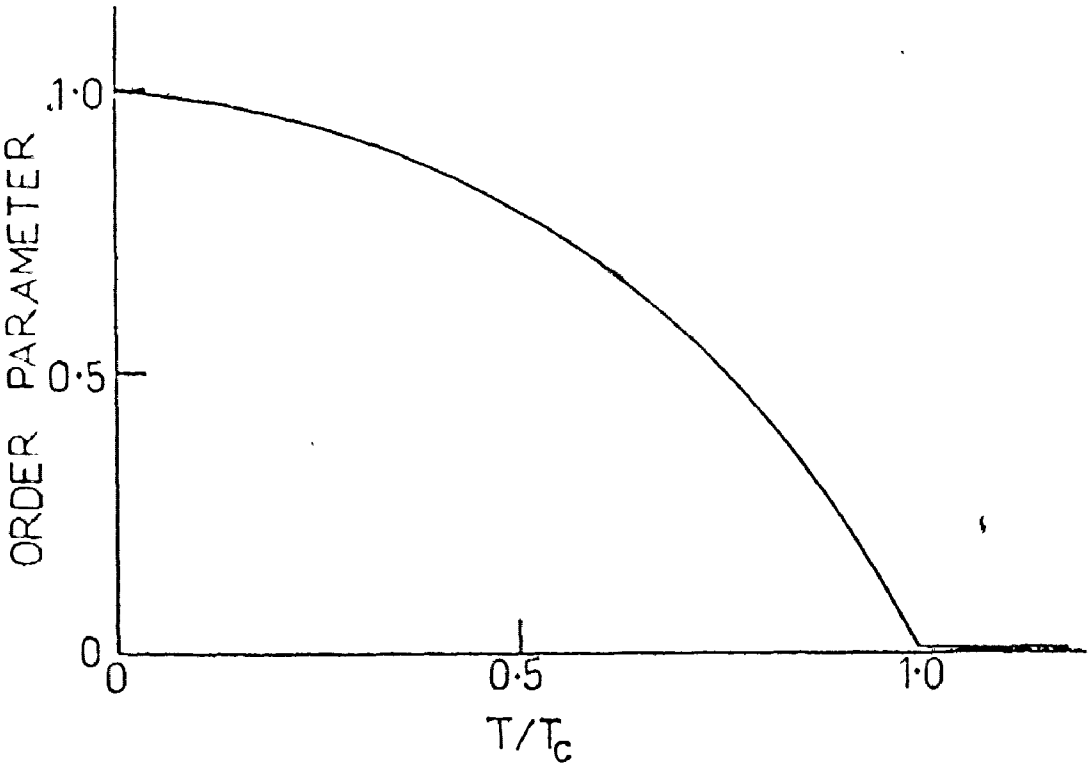

(b)

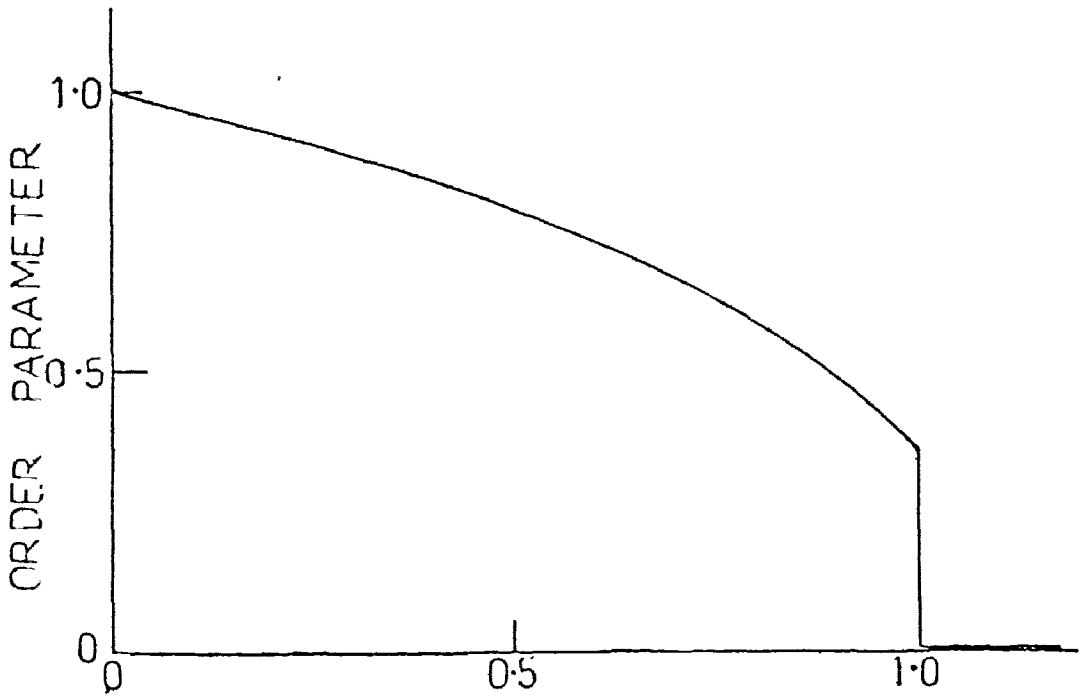

(a)

Fig. I-2. Temperature dependence of o

It has also been firmly established that ordering occurs over the composition range 40-60 atomic percent cobalt and there is much indirect evidence that ordering occurs over a wider range of composition. (W.C. Ellis and E.S. Greiner 1941, M. F. Collins and J. B. Forsyth 1963). The phase diagram of the system is shown in Figure I-3.

c. Measurement with thermal neutrons

There are direct and indirect methods of investigating the order-disorder phenomena in binary alloys. Direct methods are by neutron and x-ray diffraction techniques, and indirect methods are by measurements of properties like the resistivity and the specific heat. The success of the diffraction method depends on the fact that, when a beam of neutrons (or x-rays) is scattered by a metal, each atom contributes a component to the resultant scattered wave with a phase depending on its position and an amplitude depending on the scattering length of the atom. Thus the diffraction pattern formed by the scattered radiation furnishes information concerning the positions of atoms of different types in the metal.

The long range order in binary alloys manifests itself by the appearance of extra ("superlattice") lines in the diffraction pattern of the alloy. The intensity of the superlattice lines depends on the degree of order and on the difference between the scattering lengths of the atoms involved. Neutron scattering techniques are very suitable for the iron-cobalt

the

nearly a factor of four larger than from cobalt. The nuclear and magnetic scattering lengths of iron and cobalt are shown in Table I-1.

There are some excellent reviews and books available on phase transitions and critical phenomena. The reviews by Fisher (1967) and Guttman (1956) are among the best. Among the books, "Phase transitions and critical phenomena" by H. E. Stanley (1971), "The theory of order-disorder in alloys" by M. A. Krivoglaz and A. A. Smirnov (1965), and "Phase transitions and critical phenomena" edited by C. Domb and M. S. Green (1972-1976) should be mentioned.

The first aim of this project is to study the order-disorder transition at different compositions. The second aim is to measure the critical index of the long range order parameter in different compositions, and the third aim is to study the composition dependence of the order-disorder transition temperature and to compare the results with predictions based on simple theories of critical phenomena.

This thesis is a report of our investigation of the order-disorder transition in FeCo in the composition range 30-70 at. % cobalt. A discussion of some of the theories of phase transitions and critical phenomena is presented in chapter II. The chapter also contains a discussion of the relationship between the intensity of the diffracted neutrons and the degree of order in the alloy. Chapter III is a report of the experimental set up and measurement techniques used in the investi-

of the of

used in the investigation is included in the chapter. Chapter IV contains experimental results and discussion. The discussion includes a comparison of some of the results with those obtained in other systems, and with the predictions of theories based on the Ising model. The highlights of the results have been published in a conference proceeding and in a Physics Journal (M. F. Collins and J. A. Oyedele 1976, J. A. Oyedele and M. F. Collins 1977).

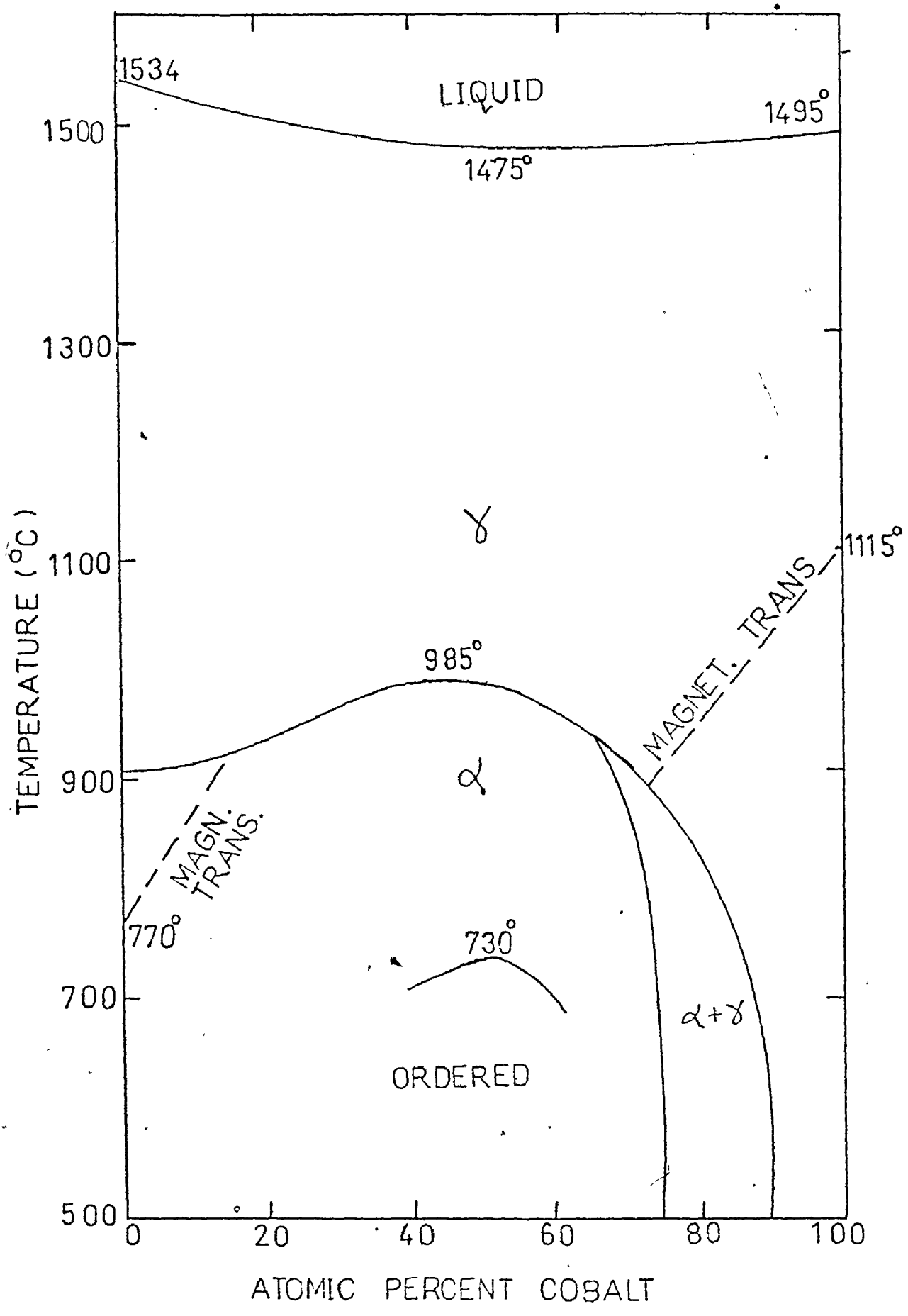
1534
LIQUID
1495°
1475°
1500
1300
1100
900
700
500
TEMPERATURE (°C)
γ
1115°
MAGNET. TRANS.
985°
α
MAGN. TRANS.
770°
730°
α+γ
ORDERED
0
20
40
60
80
100
ATOMIC PERCENT COBALT

Table I-1. General properties of iron, cobalt and their alloys

(1) Thermal neutron scattering amplitude and cross section

	Fe	Co
Nuclear coherent scattering amplitude[a]	0.95×10^{-12} cm	0.25×10^{-12} cm
Magnetic scattering amplitude[b] ($\theta = 0$)	0.60×10^{-12} cm	0.47×10^{-12} cm
Magnetic scattering amplitude[b] ($\frac{\sin\theta}{\lambda} = 0.25\ A^{-1}$)	0.35×10^{-12} cm	0.27×10^{-12} cm
Nuclear incoherent scattering cross section[b]	0.46×10^{-24} cm^2	5.21×10^{-24} cm^2
Cross section for true absorption[b]	1.4×10^{-24} cm^2	21×10^{-24} cm^2

(2) Lattice constant of FeCo alloys at room temperature

30 atomic percent cobalt[c]	2.8583 Å
50 atomic percent cobalt[c]	2.8504 Å
70 atomic percent cobalt[c]	2.8370 Å

[a] The neutron Diffraction Commission, Acta Cryst. A25, 391 (1969).

[b] G. E. Bacon, Neutron Diffraction, 3rd ed. Oxford (1975).

[c] W. B. Pearson, Vol. 4, Handbook of Lattice Spacings and Structures of Metals. Pergamon Press (1958).

CHAPTER II

THEORY

The early theories of phase transitions and critical phenomena were purely phenomenological descriptions of interacting many-particle systems in which one makes the rather unrealistic assumption that each particle or atom interacts equally with all the other atoms in the system. Such theories are the Van der Waals theory of fluid system and the molecular field theory of a magnetic system. These theories predict values of the critical-point exponents that disagree with almost all experimental measurements. More realistic models that are thought to be fairly good approximations to the true interparticle interactions in at least a few physical systems, were later studied. Unfortunately, almost all these model systems have not (or can not) been solved for a three-dimensional system and numerical approximation techniques had to be used in order to obtain predictions of critical properties for these models. Some of these theories will be discussed in this chapter, and a comparison between their predictions and experimental results will be given at the end of the chapter. The discussion on the Ising model follows the treatment of Stanley (1971).

II-1 Ising Model

This is a model which has been studied theoretically in a most extensive way because it is one of the simplest models

which displays a critical phase transition. Although it was introduced as a model for ferromagnetism, it has come to serve as a practical model for binary alloys because of the analogy between the two systems; they both have one dimensional order parameter. A quantitative discussion of the equivalence of the two systems will be given later on in this chapter. Only for one and two dimensional lattices has the model been solved exactly. The one dimensional Ising model is discussed below.

In this model, the spins are assumed to be one-dimensional 'sticks' capable of assuming the two discrete orientations +1 (up) and -1 (down). In the absence of a magnetic field, the Hamiltonian of the system could be written as

$$H = - \sum_{i=1}^{N-1} J_i S_i S_{i+1} \qquad \text{(II-1)}$$

where the spins S_i are one-dimensional unit vectors assuming only the discrete values +1 and -1, and J_i is the interaction energy between spins situated on sites i and i+1.

To obtain information about the ordering temperature in the system, one calculates the two spin correlation function

$$\Gamma_k(r) = \langle S_k S_{k+r} \rangle = Z_N^{-1} \sum_{(S)} S_k S_{k+1} \exp\left(\frac{1}{k_B T} \sum_{i=1}^{N-1} J_i S_i S_{i+1}\right) \qquad \text{(II-2)}$$

where r is a measure of the distance between spins in units of a lattice constant. This function is a measure of the probability that the spin at position k will point in the same direction as the spin at position k+r. Z_N is the partition function of the system and is given by

$$Z_N \equiv Z_N(J_1, J_2, \ldots J_{N-1}) = \sum_{S_1=-1}^{1} \sum_{S_2=-1}^{1} \cdots \sum_{S_N=-1}^{1} \exp\left(\sum_{i=1}^{N-1} j_1 S_i S_{i+1} \right) \qquad \text{(II-3)}$$

where $j_i = \beta J_i = J_i/kT$ is a dimensionless exchange energy and the N summations extend over the 2^N configuration states of the system.

In order to calculate the partition function Z_N for the N spins, one calculates the partition function for N+1 spins and then iterates.

$$Z_{N+1} = \sum_{S_1=-1}^{1} \sum_{S_2=-1}^{1} \cdots \sum_{S_N=-1}^{1} \exp\left(\sum_{i=1}^{N-1} j_i S_i S_{i+1} \right) \sum_{S_{N+1}=-1}^{1} \exp(j_N S_N S_{N+1}). \qquad \text{(II-4)}$$

The last summation in eq. (II-3)

$$\sum_{S_{N+1}=-1}^{1} \exp(j_N S_N S_{N+1}) = 2 \cosh(j_N S_N)$$

and since the spin S_N can take on only the values +1 and -1, the right-hand side of the last equation is independent of the orientation of S_N. Hence the partition function for the N+1 spins may be written in the form

$$Z_{N+1} = 2 Z_N \cosh j_N$$

iteration gives

$$Z_{N+1} = Z_1 2^N (\cosh j_1 \cosh j_2 \cosh j_3 \ldots \cosh j_N) . \qquad \text{(II-5)}$$

Since Z_1 is just the partition function for a system consis-

ting of a single Ising spin, then the 'sum over states' is simply the 'number of states' which is Z.

Hence $$Z_N = 2^N \prod_{i=1}^{N-1} \cosh J_i \ . \qquad (II-6)$$

In the uniform case, $J_i = J$ for all i.

$$\therefore \quad Z_N = 2^N \cosh^{N-1} J \ .$$

$$\therefore \ \Gamma_k(r) = \langle S_k S_{k+r} \rangle = (2^N \cosh^{N-1} J)^{-1} \sum_{\{S\}} S_k S_{k+1} \exp\left(\sum_{i=1}^{N} J_i S_i S_{i+1} \right) .$$

The nearest-neighbour correlation function is simply $\Gamma_k(1)$, which satisfies the relation

$$Z_N \Gamma_k(1) = \sum_{\{s\}} S_k S_{k+1} \exp\left(\sum_{i=1}^{N-1} J_i S_i S_{i+1} \right)$$

$$= \frac{\partial}{\partial J_k} \sum_{\{S\}} \exp\left(\sum_{i=1}^{N-1} J_i S_i S_{i+1} \right).$$

This argument can be generalized to arbitrary r, with the result

$$Z_N \Gamma_k(r) = \frac{\partial}{\partial J_k} \frac{\partial}{\partial J_{k+1}} \cdots\cdots \frac{\partial}{\partial J_{k+r-1}} (Z_N) \qquad (II-7)$$

$$\therefore \quad \Gamma_k(1) = \tanh J_k$$

and

$$\Gamma_k(r) = (\tanh J_k).(\tanh J_{k+1}).....(\tanh J_{k+r-1}) \qquad (II-8)$$

$$= \prod_{i=1}^{r} \tanh J_{k+i-1} \ .$$

In the case of uniform interaction,

$$\Gamma_k(r) = \langle S_k S_{k+r} \rangle = \tanh^r J \ .$$

The temperature at which long-range order sets in is the temperature at which the two-spin correlation function falls off sufficiently slowly with interspin distance r that the magnetization becomes non-zero. That is

$$\sigma^2 = \lim_{r \to \infty} \Gamma_k(r)$$

where $\sigma = M(T,H=0)/M(T=0,H=0)$ is the normalized zero field magnetization. From eq. (II-8), we see that so long as all the parameters J_i are finite, the values of the hyperbolic tangents are less than one and hence the products approach zero in the limit of infinite r. However in the limit of zero temperature all the parameters $J_i = J_i/kT$ approach infinity and the products in the expression for Γ_k approach 1. The linear chain therefore displays zero spontaneous magnetization for all non-zero values of the temperature, but 'suddenly' at $T = T_c = 0$, the magnetization acquires its full value. Thus the Ising model predicts no phase transition for a linear chain system.

Since lattice dimensionality plays an important role in phase transition, it is not surprising that the linear chain system does not have a phase transition.

The Ising model was solved for a two dimensional lattice by Onsager in 1944. He showed that the specific heat

possesses a logarithmic divergence at the transition temperature in contrast to the predictions of the earlier theories such as the mean field theory, of a simple discontinuity at T_c. Although the predicted logarithmic divergence of the specific heat at T_c agrees with experimental results, the values he predicted for the critical exponents disagree with experimental results.

Although the Ising model has not been solved exactly for a 3 dimensional lattice, successive approximation methods, in which a thermodynamic function of interest is expanded in ascending powers of either temperature or inverse temperature have been used to obtain theoretical predictions that are compatible with experimental results.

II-2 Critical Exponents

In recent years the study of critical phenomena has come to focus more and more on the values of the critical exponents, which describe the behaviour near the critical point of the various quantities of interest.

A general definition of a critical exponent to describe the behaviour near the critical point of a function $f(\varepsilon)$ where $\varepsilon \equiv \frac{T-T_c}{T_c}$, and T_c is the critical temperature is

$$\lambda \equiv \lim_{\varepsilon \to 0} \frac{\ln f(\varepsilon)}{\ln \varepsilon}$$

(ε is a dimensionless variable that measures the difference in temperature from the critical temperature.) It is assumed that the function $f(\varepsilon)$ is positive and con[illegible] tha-

the above limit exists. The fact that λ is the critical exponent for the function $f(\varepsilon)$ is denoted by writing

$$f(\varepsilon) \sim \varepsilon^{\lambda} .$$

In practise there are usually correction terms to the last expression. That is

$$f(\varepsilon) = A\varepsilon^{X}(1 + B\varepsilon^{Y} + \ldots.) \qquad (y > 0) \qquad (II-9)$$

There are two main reasons for focussing on critical point exponents. The first reason is the experimental result that sufficiently near the critical point the behaviour of many properties follows a power law; log-log plots of experimental data display straight-line behaviour sufficiently near the critical point, and hence the critical exponent is easily determined as the slope of this straight line region. Therefore critical exponents are measurable while the complete function may not be. A second reason for focussing on the critical exponents is that there exists a number of relations among these exponents that arise from fundamental thermodynamical and statistical mechanical considerations. These relations are believed to transcend the details of any particular system. Some of the exponents are defined below.

Magnetization exponent β

From the shape of the temperature dependence of the zero field magnetization $M_0(T)$ of a ferromagnet at constant magnetic field H=0, a relation of the form

$$\frac{M_0(T)}{M_0(0)} = D\left(\frac{T_c - T}{T_c}\right)^{\beta} (1 + \ldots.) \qquad \text{(II-10)}$$

could be written. This defines the magnetization exponent β.

Susceptibility exponents γ' and γ

These are defined in a similar manner to the magnetization exponent

$$\frac{\chi_T}{\chi_T^o} = \begin{cases} B'(-\varepsilon)^{-\gamma'}(1 + \ldots..) & \text{for } T < T_c,\ H = 0 \\ B\varepsilon^{-\gamma}(1 + \ldots..) & \text{for } T > T_c,\ H = 0 \end{cases} \qquad \text{(II-11)}$$

where χ_T^o is the susceptibility of a system of non-interacting magnetic moments (paramagnet).

Specific heat exponents α' and α

These are defined as

$$C_H = \begin{cases} p'(-\varepsilon)^{-\alpha'} & \text{for } T < T_c,\ H = 0 \\ p\varepsilon^{-\alpha}(1 + \ldots..) & \text{for } T > T_c,\ H = 0 \end{cases} \qquad \text{(II-12)}$$

An example of the relationship among the critical point exponents is

$$\alpha' + 2\beta + \gamma' \geq 2 \qquad \text{(II-13)}$$

which is obtained from the fact that the specific heat C_M must be positive.

Table II-1 gives a summary of critical point exponents and their definitions.

II-3 Landau's Theory of Critical Phase Transitions

Landau's approach is to expand the thermodynamic potential in a power series about the critical point. It must be pointed out that such an expansion about the critical point cannot be convergent; for example, if the Gibbs potential of a magnetic system G(T,H) is expanded about the critical point $T = T_c$, $H = 0$, the coefficients in this expansion will involve the partial derivatives of G(T,H) with respect to T and H evaluated at $T = T_c$ and $H = 0$. But

$$\left(-\frac{\partial^2 G}{\partial H^2}\right)_{T=T_c,H=0} = \chi_T(T=T_c,H=0)$$

and since we expect the isothermal susceptibility χ_T of a magnetic system to be infinite at the critical point, such an expansion of the Gibbs potential cannot be convergent.

Landau assumed that the singular coefficients in the expansion of the thermodynamic potential are of higher order than that of the terms used in the calculation. On this basis, he examined the lower order coefficient of the expansion in order to obtain predictions regarding the critical region.

We assume that we can expand the Helmholtz potential about $T = T_c$, and $M = 0$ in a standard Taylor series for functions of two variables.

$$A(T,M) = \sum_{j=0}^{\infty} L_j(T)M^j = L_0(T) + L_2(T)M^2 + L_4(T)M^4 + \ldots . \quad (II-14)$$

$L_j(T) = 0$ for j odd, because $A(T,M)$ is an even function of M. The coefficients $L_j(T)$ themselves are expanded about $T = T_c$.

$$L_j(T) = \sum_{k=0}^{\infty} L_{jk}(T-T_c)^k = L_{j0} + L_{j1}(T - T_c) + \ldots . \quad \text{(II-15)}$$

$$\therefore \quad H(M,T) = \left(\frac{\partial A}{\partial M}\right)_T = \sum_{j=1}^{\infty} jL_j(T)M^{j-1} = 2L_2(T)M + 4L_4(T)M^3 + \ldots . \quad \text{(II-16)}$$

and

$$\chi_T^{-1}(T,M) = \left(\frac{\partial^2 A}{\partial M^2}\right)_T = \left(\frac{\partial H}{\partial M}\right)_T = \sum_{j=2}^{\infty} j(j-1)L_j(T)M^{j-2}$$

$$= 2L_2(T) + 12L_4(T)M^2 + \ldots . \quad \text{(II-17)}$$

The restrictions on the nature of the coefficients $L_j(T)$ are based upon what is known about the magnetic system. For example, in the limit as $T \to T_c^+$, we expect that the zero-field susceptibility approaches infinity; from eq. (II-17), we have

$$\chi_T^{-1}(T,0) = 2L_2(T) = 2(L_{20} + L_{21}(T-T_c) + L_{22}(T-T_c)^2 + \ldots .) \quad \text{(II-18)}$$

so that we choose $L_{20} = 0$ for $\chi_T(T,0)$ to approach infinity at $T \to T_c^+$.

Magnetization exponent β

From the equation of state above for $H(M,T)$, (eq. (II-16)), it follows that for $H = 0$ and M small,

$$H = 0 = [L_{21}(T-T_c) + \ldots .] + 2M^2[L_{40} + L_{41}(T-T_c) + \ldots .] \quad \text{(II-19)}$$

so that

$$M = (L_{21}/2L_{40})^{1/2}(T_c-T)^{1/2} . \qquad (II-20)$$

Thus $\beta = \frac{1}{2}$ in the Landau theory.

Susceptibility exponents γ and γ'

From eq. (II-18), we have

$$\chi_T^{-1}(T,M) = 2[L_{21}(T-T_c) + ...] + 12M^2(L_{40}+L_{41}(T-T_c)+...). \qquad (II-21)$$

For $T > T_c$, $M = 0$ when $H = 0$ and the zero-field susceptibility is

$$\chi_T^{-1}(T,0) = 2L_{21}(T-T_c) + ...$$

$\therefore \gamma = 1$.

For $T < T_c$, the zero-field magnetization is of course non-zero; on substituting the expression for M from eq. (II-20), we obtain

$$\chi_T^{-1}(T,0) = 4L_{21}(T_c-T) .$$

Thus $\gamma' = 1$.

Other exponents could be obtained in similar fashions.

Landau's theory can be shown to be equivalent to the approaches of Van der Waals, Bragg-Williams, and mean field theory. The predicted critical exponents depend only on the dimensionality of the system. The agreement with experiment is usually poor; though ferroelectric and superconducting critical phase transitions seem to fit the theory. This is

connected with the fact that these phenomena have long range interactions and the theory becomes good for infinite range interactions.

II-4 Series Expansion Methods

Series expansion methods are based on expanding the thermodynamic function of interest in ascending powers either of temperature (a low-temperature expansion) or of inverse temperature (a high-temperature expansion). The technique will be illustrated by calculating the temperature dependence of the specific heat using the high temperature expansion.

The basic idea is to expand the exponential $\exp(-\beta H)$ as a power series in its argument

$$\exp(-\beta H) = 1-\beta H + \frac{1}{2}(\beta H)^2 + \ldots\ldots \qquad \text{(II-22)}$$

where $\beta = 1/kT$, and H is the Hamiltonian of the system. The motivation for such an expansion is that the partition function $Z_N(T,H)$ is directly related to $\exp(-\beta H)$ through

$$Z_N(T,H) = \mathrm{Tr}\{\exp(-\beta H)\} \qquad \text{(II-23)}$$

where the symbol 'Tr' denotes a summation over all the allowed states of the system in the case of a discrete (finite) number of states (e.g. for the Ising model) and denotes an integral over all allowed portions of the phase space of each magnetic moment in the case of a system in which the constituent magnetic moments are free to assume a continuum of orientation (e.g.

the classical Heisenberg model).

For the Ising model

$$Z_N(T,H) = Tr(1)[1-\beta tr(H) + \frac{1}{2}\beta^2 tr(H^2) + ...] \qquad (II-24)$$

where $trH' = \frac{TrH'}{Tr(1)}$ and $Tr(1)$ denotes the total number of states of the system; $Tr(1) = 2^N$ for N Ising spins.

If one can calculate the first L terms in an expansion of the partition function, then one can obtain expressions for analogous terms in the expansion of other thermodynamic functions of interest. For example the Gibbs potential is

$$G(T,H) = -kT\ln Z_N(T,H)$$

$$\ln Z_N(T,H) = \ln(Tr(1)) + \ln(1-\beta tr(H) + \frac{1}{2}\beta^2 tr(H^2) + ...)$$

$$= \sum_{l=0}^{\infty} (\frac{C_l}{l!})\beta^l \qquad (II-25)$$

where the coefficients C_l are called the cumulants, corresponding to the moments b_l. The first few cumulants C_l can be obtained using the expansion $\ln(1+x) = x - \frac{1}{2}x^2 + \frac{1}{3}x^3 + ...$. Thus

$$C_0 = \ln(Tr(1))$$

$$C_1 = -b_1 = -Tr(H)$$

$$C_2 = b_2 - b_1^2 = tr(H^2) - (tr(H))^2$$

and so on. Therefore by calculating the first few moments b_l, one can obtain the first few coefficients in the expansion of the Gibbs potential and hence the first few coefficients in

any of the thermodynamic functions derived from G(T,H). For example, the magnetic specific heat C_H is

$$C_H = -T\left(\frac{\partial^2 G}{\partial T^2}\right)_H = k\beta^2 \frac{\partial^2}{\partial \beta^2} (\ln Z_N)$$

and from the above expression for $\ln Z_N$ (eq. (II-25)), and the cumulants C_l, the leading term in an expansion in powers of β of the specific heat involves the cumulant C_2;

$$C_H \approx k\beta^2 C_2 = \frac{1}{kT^2} [tr(H^2) - (tr(H))^2]$$

Thus the specific heat is predicted to fall off with temperature as $1/T^2 + O(1/T^3)$ above T_c.

The low temperature expansion method has been used to calculate the temperature dependence of the zero field magnetization of the Ising model for three-dimensional lattices.

II-5 Padé Approximant Techniques

The [M,N] Padé approximant to a function F(Z) is the ratio of a polynomial $P(Z) = \Sigma P_r Z^r$ of degree M to a polynomial $Q(z) = \Sigma q_s Z^s$ of degree N. The coefficients P_r and q_s are chosen so that the expansion of P(Z)/Q(Z) agrees with the expansion F(Z) for the first N+M+1 terms. In other words one equates coefficients of powers of Z in the identity

$$F(Z)Q(Z) - P(Z) \equiv AZ^{M+N+1} + BZ^{M+N+2} + \ldots . \qquad \text{(II-26)}$$

with $q_0 = 1$.

Given the polynomial expansion of F(Z) to sufficient terms, the coefficient P_r and q_s may be calculated by solving a set of N simultaneous linear equations for the q_r followed by direct substitution in M linear equations for the P_r. Thus one has essentially 'fitted' the function F(Z) to the ratio of two polynomials.

The motivation for this procedure can be shown by applying the Padé approximant method to a thermodynamic function, such as the magnetization, which has a power law singularity,

$$M = \sum_{l=0}^{\infty} a_l g_l \sim (g_c - g)^{\beta} \qquad \text{(II-27)}$$

where g_l is a function of temperature, and β is a critical point exponent. If one can calculate L+2 coefficients A_l (l=0, 1, ... L+1) in the series for M, then by differentiation, we can obtain L+1 coefficients (l=0, 1....L) in the series for logarithmic derivative of M. Choosing the function F(Z) to be given by this logarithmic derivative series, we obtain

$$F(g) = \frac{\partial}{\partial g} (\ln M) = \sum_{l=0}^{\infty} f_l g^l \sim \frac{\beta}{(g_c - g)} .$$

Therefore the logarithmic derivative series is predicted to have a simple pole at $g = g_c$ with a residue equal to β. Thus if we form the Padé approximants of the logarithmic derivative series - that is if we 'fit' the function F(g) of the last expression to the ratio of two polynomials - then we might expect to find that the of

is the root $g = g_c$ and that the residue corresponding to this root is precisely the critical point exponent β.

Predictions on the critical point exponent β for a 3-dimensional Ising model have been obtained by forming a Padé approximant to

$$u^{-3}(u_c-u)\ \frac{d}{du}\ \ln(I_0/Nm) \qquad (II-28)$$

where $u^{1/2} = \exp(-2J/kT)$ and (I_0/Nm) is the normalized spontaneous magnetization.

II-6 Application to Binary Alloys

The equivalence of the ordering phenomena in binary alloys to that in an Ising antiferromagnet will be discussed. The relationship between the intensity of the scattered neutrons and the degree of order in the alloy will also be discussed.

Consider a binary alloy composed of equal amounts of A and B metals and having a b.c.c. structure. It is assumed that the alloy can undergo a critical phase transition. At sufficiently low temperature the alloy is ordered such that the cube corners are predominantly occupied by one type of atoms - say the A atoms - and the cube centres are predominantly occupied by the B atoms (Figure 1-1(a)). As the temperature is raised, the occupation of lattice sites becomes more and more random until, at the critical temperature T_c, the average occupation of a lattice site is entirely random. The occupation of lattice sites thus corresponds to an antiferromagnetic

structure in which spin up, for instance, corresponds to occupation by A atom and spin down to occupation by B atom.

The occupation of lattice sites can be described quantitatively by pseudo-spin variable or occupation variable S_i defined by

$$S_i = \begin{cases} +1 \text{ if site is occupied by A atom} \\ -1 \text{ if site is occupied by B atom} . \end{cases}$$

One can introduce a staggered spin variable σ_i that takes into account the type of site that is being occupied and the type of atom that occupies the site.

$$\sigma_i = S_i \exp i\underline{\tau}\cdot\underline{r}_i \quad . \qquad \text{(II-29)}$$

where τ is a reciprocal lattice vector with an odd sum of Miller indices and r_i is the lattice vector for site i. The phase factor $\exp(i\underline{\tau}\cdot\underline{r}_i)$ and $\exp(-i\underline{\tau}\cdot\underline{r}_i)$ will both be +1 if r_i terminates at a cube corner and -1 if r_i terminates at a cube centre. That is

$$\sigma_i = 1 \begin{cases} \text{if A atom is on site i and i is a cube corner} \\ \text{or} \\ \text{if B atom is on site i and i is a cube centre} \end{cases}$$

$$= -1 \begin{cases} \text{if A atom is on site i and i is a cube centre} \\ \text{or} \\ \text{if B atom is on site i and i is a cube corner} . \end{cases}$$

Thus σ_i is +1 for "right" occupation of site i, and -1 for "wrong" occupation of site i.

Let $\varepsilon_{AA}(r_{ij})$ represent the configuration energy when lattice sites i and j are both occupied by A atoms. The energies $\varepsilon_{AB}(r_{ij})$ and $\varepsilon_{BB}(r_{ij})$ are defined analogously.

The configurational energy H_c for the system is then

$$H_c = \frac{1}{4} \sum_{ij} (\varepsilon_{AA}(r_{ij})[S_i+1][S_j+1] + \varepsilon_{BB}(r_{ij})[1-S_i][1-S_j] + \varepsilon_{AB}(r_{ij})([S_i+1][1-S_j]+[1-S_i][S_j+1])). \quad \text{(II-30)}$$

Utilizing the fact that $\sum_i S_i = 0$ for an alloy of 50:50 composition, eq. (II-30) becomes

$$H_c = \text{constant} - \sum_{ij} J_{ij}\sigma_i\sigma_j \quad \text{(II-31)}$$

with

$$4J_{ij} = [2\varepsilon_{AB}(r_{ij}) - \varepsilon_{AA}(r_{ij}) - \varepsilon_{BB}(r_{ij})]\exp(i\underline{\tau}\cdot\underline{r}_{ij}) .$$

Apart from the constant, H_c has the form of the Ising Hamiltonian in zero field (eq. (II-1)).

The long range order parameter S could be related to the pseudo-spin variable S_i by defining S as the average of the occupation variable throughout the lattice on the corner sites or the centre sites, or the weighted average occupation of all lattice sites ascribing a weight factor of +1 to the corner sites and -1 to the centre sites. The weight factor is conveniently expressed by $e^{i\underline{\tau}\cdot\underline{r}_i}$, where τ and r_i are as defined earlier.

$$\therefore \quad S = \frac{1}{N}\sum_i \sigma_i = \frac{1}{N}\sum_i S_i e^{i\underline{k}\cdot\underline{r}_i} \qquad \text{(II-32)}$$

where N is the number of atoms, and $0 \leq S \leq 1$. $S = -1$ corresponds to the same physical state as $S = 1$.

The relationship between the intensity of the scattered neutrons and the degree of long range order in an alloy with a b.c.c. lattice can be obtained as follows.

Let us consider the elastic coherent nuclear scattering. For a lattice in which site i is occupied by an atom with nuclear scattering length b_i, the scattering cross section is given by

$$\frac{d\sigma}{d\Omega} = \sum_{i,r} b_i b_{i+r} e^{i\underline{k}\cdot\underline{r}} e^{-2W} \quad . \qquad \text{(II-33)}$$

The scattering vector $\underline{k}$ is the difference between the incoming and scattered neutron wave vectors. e^{-2W} is the Debye-Waller factor which takes into account the fact that the atoms are not rigidly fixed and therefore vibrate around their equilibrium positions. $\exp(i\underline{k}\cdot\underline{r})$ is the phase of the scattered radiation.

Since the occupation of lattice sites is described by the occupation variable S_i, b_i can be expressed as

$$b_i = \frac{(b_A+b_B)}{2} + \frac{(b_A-b_B)}{2} S_i \qquad \text{(II-34)}$$

where b_A and b_B are the coherent nuclear scattering lengths for atoms of type A and B respectively. Inserting eq. (II-34) in eq. (II-33) and utilizing $\sum_i S_i = 0$ for 50:50 alloys, we get

$$\frac{d\sigma}{d\Omega} = \left(\frac{b_A+b_B}{2}\right)^2 N \sum_r e^{i\underline{k}\cdot\underline{r}_e - 2W} + \left(\frac{b_A-b_B}{2}\right)^2 \sum_{i,r} S_i S_{i+r} e^{i\underline{k}\cdot\underline{r}_e - 2W} \qquad \text{(II-35)}$$

where N is the number of atoms.

Using equations (II-29) and (II-32), and defining

$$\langle \sigma_o \sigma_r \rangle \equiv \frac{1}{N} \sum_i \sigma_i \sigma_{i+r} ,$$

eq. (II-35) becomes

$$\frac{d\sigma}{d\Omega} = \left(\frac{b_A+b_B}{2}\right)^2 N \sum_r e^{i\underline{k}\cdot\underline{r}_e - 2W} \delta(\underline{k}-\underline{\tau}_e) + N^2 \left(\frac{b_A-b_B}{2}\right)^2 e^{-2W} S^2 \delta(\underline{k}-\underline{\tau}) +$$

$$+ N\left(\frac{b_A-b_B}{2}\right)^2 e^{-2W} (\langle \sigma_o \sigma_r \rangle - \langle \sigma_o \rangle^2) e^{i(\underline{k}-\underline{\tau})\cdot\underline{r}} \qquad \text{(II-36)}$$

where $\underline{\tau}_e$ is the reciprocal lattice vector with an even sum of Miller indices.

The first term in eq. (II-36) is independent of the ordering process in the alloy (no dependence on S, or σ_i) and contributes only when the reciprocal lattice vector is an even sum of Miller indices. This term gives the fundamental peaks in the neutron diffraction pattern of the b.c.c. lattice.

The contribution of the ordering process to the differential cross section is from the second and third terms. It can be shown that the last term in eq. (II-36) is related to the wave vector dependent susceptibility $\chi_T(q)$, $\underline{q} \equiv \underline{k}-\underline{\tau}$. Above the transition temperature - where there is no long range order - the second term in eq. (II-36) vanishes and there remains a so-called diffuse peak intensity which is proportional to the susceptibility. Well below the transition temperature,

the third term in eq. (II-35) is, for $\underline{k} \approx \underline{\tau}$, negligibly small compared to the second term. Omitting the first term that gives the fundamental peak and the third term that is negligibly small at $\underline{k} \approx \underline{\tau}$ and $T < T_c$, in eq. (II-36) we have

$$\frac{d\sigma}{d\Omega} \propto (b_A - b_B)^2 S^2 \; ; \; \underline{k} = \underline{\tau}, \quad T < T_c \; . \tag{II-37}$$

This reflection at $\underline{k} = \underline{\tau}$, and $T < T_c$ is called the superlattice reflection. Since $(b_A - b_B)$ is a constant, the intensity of the superlattice peak varies as the square of the long range order parameter; it is therefore a measure of the degree of long range order in the alloy. As can be observed in the second term in eq. (II-36), the superlattice peak is sharp at all temperatures.

In some alloys, the atoms have magnetic as well as nuclear scattering amplitudes. In such alloys there is a contribution of magnetic scattering to the superlattice peak. The expression for the magnetic contribution to the superlattice peak is similar to that for the nuclear contribution (eq. (II-37)) but the magnetic scattering lengths of the atoms should be used instead of the nuclear scattering lengths.

In practice, the reflections described by eq. (II-36) do not occur as single lines but as peaks with finite widths. The total intensity of any peak therefore depends on its height and width and is called the integrated intensity. The conversion of the intensity calculated above (eq. (II-36)) to integrated intensity involves certain instrumental and geometrical

factors of the experimental set up. Since we used powder diffraction techniques in our investigation, we shall quote the expression for the integrated intensity of the superlattice reflection from a powder sample having the form of a parallel-sided slab. This is given by (Bacon 1975),

$$I = \frac{CJ\,F^2\,e^{-\mu t \sec\theta}}{\sin^2 2\theta} \qquad \text{(II-38)}$$

and

$$F^2 = S^2[(b_{Fe}\exp(-W_{Fe}) - b_{Co}\exp(-W_{Co}))^2 + q^2(p_{Fe}\exp(-W_{Fe}) - p_{Co}\exp(-W_{Co}))^2]$$

where S is the degree of long range order. b and p are the nuclear and magnetic scattering lengths and W is the Debye-Waller factor. q is the magnetic interaction vector and 2θ is the angular position of the reflection. t and μ are respectively the thickness and the linear absorption coefficient of the sample. $\exp(-\mu t \sec\theta)$ is the correction for true absorption of neutrons in the sample. J is the number of cooperating planes or the number of reciprocal lattice vectors having a magnitude equal to that of the reflection being measured. C is a constant that depends mainly on the wavelength of the neutrons, the number of neutrons in the incident monochromatic beam, the distance from sample to counter, and the number of unit cells per cm^3 in the sample.

Table II-1. Definitions of critical point exponents

Exponent	Quantity	Definition	Conditions		
		Fluids			
			ε	$p-p_c$	$\rho-\rho_c$
β	$\rho_L-\rho_G$	$\sim(-\varepsilon)^{\beta}$	<0	0	$\neq 0$
α'	C_V	$\sim(-\varepsilon)^{-\alpha'}$	<0	0	0
α	C_V	$\sim\varepsilon^{-\alpha}$	>0	0	0
γ	k_T	$(-\varepsilon)^{-\gamma'}$	<0	0	$\neq 0$
γ	k_T	$\sim\varepsilon^{-\gamma}$	>0	0	0
δ	$p-p_c$	$\sim\lvert\rho_L-\rho_G\rvert^{\delta}\operatorname{sgn}(\rho_L-\rho_G)$	0	$\neq 0$	$\neq 0$
ν'	ξ	$\sim(-\varepsilon)^{-\nu'}$	<0	0	$\neq 0$
ν	ξ	$\sim(\varepsilon)^{-\nu}$	>0	0	0
		Magnets			
			ε	H	M
β	M	$\sim(-\varepsilon)^{\beta}$	<0	0	$\neq 0$
α'	C_H	$\sim(-\varepsilon)^{-\alpha'}$	<0	0	0
α	C_H	$\sim\varepsilon^{-\alpha}$	>0	0	0
γ'	χ_T	$\sim(-\varepsilon)^{-\gamma'}$	<0	0	$\neq 0$
γ	χ_T	$\sim\varepsilon^{-\gamma}$	>0	0	0
δ	H	$\sim\lvert M\rvert^{\delta}\operatorname{sgn}(M)$	0	$\neq 0$	$\neq 0$
ν'	ξ	$\sim(-\varepsilon)^{-\nu'}$	<0	0	$\neq 0$
ν	ξ	$\sim\varepsilon^{-\nu}$	>0	0	0
η	$\Gamma(r)$	$\sim\lvert r\rvert^{-(d-2+\eta)}$	0	0	0
Δ_1'	$\frac{\partial^1 G}{\partial H^1}\equiv G(1)$	$\sim(-\varepsilon)^{-\Delta_1}{}_G(1-1)$	<0	0	0

Table II-2. Comparison of theoretical predictions with experimental results. (After H.E. Stanley, Introduction to Phase Transitions and Critical Phenomena. Oxford University Press (1971).)

Exponent	Experimental Results			Exact and Approximate Theoretical Values		
	Fluid (Co_2)	Magnet (Ni)	Alloy β-brass	Landau Mean Field	Ising (d=2)	Ising (d=3) (approximation)
below T_c						
α'	~ 0.1	-0.3	~ 0[a]	0	0	$\sim \frac{1}{16}$
β	0.34	.42	0.304[b]	$\frac{1}{2}$	$\frac{1}{8}$	$\sim \frac{5}{16}$
γ'	~ 1.0			1	$1\frac{3}{4}$	$\sim 1\frac{5}{16}$
at $T=T_c$						
δ	4.2	4.22		3	15	~ 5
above T_c						
α	~ 0.1	0	$\sim \frac{1}{8}$[a]	0	0	$\sim \frac{1}{8}$
γ	1.35	1.35	1.25	1	$1\frac{3}{4}$	$\sim 1\frac{1}{4}$

[a] P. K. Kumar and L. Muldawer, Phys. Rev. B 14, 1972 (1976).

[b] J. C. Norvell and J. Als-Nielsen, Phys. Rev. B 2, 277 (1970).

[c] O. W. Dietrich and J. Als-Nielsen, Phys. Rev. 153, 711 (1967).

CHAPTER III

EXPERIMENTAL APPARATUS AND TECHNIQUES

III.1 Specimens

Alloys with twelve different compositions were prepared separately from weighed amounts of Johnson-Mathey 4N iron and cobalt. The materials were melted together in an arc melter and cast into square plates 38 mm × 38 mm and 4 mm thick. Since each plate will attenuate a neutron beam having intensity I_0 to $I_0\exp(-n\sigma t)$, where n is the number of atoms per unit volume in the alloy, t is the thickness of the plate, and σ is the weighted mean of the cross sections (including elastic, inelastic and absorption cross sections) of the atoms, the thickness of each plate should be as small as possible in order to minimize the attenuation. But it is also necessary that each plate should be thick enough to give sufficiently intense reflections. A compromise was made by grinding down the thickness of each sample to 2 mm which was the thickness that gives an attenuation of about 25%.

After the experiment, we analysed chemically the twelve specimens. With the exception of the two specimens that were closest to the equiatomic composition, the analysis was done to measure both the concentration of iron, and the concentration of cobalt. The analysis for each sample was done as follows.

where N and V(ml) are respectively the normality and volume (in millilitre) of the potassium permanganate used in the titration. There was no interference from the cobalt in the above procedure; the technique had been satisfactorily used in blank titrations for iron, i.e. titrations to determine the amount of iron in solutions containing known amounts of iron and cobalt.

The determination of the amount of cobalt in the solution was difficult because of interference from iron. Different masking agents were tried in the attempt to mask or complex the iron by doing blank titrations for cobalt in solutions containing cobalt and the masking agent, and in solutions containing a mixture of cobalt, iron, and the masking agent. From these trials, sodium fluoride was found to be a suitable masking agent. The titration used was one in which the titrant forms a complex with the titrate (a complexometric titration). The titrant was the disodium salt of ethylenediaminetetraacetic acid (EDTA). In the analysis the iron was first of all masked and three drops of xylenol orange indicator were added to the solution in order to recognize the end point of the titration; its colour changes sharply at the end point. Hexamethylenetetramine (hexamine) was added to the solution so as to bring its pH to 6 - which is the pH at which the complex formed is most stable - and the solution was heated to about 40°C. Near the estimated end point, 5 drops of 0.001 M phenanthroline were added to the solution so as to make the colour

change at the end point easier to recognize. At the end point, the colour of the solution changes from purple to yellow. The relationship between the volume of EDTA used and the amount of cobalt in the solution is (A.L. Vogel 1961),

$$V(ml) \times N \times 0.05893 = \text{weight of cobalt (gms)} . \qquad \text{(III-2)}$$

N and V(ml) are respectively the normality and volume (in millilitre) of the EDTA used.

The technique used in calculating the concentrations of iron and cobalt with their errors from the results of the titrations will be illustrated by discussing the analysis done for one of the samples; the 45.1 atomic % cobalt sample.

For this sample, a piece weighing 4.5750±0.0005 gms was used to make 500 mls of solution. Therefore the weight of iron and cobalt in 25 mls is 0.2288 gms. The average volume of 0.1 N$KMnO_4$ used in three titrations of three 25 mls of the solution was 21.92±0.02 mls, and the average volume of 0.1 MEDTA used in three other similar titrations was 17.98±0.06 mls.

$\therefore$ The weight of iron in 25 mls = $(21.92\pm0.02)\times(0.1000\pm0.0004)\times$
$\times\ 0.05585$
$= 0.1224\pm0.0006$ gms

and the weight of the cobalt in 25 mls = $(17.98\pm0.06)\times(0.1000\pm0.0005)\times$
$\times\ 0.05893$
$= 0.1060\pm0.0009$ gms.

If Y represents the number of cobalt atoms; then

$$\frac{\text{number of Co atoms}}{\text{number of Fe atoms}} = \frac{Y}{1-Y} = \left(\frac{\text{wt. of Co}}{\text{atomic wt. of Co}}\right) / \left(\frac{\text{wt. of Fe}}{\text{atomic wt. of Fe}}\right)$$

$$= \left(\frac{\text{wt. of Co}}{\text{wt. of Fe}}\right) \times B$$

and $$B = \frac{\text{atomic wt. of Fe}}{\text{atomic wt. of Co}} = \frac{55.85}{58.93} .$$

If W_T' and W_{Co}' represent the total weight of FeCo and weight of cobalt (both in 25 mls) respectively, and noting that Wt. of Fe = Wt. of FeCo - Wt. of Co

$$Y = \frac{(B \times W_{Co}')}{W_T' + (B-1)W_{Co}'}$$

$$= \frac{0.9477 \times (0.1060 \pm 0.0009)}{0.2288 - 0.0523(0.1060 \pm 0.0009)}$$

$$= 0.4501 \pm 0.0039$$

having used the expansion $(1+x)^{-1} = (1-x)$ for x small. Therefore the concentration (atomic) of cobalt determined from the titration for cobalt is

$$45.0 \pm 0.4\%. \qquad \text{(III-3)}$$

Similarly if X represents the number of iron atoms, then

$$\frac{\text{numer of Fe atoms}}{\text{number of Co atoms}} = \frac{X}{1-X} = \frac{(\text{wt. of Fe})}{(\text{atomic wt. of Fe})} / \frac{(\text{wt. of Co})}{(\text{atomic wt. of Co.})}$$

$$= \frac{\text{wt. of Fe}}{\text{wt. of Co}} \times k$$

and

$$k = \frac{1}{B} = \frac{58.93}{55.85} .$$

Denoting the weight of Fe by W'_{Fe} and noting that the weight of Co = wt. of FeCo - wt. of Fe, we have

$$X = \frac{k \times W'_{Fe}}{W'_T + (k-1)W'_{Fe}}$$

$$= \frac{1.055(0.1224 \pm 0.0006)}{0.2288 + 0.0550(0.1224 \pm 0.0006)}$$

$$= 0.5482 \pm 0.0026 .$$

Therefore the concentration (atomic) of iron as determined from the titration for iron is

$$54.8 \pm 0.3\% . \qquad \text{(III-4)}$$

Since the concentration of iron plus the concentration of cobalt should equal 100, then the measured concentration of iron implies that the concentration of cobalt should be

$$100-(54.8 \pm 0.3) = 45.2 \pm 0.3\% . \qquad \text{(III-5)}$$

The concentration of cobalt in the sample was taken to be the mean of the values measured directly for cobalt (III-3) and that deduced from the measured concentration of iron (III-5). That is

$$\text{Concentration of cobalt} = ((0.4)^{-2}+(0.3)^{-2})^{-1} \times (45.0/(0.4)^2+45.2/(0.3)^2$$

$$= 45.1\% .$$

The error is $((0.4)^{-2}+(0.3)^{-2})^{-1/2} = 0.2\%$.

Therefore the concentration of cobalt in the sample is 45.1 ± 0.2 atomic %.

The analysis for the concentration of iron and cobalt in the other samples was done in the same way. The sum of the concentration of iron, and the concentration of cobalt measured in each specimen added up to 1 within the limits of experimental error as shown in Table III-1. For the two nearly equiatomic compositions, the analyses was done to determine only the concentration of iron in each specimen, and it was assumed that the sum of the concentration of iron and the concentration of cobalt in each of the two specimens add up to 1. These two specimens were the first to be studied and analysed; and at that time a satisfactory procedure had not been devised to mask the iron. By the time we solved this problem - about 6 months later - somebody had accidentally thrown away the solutions of the two specimens, and unfortunately there were no pieces of these samples left to prepare more solutions as we had used them up during the early part of the analysis. Since the sum of the concentration of iron and the concentration of cobalt in the other specimens added up to 1, and since all the specimens were prepared in the same fashion and from the same ingredients, the assumption that the concentration of iron and cobalt in each of these two specimens add up to 1 is reasonable. The two specimens were found to contain 49.5 and 50.2 (±0.3) atomic % cobalt respectively. The concentration of cobalt measured in each sample is shown in Table III-1. With the exception of 49.4 atomic % cobalt, these amounts were within 0.7% of the compositions calculated from the weights

Table III-1. The calculated and measured concentration (atomic %) of iron and cobalt in the samples

Co (calculated)	Co (measured) (A)	Fe (measured) (B)	Fe+Co (A+B)	Co (100-B) (C)	Mean Co (from A and C)
70.0	69.7±0.4	30.5±0.2	100.2	69.5±0.2	69.5±0.2
65.0	64.8±0.4	35.3±0.2	100.1	64.7±0.2	64.7±0.2
60.0	60.0±0.4	40.1±0.2	100.1	59.9±0.2	59.9±0.2
55.0	55.0±0.3	44.9±0.2	99.9	55.1±0.2	55.1±0.2
52.5	52.2±0.3	47.8±0.2	100.0	52.2±0.2	52.2±0.2
50.0		49.8±0.3		50.2±0.3	50.2±0.3
50.0		50.6±0.3		49.4±0.3	49.4±0.3
47.5	47.6±0.3	52.5±0.3	100.1	47.5±0.3	47.5±0.2
45.0	45.0±0.4	54.8±0.3	99.8	45.2±0.3	45.1±0.2
40.0	40.0±0.2	60.0±0.3	100.0	40.0±0.3	40.0±0.2
35.0	34.7±0.2	65.5±0.3	100.2	34.5±0.3	34.6±0.2
30.0	29.7±0.2	70.5±0.3	100.2	29.5±0.3	29.6±0.2

of the starting ingredients. In the case of 49.4 atomic % cobalt, this difference was about 1.2%.

III-2 Furnace

The furnace used was constructed of stainless steel and it had a cylindrical shape. At the height of the neutron beam the outside wall thickness was machined down to less than 0.02 inches so that there should be little scattering of neutrons by the outside wall of the furnace. A schematic diagram of the furnace is shown in Figure III-1. It was evacuated by an oil diffusion pump to prevent the sample from oxidizing. The heater arrangement consisted of a vertical cylindrical heater 6 inches high and 3.5 inches in diameter, which supplied most of the heat, and two small auxilliary heaters situated at the top and bottom of the cylinder to compensate for heat losses at the ends of the cylinder and so reduce the temperature gradient in the specimen. The cylindrical heater was Kanthal Al strip wired in a parallel arrangement of 15 strips with resistance 0.1 Ω. The strip was 3 mm wide and 0.33 mm thick. Although the neutron beam passed through the cylinder heater, there was little attenuation and scattering of neutrons by the heater.

Electrical conductors from outside the furnace to the main heater were iron rods 3/8 inches in diameter. They also acted as mechanical supports for the heater. They were of large diameter so that their electrical resistance was very

Figure III-1

Schematic diagram of the vacuum furnace, with important components numbered in the following order.

1. Specimen
2. Main heater
3. Electrode and support for main heater
4. Teflon vacuum seal and electrical insulation
5. Auxiliary heater
6. Vacuum line to diffusion pump
7. Specimen support
8. Radiation shields
9. Chromel-alumel thermocouple measuring specimen temperature
10. Swagelock fitting
11. Flange
12. Cooling pipe
13. Thermocouple providing reference signal to temperature controller
14. Thermocouple acting as sensor to cut power to furnace in case of over heating
15. O-ring vacuum seal

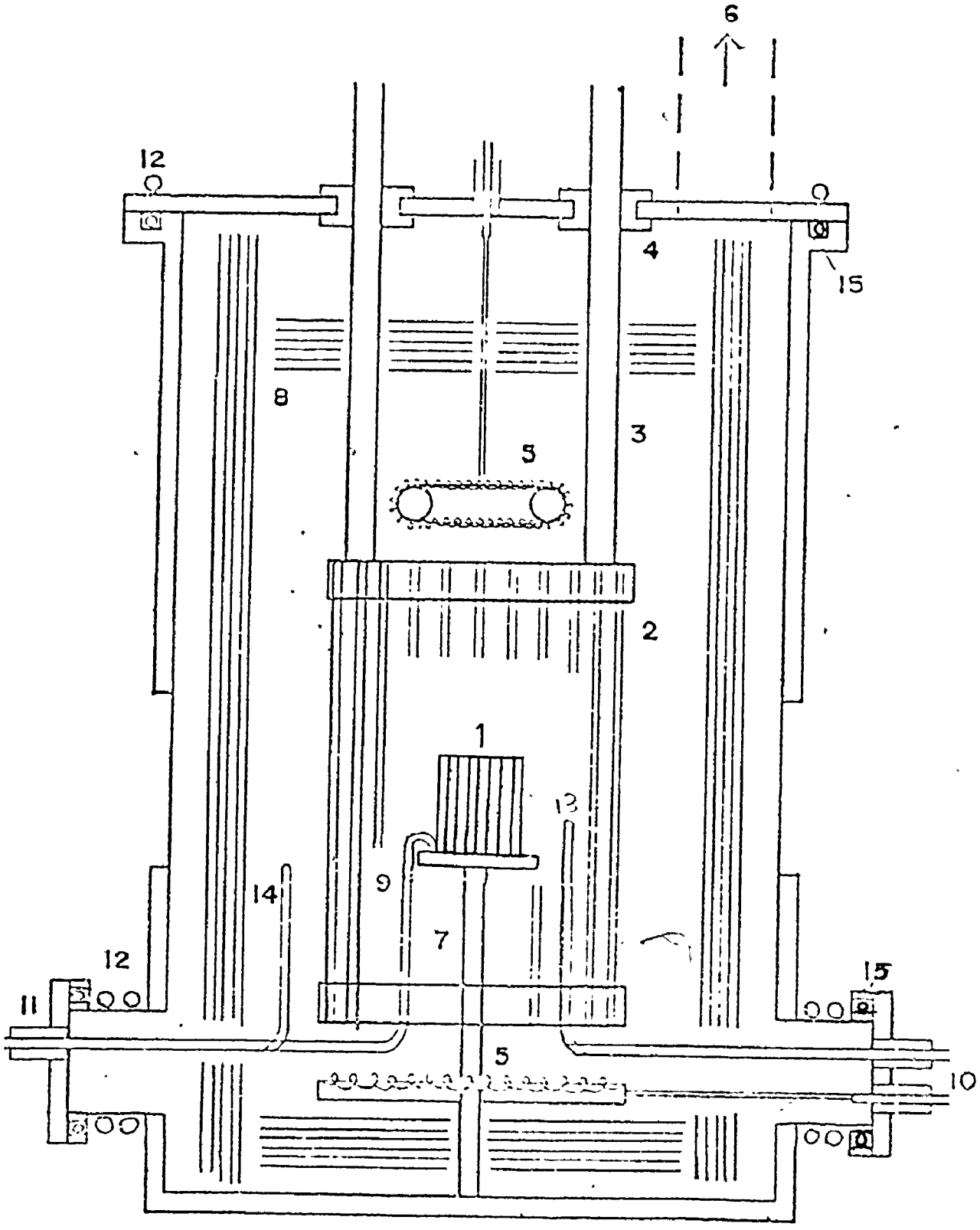

Fig. III-1. Schematic diagram of the vacuum furnace.

small compared with that of the heater element. The rods were secured vertically in the lid of the furnace by a set of teflon rings that acted as an insulator and held the O-ring for the vacuum seal. As the heater resistance was small a step-down transformer (220 V primary, 14 V secondary; 2 KVA) was placed after the temperature controller.

The two auxiliary heaters situated above and below the main heater cylinder were of Kanthal Al wire. Their resistance was 25 Ω, with each having a separate variable transformer power supply. The power to the auxiliary heaters could be adjusted independently to minimize the axial temperature gradient in the specimen.

The auxiliary heater terminals were 1/8 inch diameter brass rods secured into flanges using nylon swagelock fittings. The nylon fittings acted both as insulator and as vacuum seal. The flanges were attached by screws near the base of the furnace using O-rings for vacuum seals. All the O-ring seals on the furnace were water cooled.

The heaters were enveloped by five cylindrical stainless steel shields whose axes were along that of the main heater, and by six shields positioned above and below the heaters. The 0.002 inches thickness of the shields at the side did not attenuate the neutron beam to any significant extent.

The temperature of the specimen was measured using an ungrounded chromel-alumel thermocouple enclosed in a 1/8 inch diameter stainless-steel sheath. There were two other such

thermocouples inside the furnace; one was positioned between the specimen and the main heater so that it could monitor the incident radiation, and the other was positioned between the main heater and the radiation shields. The cold junctions of all the thermocouples were kept at 0°C by an ice-point reference unit that was stable to better than 0.1°K over long periods.

The voltage of the specimen thermocouple was measured using a six-digit D.C. differential voltmeter. The accuracy of the instrument was 4 μV corresponding to an accuracy of the temperature measurement of 0.1°K. The amplified output of the error signal, from the balance voltage of the voltmeter, was fed into a chart recorder to give a record of the specimen temperature during an experiment.

The temperature was controlled by a proportional temperature controller (Figure III-2) with a continuously variable setpoint between 15 MV and 35 MV (∿ 650°K to ∿ 1150°K). The setpoint could be set with an accuracy of 4 μV (0.1°K). The signal to the temperature controller was provided by the thermocouple that was positioned between the main heater and the specimen. The power input to the heater was varied by the controller in proportion to the difference between the thermal emf of the feedback thermocouple and the setpoint voltage. When the difference was zero the power to the heaters had a pre-set constant value. With this arrangement the stability of the specimen temperature near T_c was 0.2-0.3°K

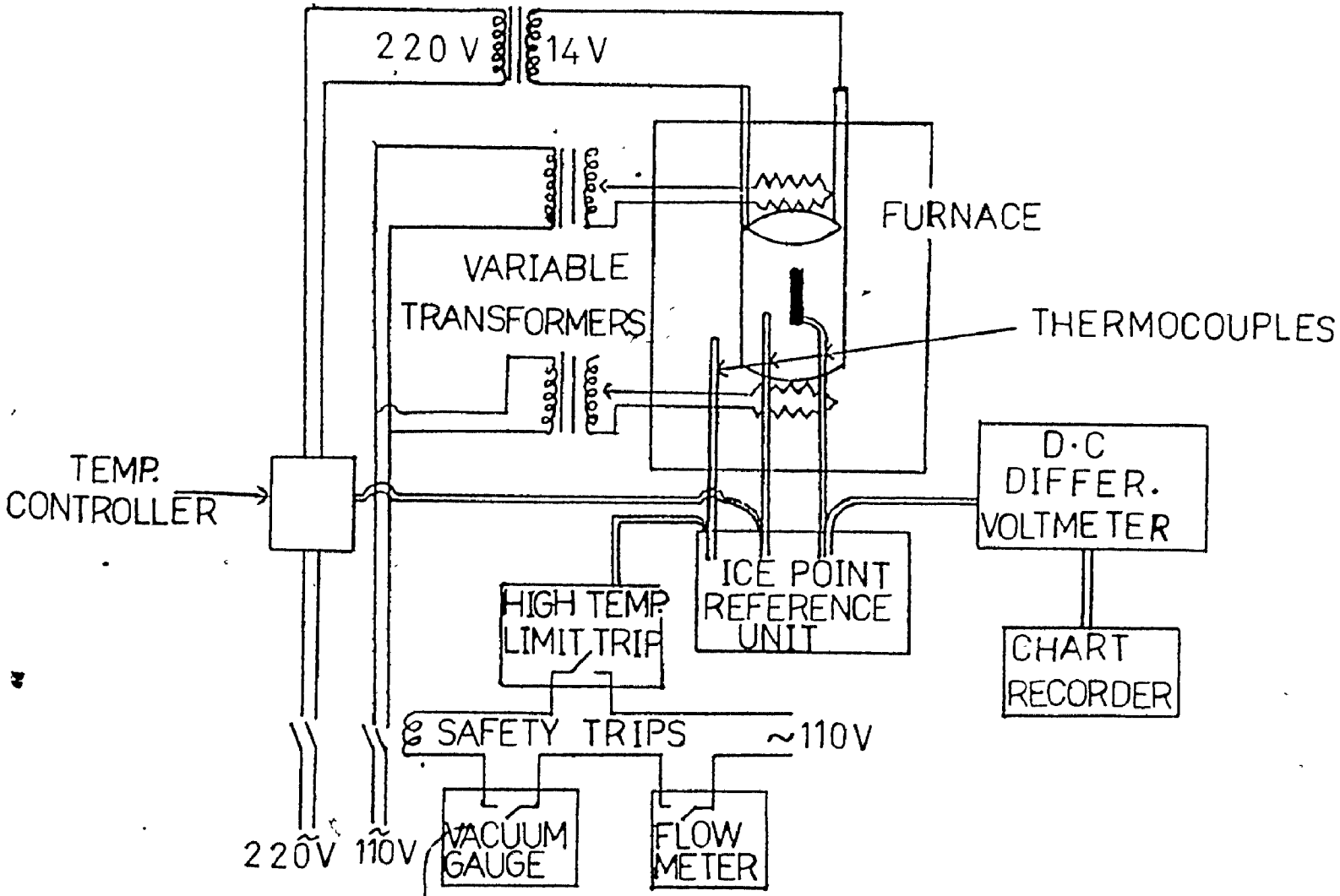

Fig. III-2. Schematic diagram of the temperature control and measurement apparatus.

over 24 hour periods and the response-time to a change in the setpoint was less than 1 minute.

There were three safety trips that could switch off the power to the heaters. These trips were installed to protect the sample and the furnace from a deterioration of the vacuum, a decrease in the water flow to cool the O-ring seals, and from overheating of the crystal. The temperature sensor for the overheating trip was the thermocouple that was positioned between the main heater and the radiation shields.

The sample to be investigated was attached to the end of a ceramic tube that was fixed to the bottom of the furnace. The ceramic tube had a low thermal conductivity so that the sample was effectively thermally isolated from the outside.

III-3 Triple-axis Spectrometer

Measurements on the first set of samples to be investigated were taken with the spectrometer (B.N. Brockhouse et al 1968) at the McMaster University Nuclear Reactor. The compositions were 45.1, 49.4, 50.2 and 55.1 atomic % cobalt. The spectrometer was a triple-axis spectrometer but it was used in a double-axis mode of operation. Neutrons of energy E_0 are selected from the continuous spectrum of the reactor by Bragg reflection from (220) planes of the Cu monochromating crystal, with monochromating angle θ_M. This monochromatic beam of neutrons passes through a beam tube to the centre of the specimen table and is scattered by the specimen through an angle ϕ into a helium-3 counter. A fission counter, situated

before the specimen table, is used to monitor the incident beam flux. A schematic diagram of the spectrometer is shown in Figure III-3.

The reactor power was 1.5 M.W. and the neutron beam area was about 4.0 square inches. A copper powder was used to calibrate the spectrometer. The results of the calibration show that the neutron beam had a wavelength of 0.996 A and that the Bragg peaks had less than 0.1% contamination from half wavelengths.

III-4 Double-axis Spectrometer

Due to the much higher neutron flux of the NRU reactor at the Chalk River Nuclear Laboratories, measurements on the rest of the specimens were taken at the reactor using the McMaster University double axis spectrometer. The spectrometer was constructed such that the monochromator compartment was surrounded by lead bricks and was totally submerged in water inside a tank. Photographs of the compartment before and after shielding are shown in Figure III-4. Since this was the first experiment performed with the instrument, a number of commissioning problems had to be overcome before the spectrometer could be used. The first problem was that the centre of the neutron beam reflected from the monochromator did not coincide with the centre of the specimen table along the horizontal plane. This problem was due to a misalignment between the centre of the mono-

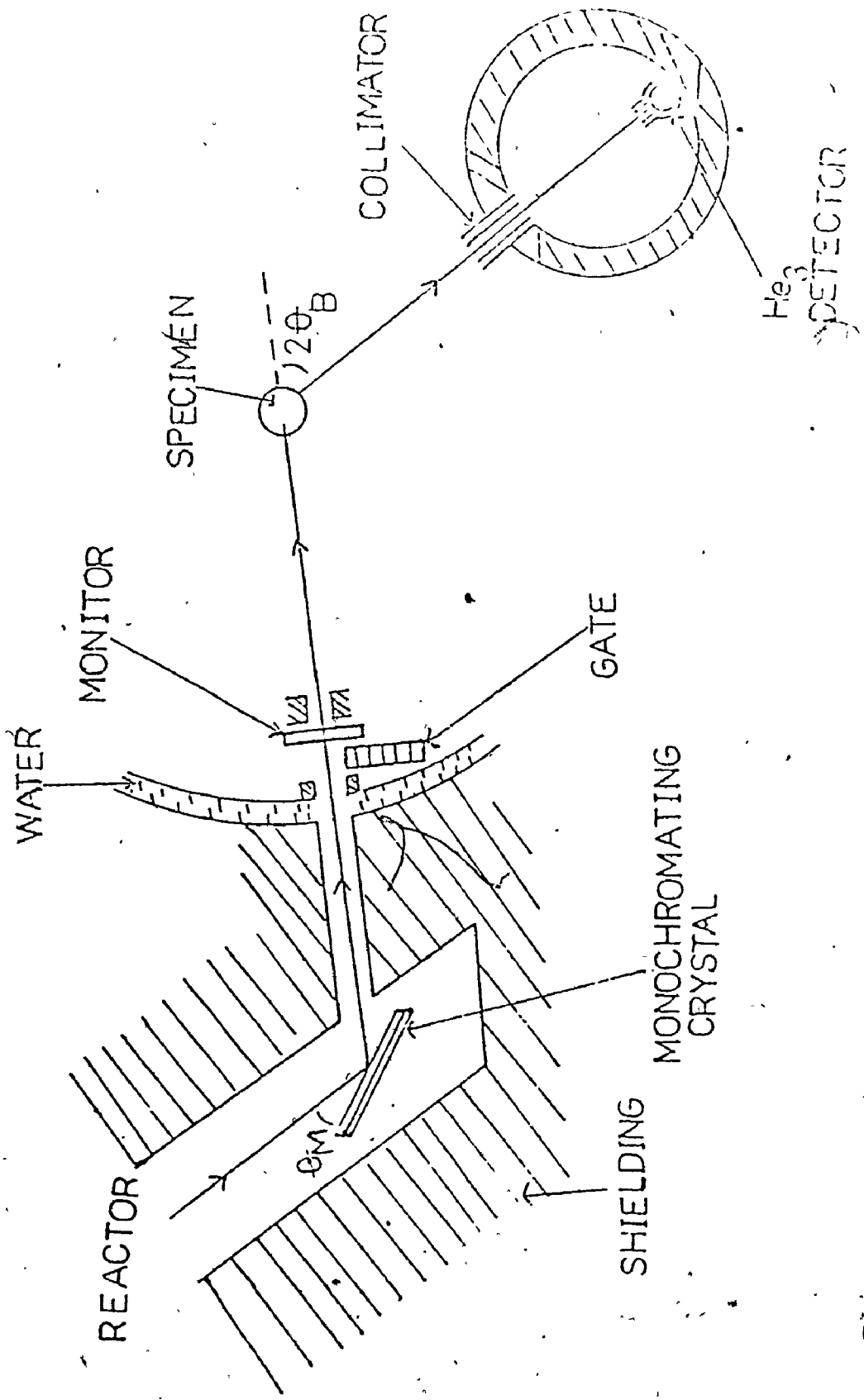

Fig. III-3. Schematic diagram of the McMaster University triple axis spectrometer in the double axis mode of operation.

chromator and that of the specimen table, and we thought that it could be easily corrected by rocking the monochromator. But by using a neutron camera, we found that no matter how we rocked the monochromator, the beam would either be to the right or left half of the centre of the specimen table as shown in Figure III-5. Other reasons were proposed for this problem - like a possible misalignment between the centre of the neutron beam coming out of the reactor, and the centre of the monochromator - but none led to a satisfactory solution. It was finally discovered that the misalignment is in the beam tube itself; the part between the monochromator and the monitor, and the part between the monitor and the specimen table - this part contains the collimator - are misaligned. The collimator had been inserted in the tube to reduce the horizontal divergence of the neutron beam; its Soller slits were made of stainless steel coated with cadmium. By adjusting the collimator so that its centre coincided with that of the beam tube, the misalignment was corrected as could be seen in Figure III-6(a).

The second problem was that the diffraction pattern of the furnace with the sample enclosed inside was very different from that obtained on the McMaster University triple axis and from what was expected for the wavelength used. The problem was initially thought to be due to higher order contamination in the neutron beam, or half wavelength neutrons,

Fig. III-4. Photographs of the monochromator compartment before (a) and after (b) shielding with lead bricks and water.

(a)

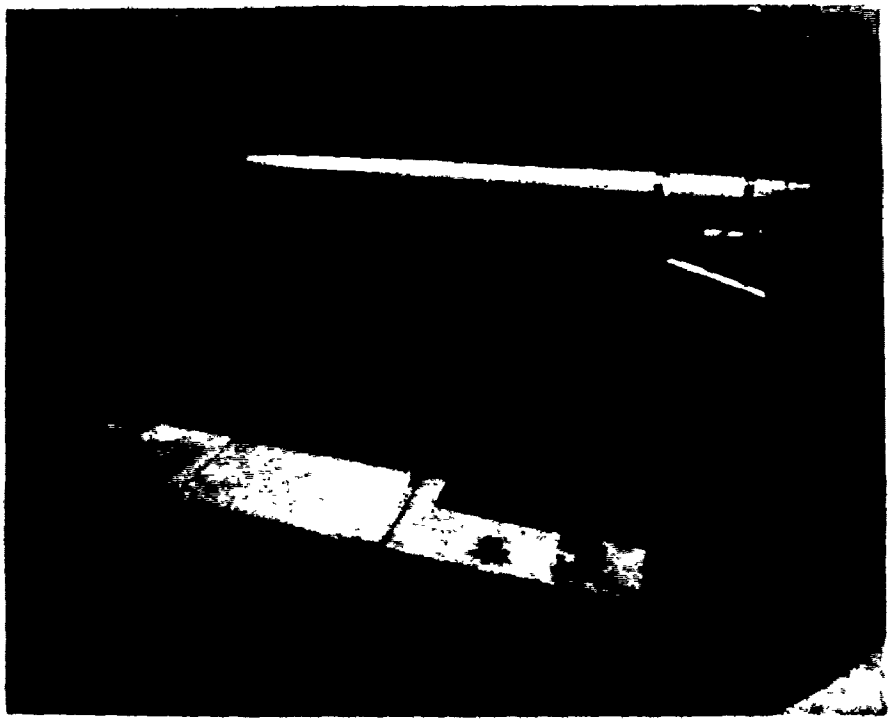

(b)

Figure III-5

Photographs of the neutron beam incident on the specimen table of the double axis spectrometer. Due to misalignment between the collimator and the beam tube, the beam was either to the left (a) or to the right (b) of the centre of the table. The black cross on the photographs is due to a strip of cadmium attached to the colimator to identify its centre.

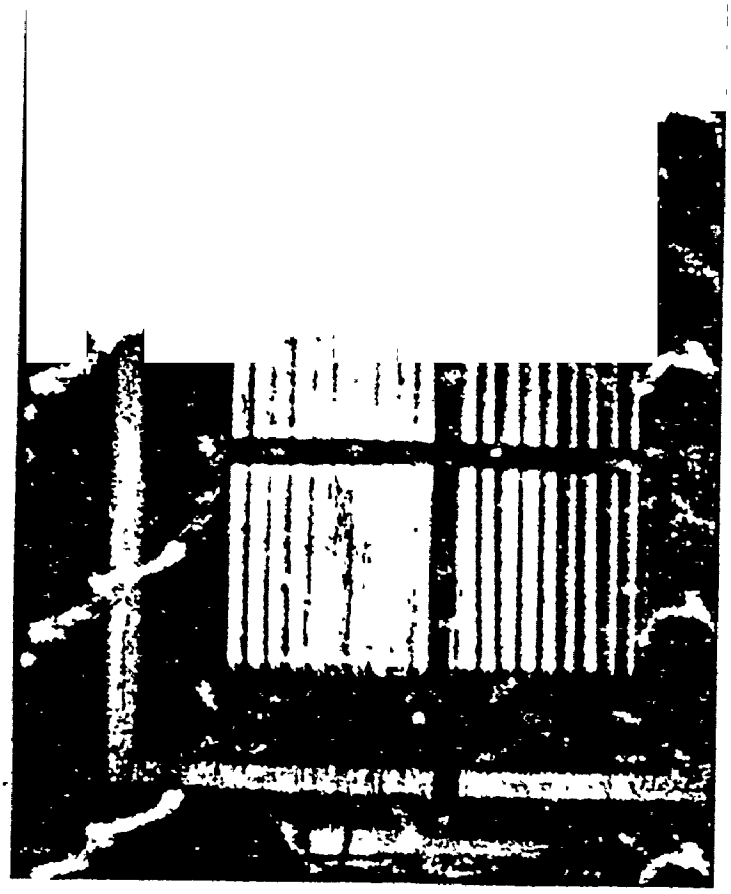

(a)

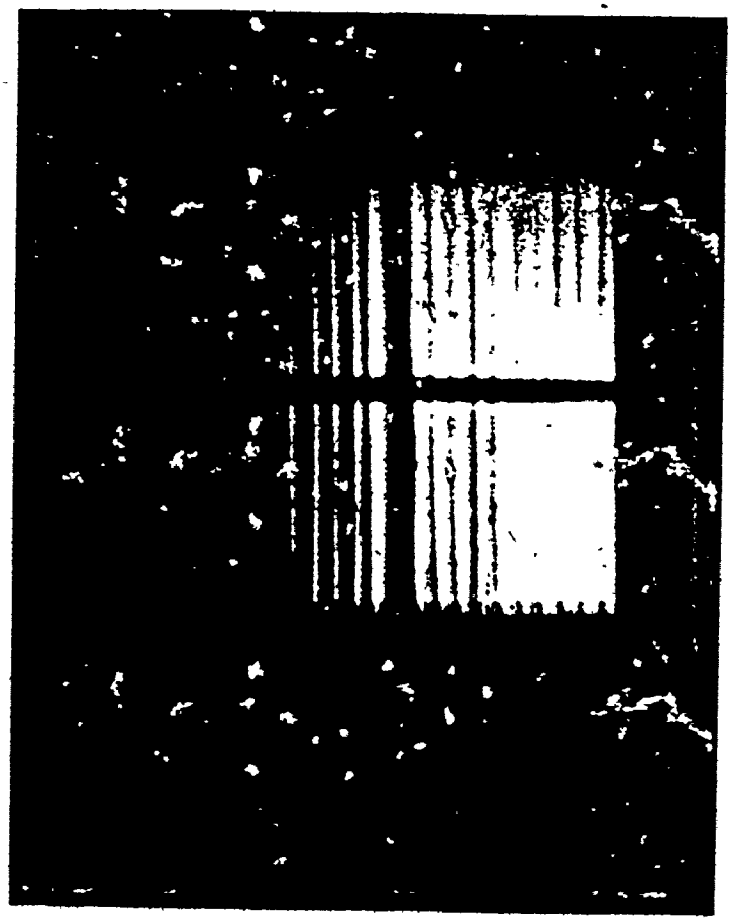

(b)

Figure III-6

Photographs of the neutron beam incident on the specimen table of the double axis spectrometer. The beam centre coincides with the centre of the specimen table. The black cross on the photograph is due to a strip of cadmium attached to the collimator to identify its centre. In addition to the main beam, some neutrons that leaked out of the beam tube were incident on the specimen table as can be seen in the areas surrounding the main beam in (a). The size of the neutron beam used in the experiment is shown in (b).

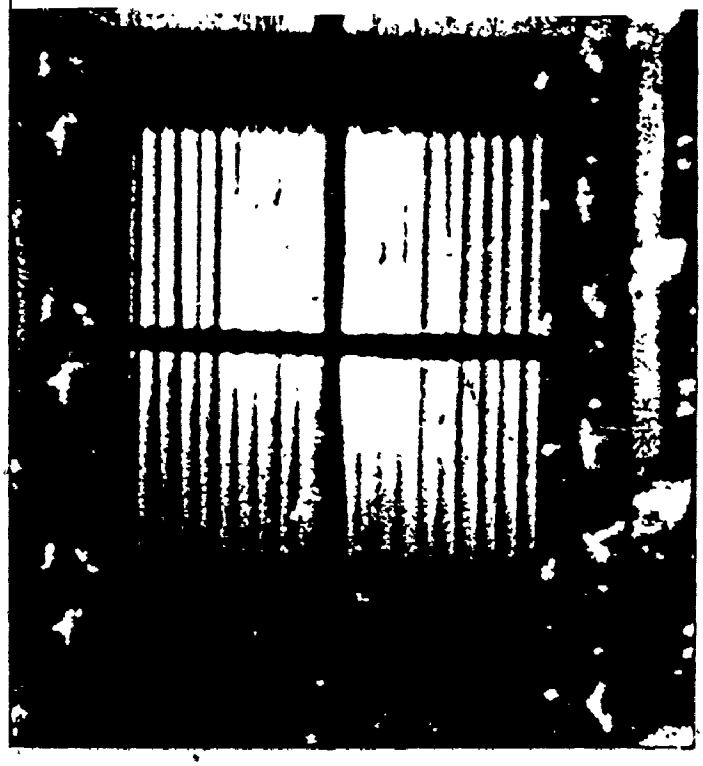

(a)

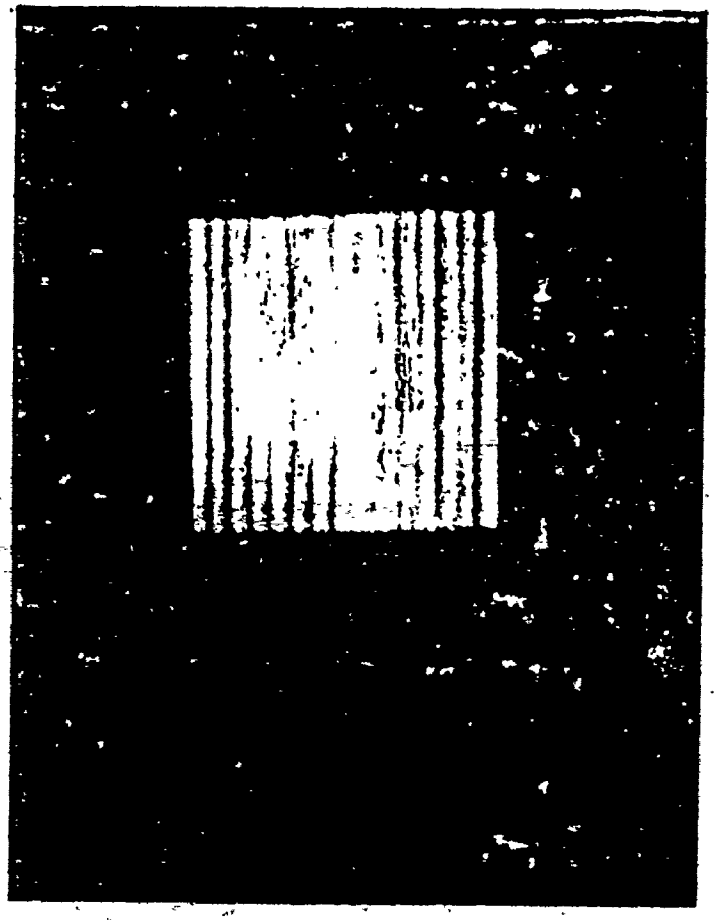

(b)

or to the possibility of much gamma radiation getting into the detector. Along these lines of thought, different attempts were made to correct the problem - like changing the wavelengths of the neutrons and adjusting the electronics of the detecting system so as to discriminate more against gamma radiation - but no satisfactory solution was obtained. The solution was finally obtained by using a neutron camera to study the neutron distribution around the specimen table. It was then observed that neutrons were incident over a distance of about 6 ins. around the centre of the specimen table instead of over 2 to 2.5 ins corresponding to the width of the beam tube. Figure III-6(a) shows the neutron distribution over a distance of about 3.25 inches around the centre of the specimen table. Although the neutron intensity at distances much more than 2.5 ins around the centre was small, it was sufficiently large to cause the problem. This unexpected neutron distribution is due to the fact that not all the neutrons reflected by the monochromator passed through the beam tube to the specimen table, but because of a divergence in the beam near the monochromator, some neutrons leaked out of the beam tube at glancing angles but outside the soller slit collimation and these were subsequently scattered into the counter. This was corrected by reducing the size of the neutron beam incident on the monochromator and by inserting extra shielding to eliminate the halo. The area of the neutron beam

incident on the specimen table was also reduced to a value close to that of the samples to be investigated. This reduced the background scattering significantly. Figure III-6(b) shows the size of the neutron beam that was used in the experiment. Figures III-7 and III-8 show respectively the schematic diagram of the double axis spectrometer and the diffraction pattern of the furnace plus sample both before and after the radiation problem was solved.

The measurement techniques are similar to those used for the other samples at the McMaster University nuclear reactor. The reactor power was 114 M.W. for most of the time and the neutron beam area was 2.25 square inches. The (220) plane of a copper monochromating crystal was used to select the wavelength used, and a fission counter situated before the specimen table, monitored the incident beam flux. The specimen was calibrated with a copper powder. The results of the calibration show that the beam had a wavelength of 1.005 A and that the Bragg peaks had less than 0.1% contamination from half wavelengths. Photographs of the experimental set up on the double axis spectrometer are shown in Figure III-9.

The intensity of the neutron beam on the double axis spectrometer was about 2 orders of magnitude larger than that on the triple-axis spectrometer.

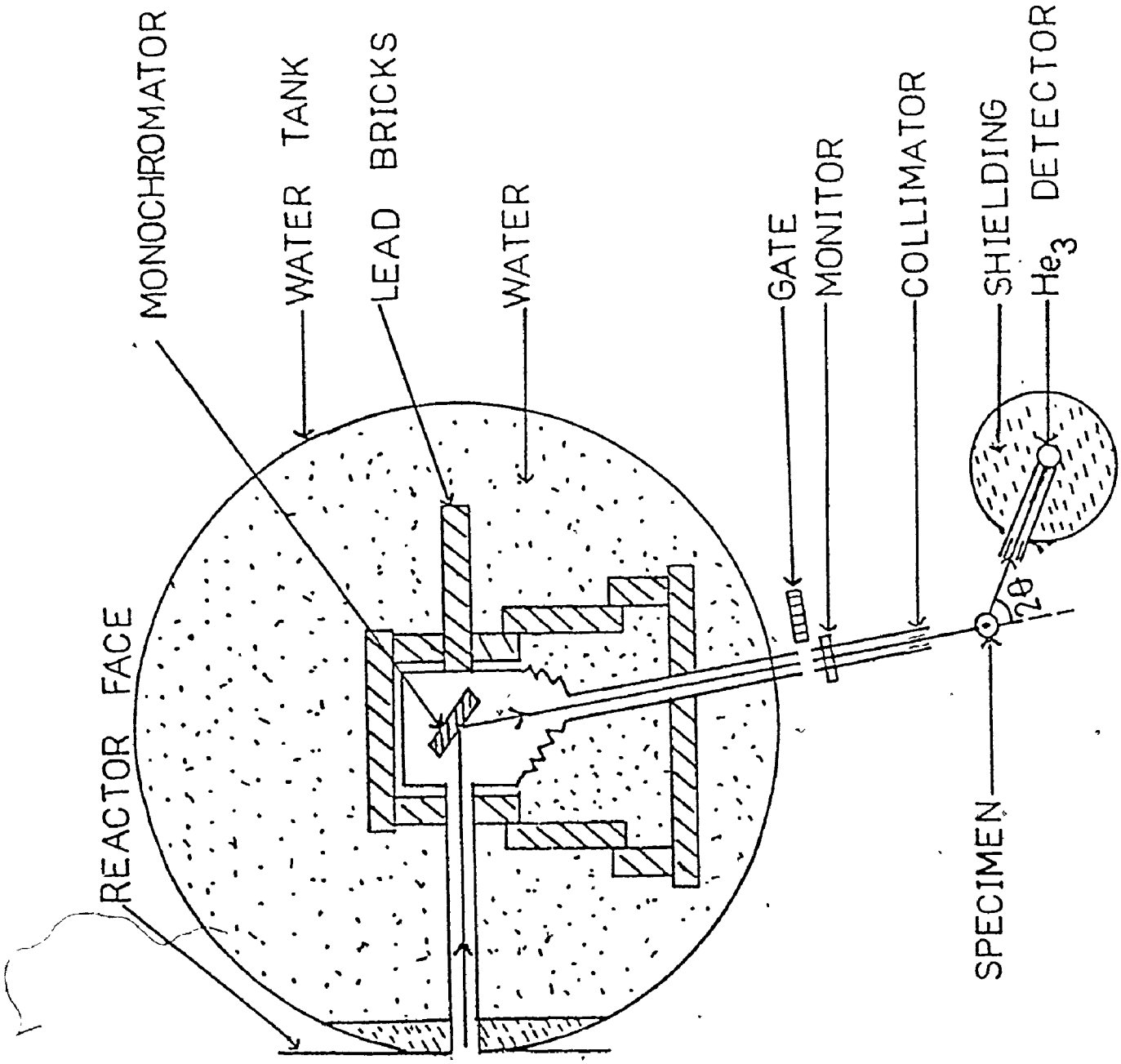

Fig. III-7. Schematic diagram of the McMaster University (E-3) double-axis spectrometer at Chalk River.

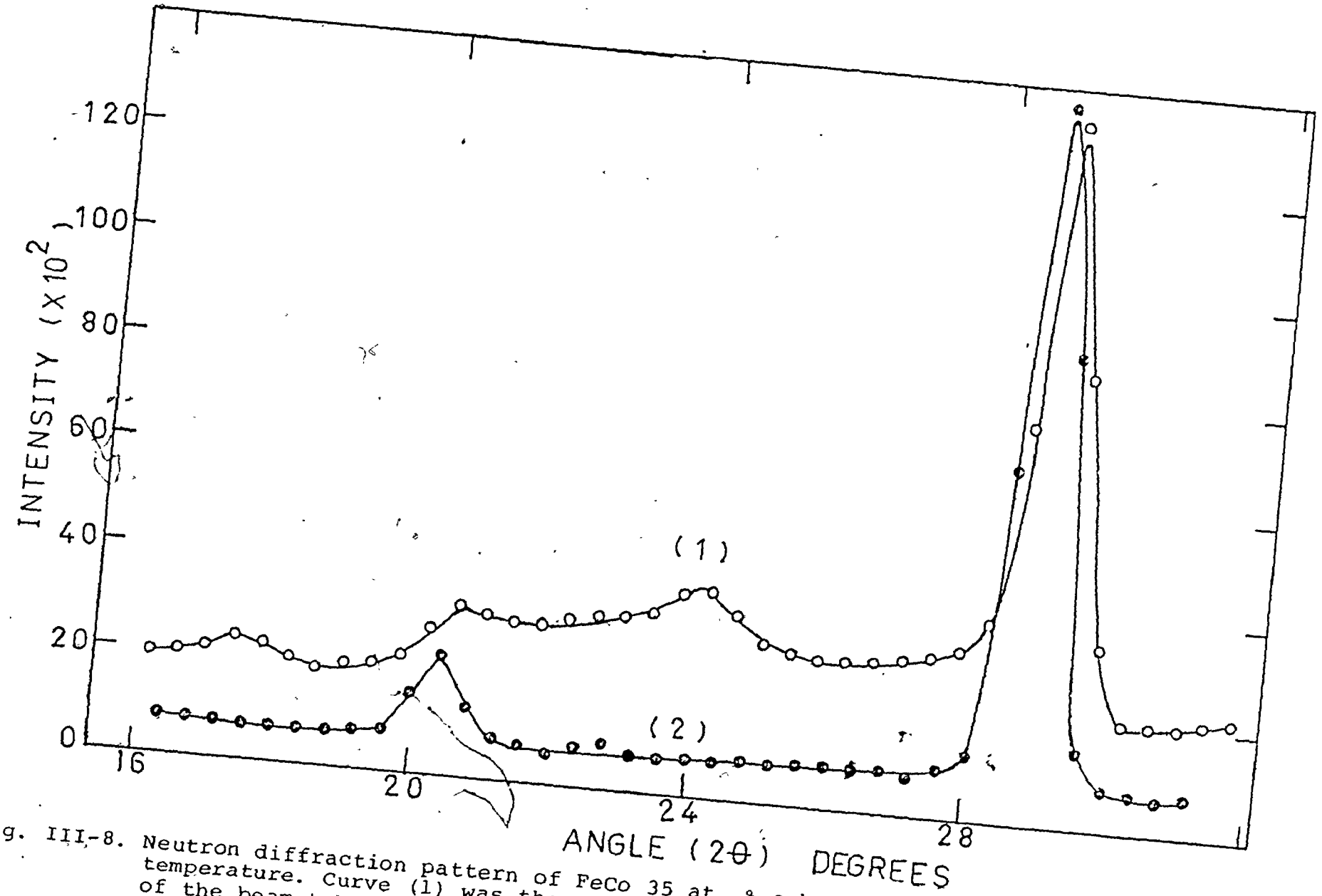

Fig. III-8. Neutron diffraction pattern of FeCo 35 at. % cobalt (inside furnace) at room temperature. Curve (1) was the pattern obtained when radiation was leaking out of the beam tube (of the double axis spectrometer) and curve (2) was the pattern obtained after the radiation problem was solved.

Figure III-9

Photographs of the experimental set up on the double axis spectrometer. The furnace and the electrical leads are shown in (a). On the left hand side of (b) is shown the control panel of the spectrometer (monochromator orientation, detector position etc.) and on the right hand side is shown the furnace temperature and measurement control panel.

(a)

(b)

CHAPTER IV

EXPERIMENTAL RESULTS AND DISCUSSION

IV-1 General Remarks

The diffraction patterns of the empty furnace, and specimen plus furnace were taken at both low and high temperatures. There was no difference in the diffraction patterns of the empty furnace at low, and at high temperatures; the diffraction pattern at room temperature is shown in Figure IV-1. But some of the peaks in the diffraction pattern of the specimen plus furnace at low temperatures disappear at high temperatures as shown in Figures IV-2 and IV-3 for a sample of 50.2% cobalt. The fact that the diffraction pattern of the empty furnace remains unchanged with temperature whereas there is much difference in the diffraction pattern of the specimen plus furnace at low and high temperatures indicates that this difference is due to the order-disorder phenomena in the specimen. The peaks that appear at low temperatures but disappear at high temperatures are the superlattice peaks. The diffraction patterns of 34.6 and 69.5% cobalt are shown in Figures IV-4 and IV-5. Similar patterns were obtained from the other samples.

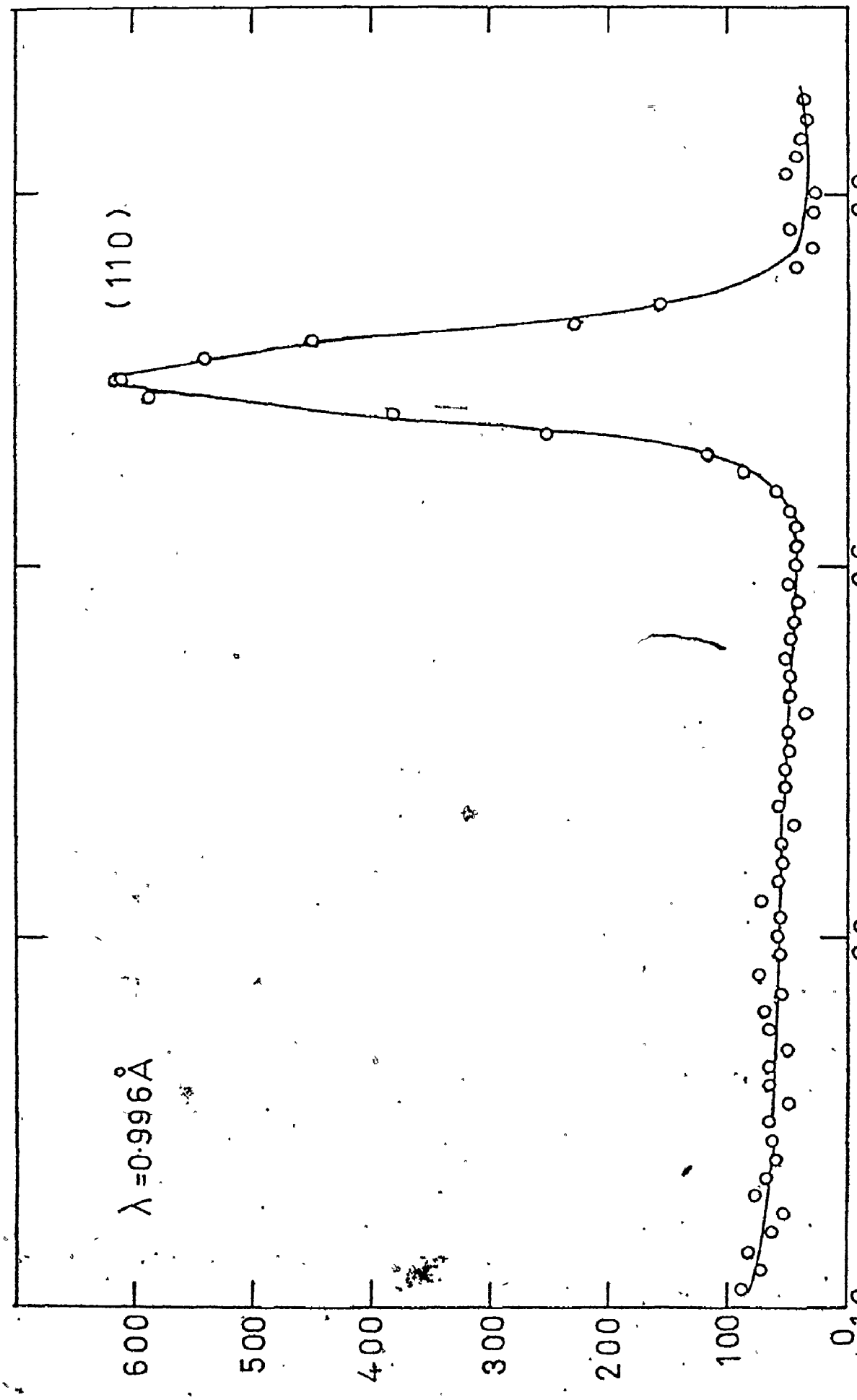

Fig. IV.1. Neutron diffraction pattern of the furnace at room temperature (using the McMaster triple axis spectrometer).

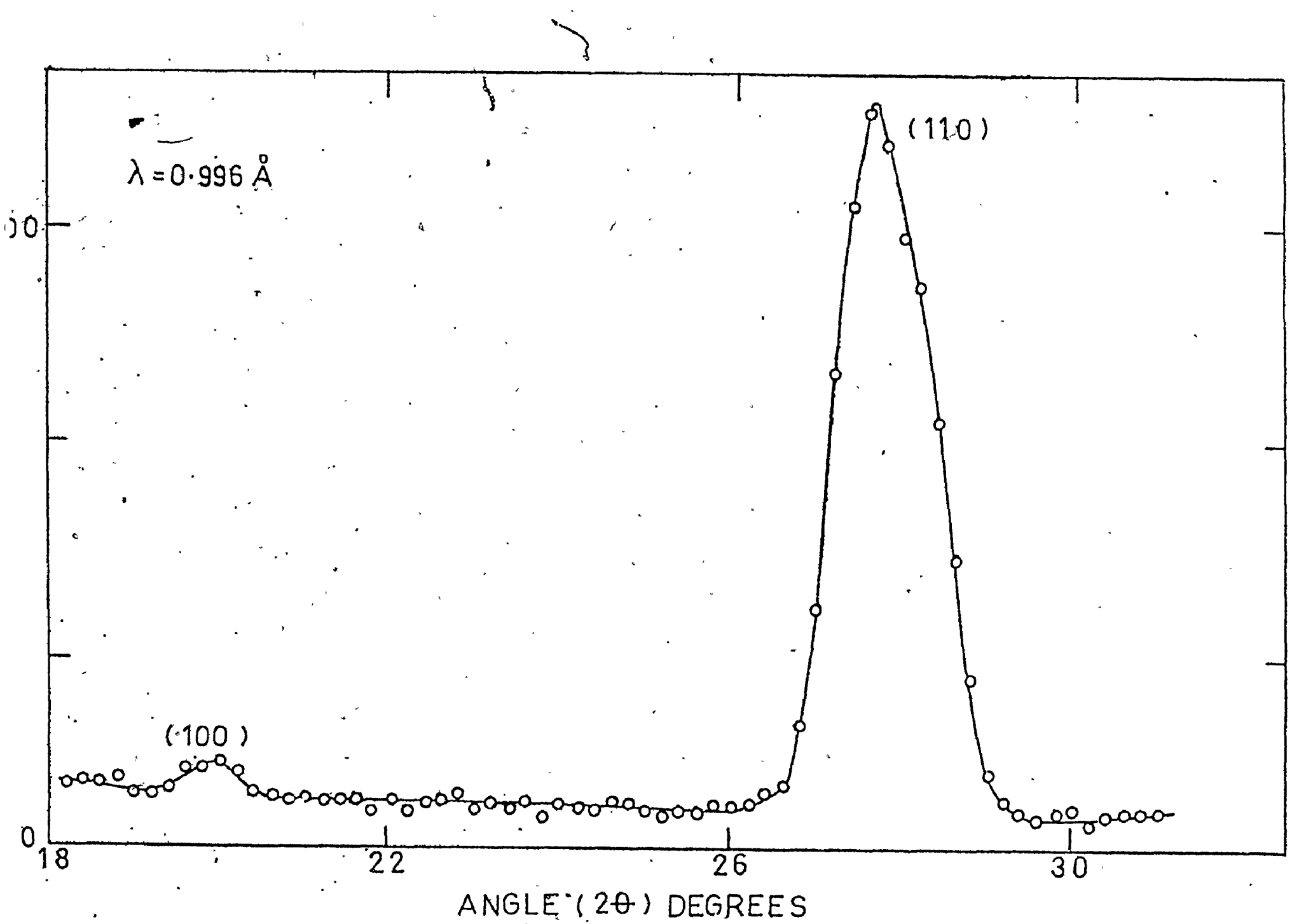

Fig. IV-2. Neutron diffraction pattern of FeCo 50.2 at. % cobalt at T = 690°C.

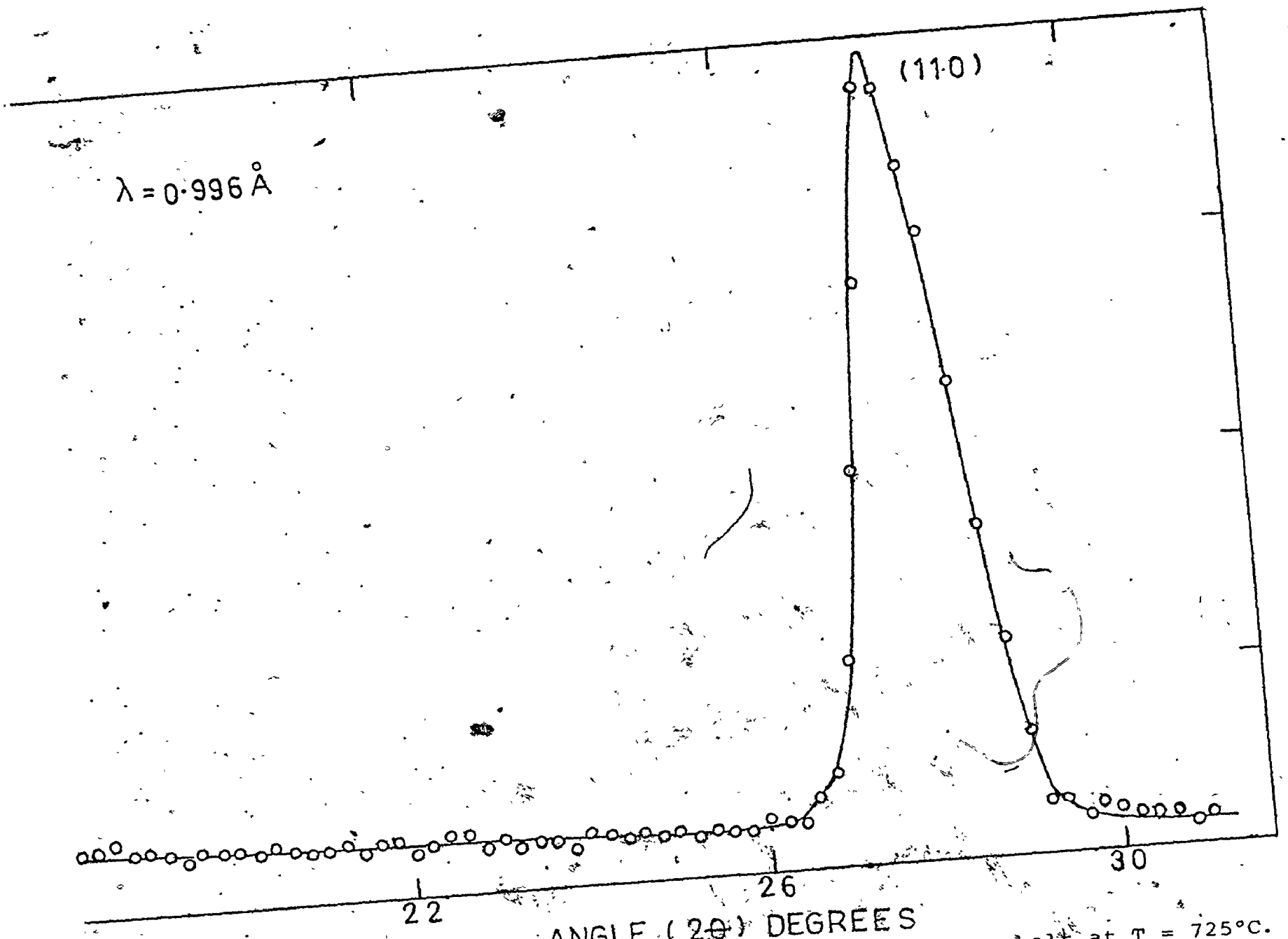

Fig. IV-3. Neutron diffraction pattern of FeCo 50.2 at.% cobalt at T = 725°C.

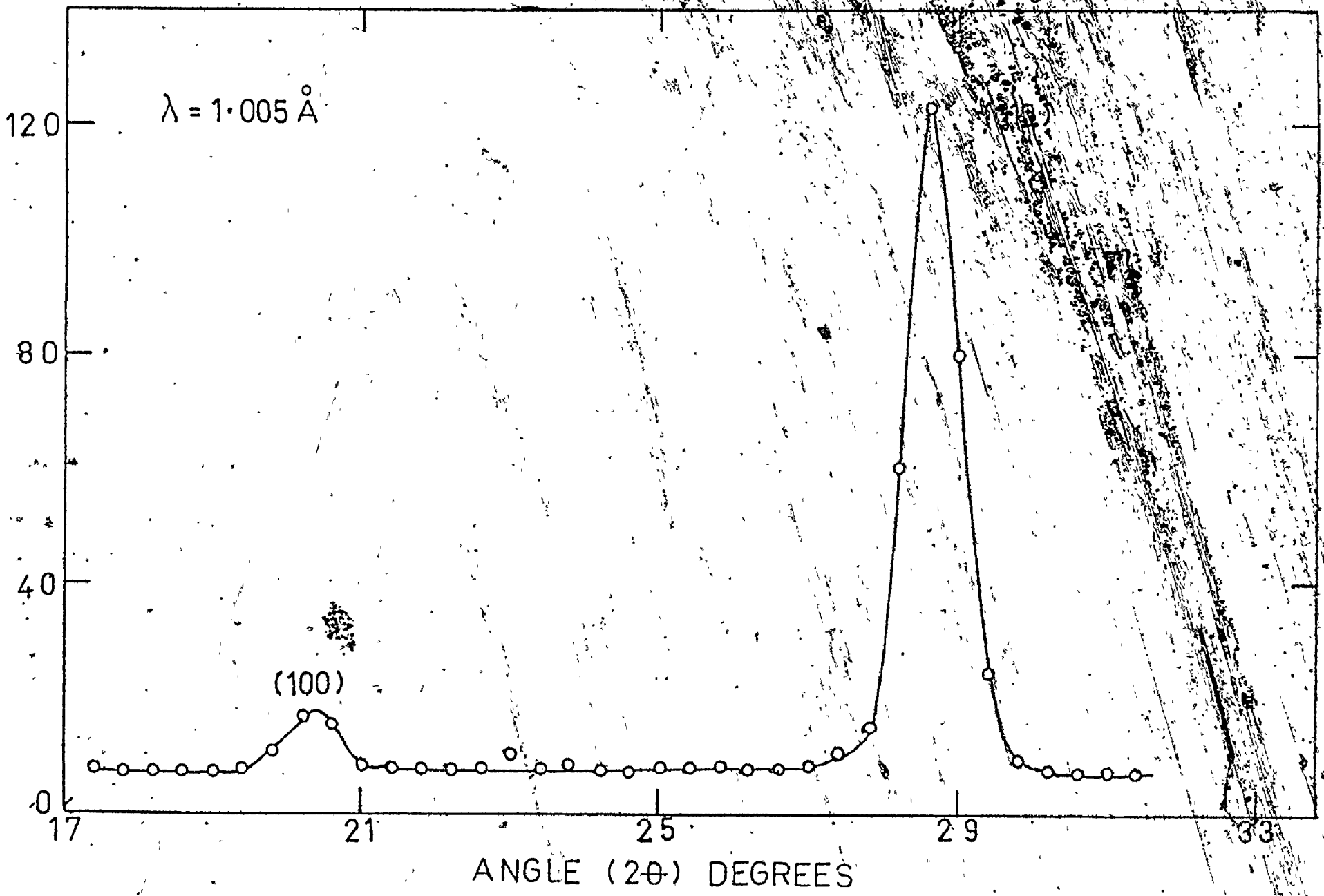

Fig. IV-4. Neutron diffraction pattern of FeCo 34.6 at.% cobalt at 596.7°C

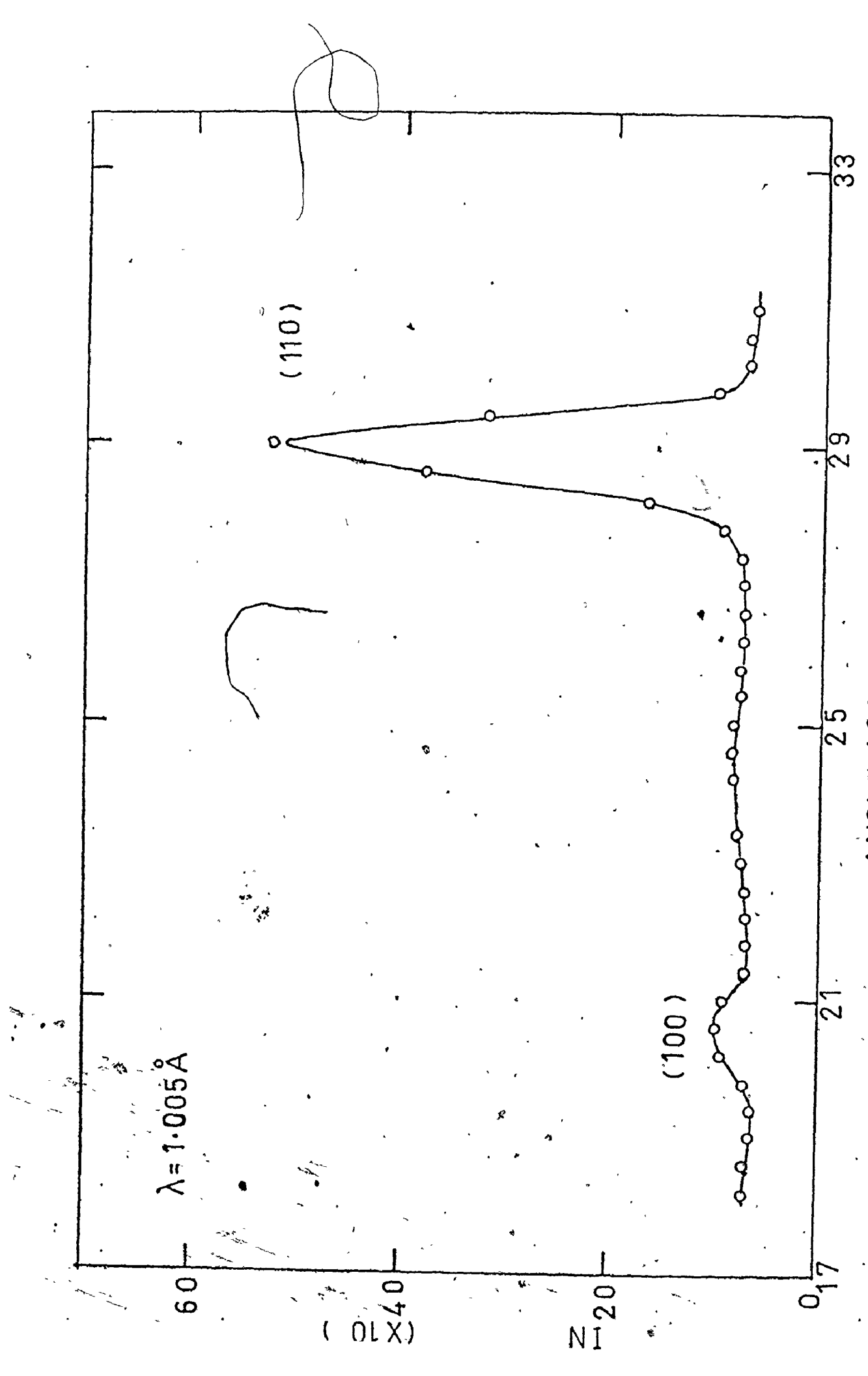

Fig. IV-5. Neutron diffraction pattern of FeCo 69.5 at.% cobalt at 440.7°C.

IV-2 Method of Collecting Data

Measurements were made while the specimen was maintained in the neutron beam at a controlled temperature by means of a vacuum furnace. The temperature was stable to better than 1°C at around 725°C. The long range order in each specimen was determined by measuring the intensity of the (100) superlattice peak. Powder specimens were used so extinction effects should not be important. Since the lattice parameter of the alloys varies slowly with temperature (W. B. Pearson 1967), relaxed collimation was employed throughout the experiment to minimize the shift, if any, of the peak centre with temperature.

In each specimen, the width (F.W.H.H.) of the (100) superlattice peak was measured at low temperatures and close to T_c, and was found to be the same to within experimental error. If the order is long range, the peaks should be sharp with width independent of temperature as discussed in section II-6. As the measured width of 0.80 degrees was equal to the instrumental resolution width it can be concluded that the samples had long range order. The (100) superlattice peak in 34.6, 47.5, 50.2, and 69.5% cobalt are shown in Figures IV-6 to IV-9 respectively. With the coarse resolution used, there was no detectable shift of the peak centre with temperature for either the fundamental or the superlattice peak over the temperature range used.

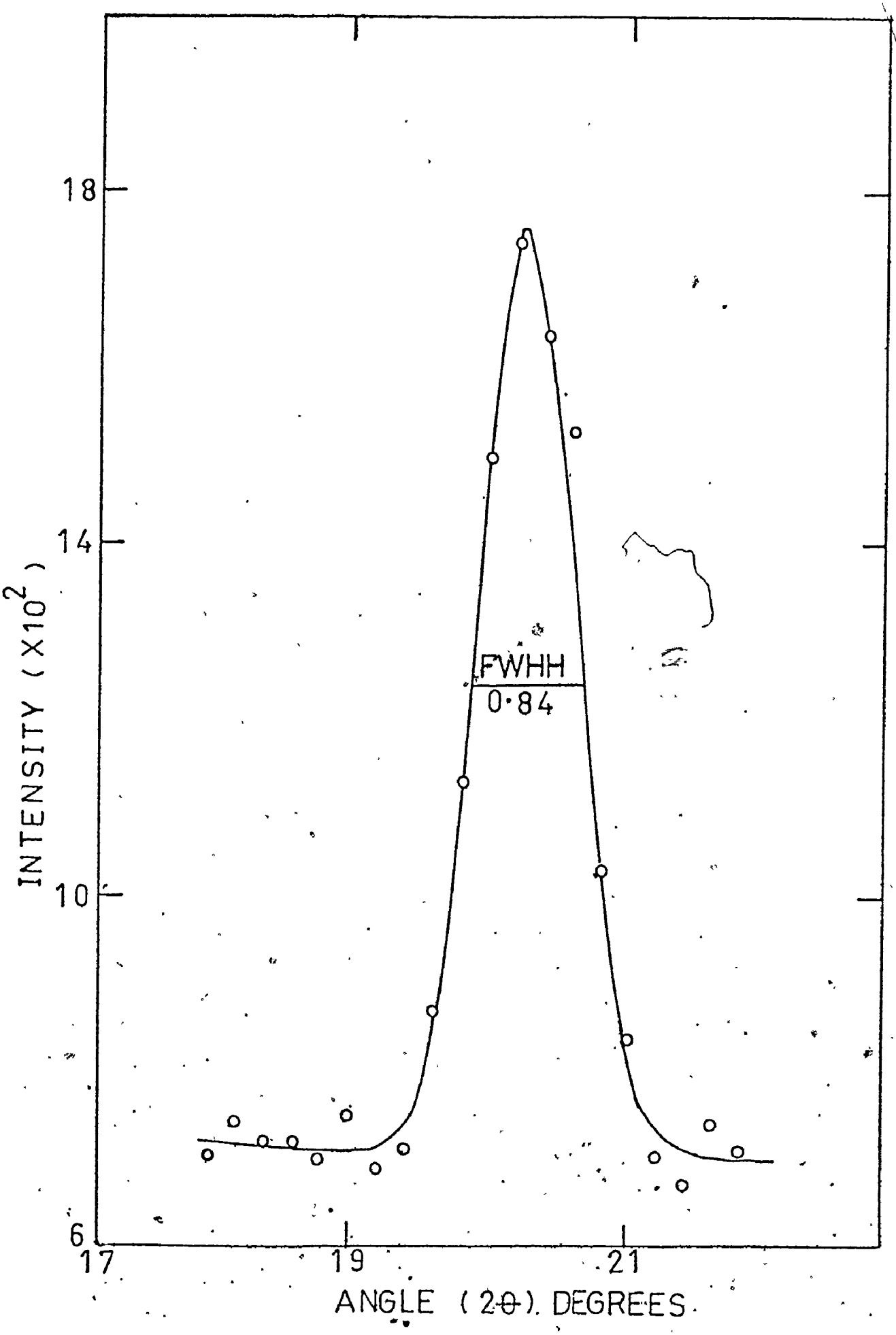
18
14
10
6
INTENSITY (X10^2)
FWHH
0·84
17
19
21
ANGLE (2θ). DEGREES.

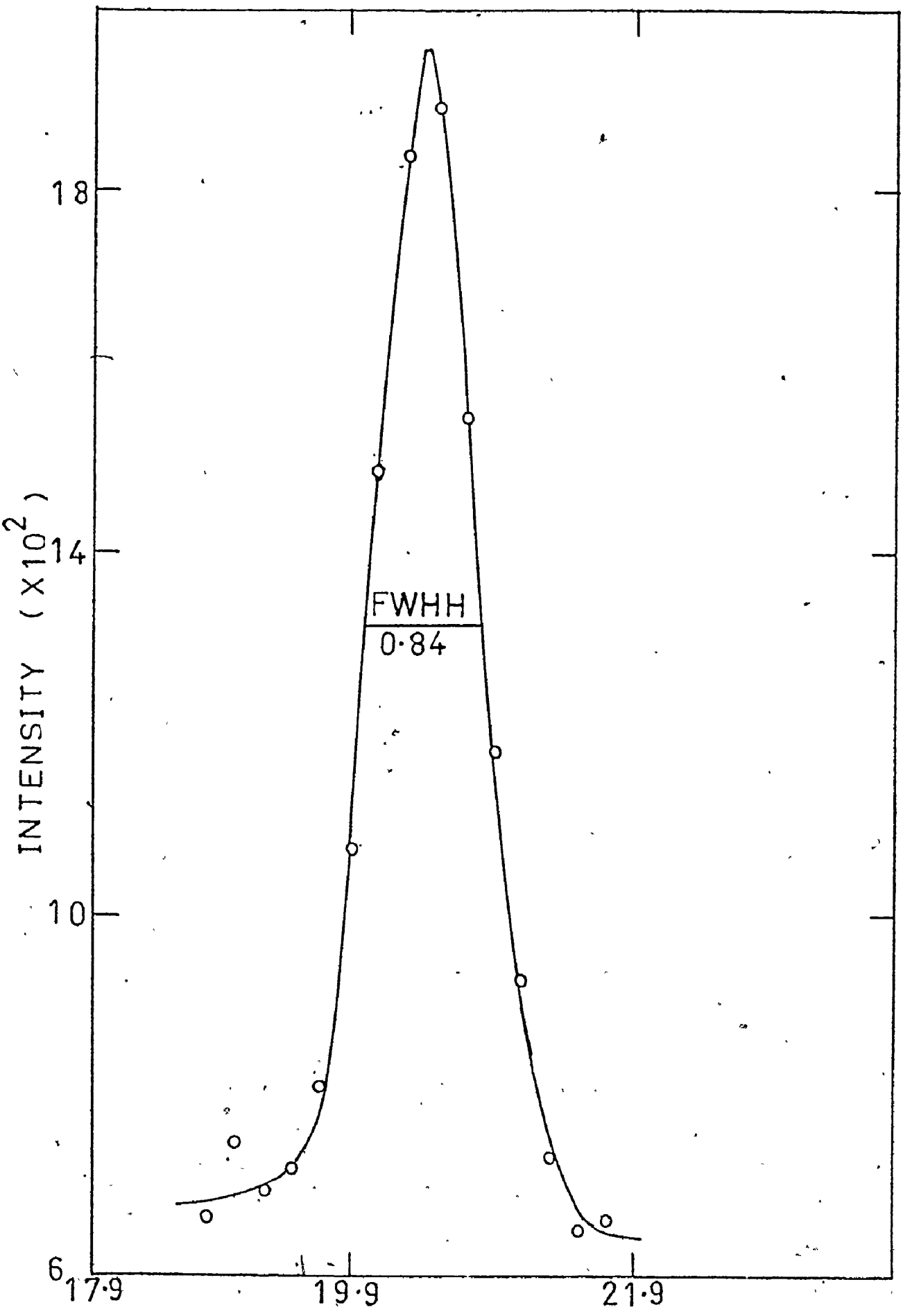
18
14
10
6
INTENSITY (X10^2)
FWHH
0·84
17·9
19·9
21·9

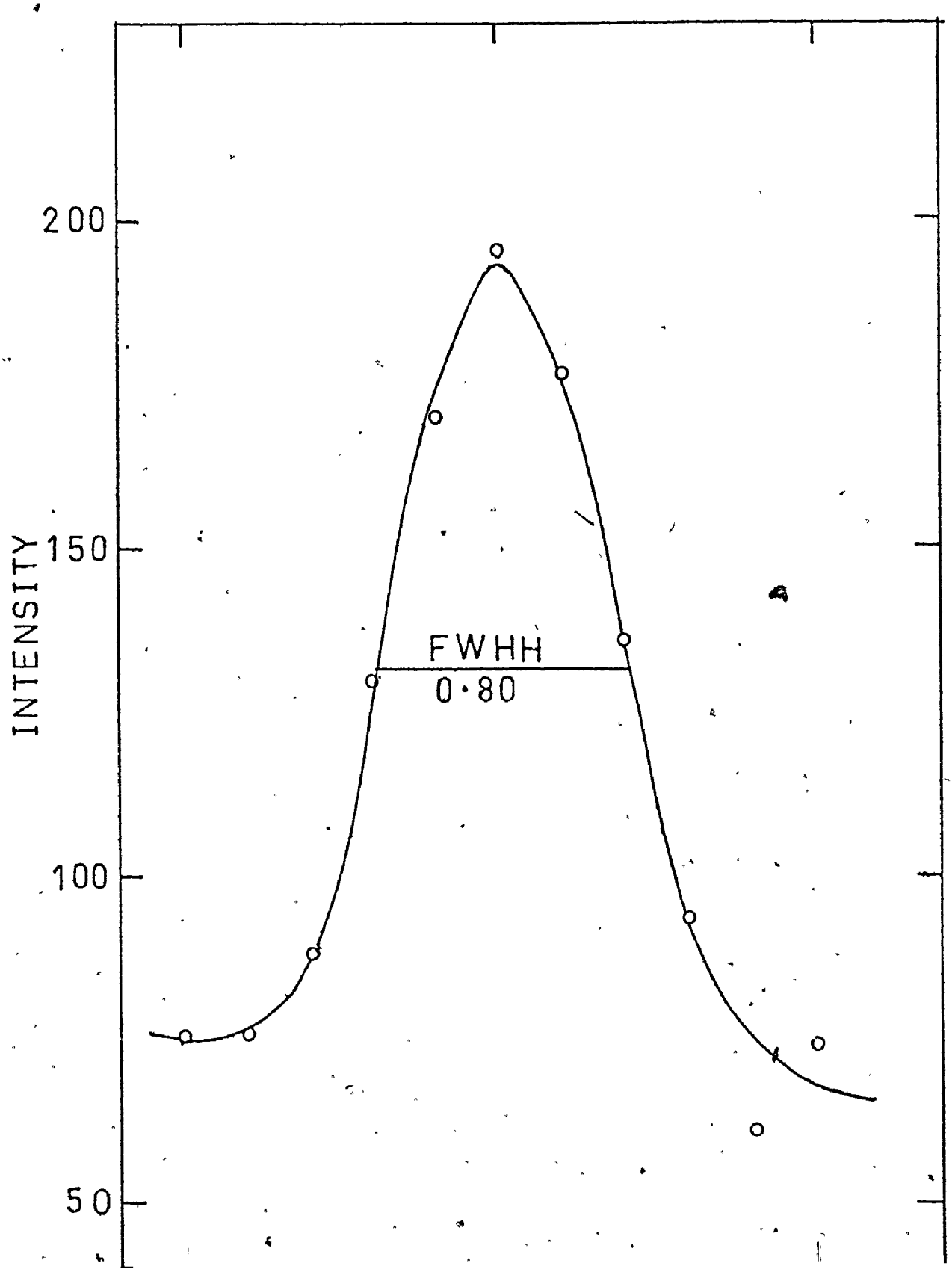
200
150
100
50
INTENSITY
FWHH
0·80

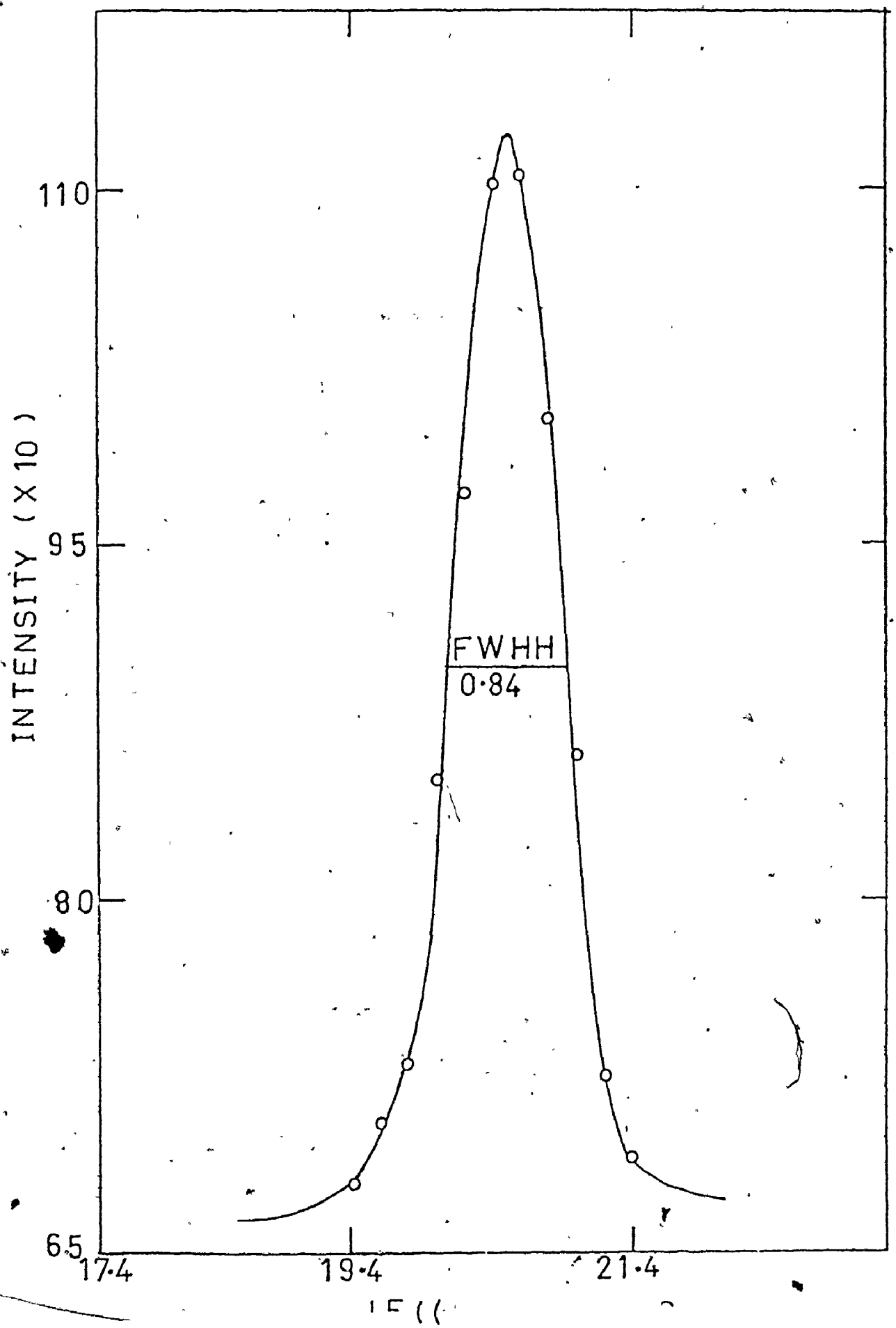
110
95
80
65
INTENSITY (X10)
FWHH
0·84
17·4
19·4
21·4

To determine the order parameter, it is necessary to measure the integrated intensity of the superlattice peak as a function of temperature. But since the peak widths (and shapes) were found to be independent of temperature at a few trial temperatures, measurements were just made of the peak height intensity of the superlattice peak as a function of temperature. The alloy was allowed to reach or relax to equilibrium after a change of temperature before the peak height intensity at the new temperature was measured; this is because the relationship between the peak intensity and the degree of order in the alloy (eq. (II-38)) is for an equilibrium and not dynamic phenomena. The constancy of the peak height intensity with time signifies the achievement of equilibrium. In order to reduce the statistical error in the counting process, the peak height intensity at a given temperature was measured several times for the same monitor setting and the mean was taken. To illustrate this method of collecting data, part of the data for the 59.9 atomic % Co alloy will be considered below.

At a temperature of 600.5°C, the peak height intensity of the (100) peak was measured ten times for a monitor setting of 1×10^5 neutrons/cm^2 (80 seconds), and the following values were obtained respectively.

1584
1672
1633
1598
1649
1584
1638
1577
1558
1548

$$\text{Total} = 16041 \pm \sqrt{16041} \quad (= 127)$$

$$\text{Mean} = 1604.1 \pm \frac{\sqrt{16041}}{10} \quad (= 13)$$

The relative error in the mean intensity for this temperature is therefore less than 1%. The errors in the mean intensities measured at other temperatures and in other samples were calculated in the same way and found to be less than 1% of the corresponding intensity. The measurements were repeatable and showed no hysteresis effects. The data for 34.6, 47.5, 50.2, and 59.9% cobalt are shown in Tables IV-1 to IV-4 respectively.

Very close to T_c, where there is critical scattering as well as scattering due to long range order (eq. (II-36)), the above method of collecting and interpreting data may run into difficulties. To calculate properly the magnitude of the critical scattering, it would be necessary to know more about the iron-cobalt system than is currently known. However, an estimate of the effect can be made by examining the apparent rounding of the data at the critical temperature for the stoichiometric alloy. The peak intensity varies with temperature in the same

way as the square of the order parameter except for a rounding within two degrees of T_c. This observation and the temperature independence of the scattering at the superlattice position at higher temperatures indicates that the measurements can be interpreted as giving the superlattice peak intensity except within about two degrees of T_c.

IV-3 Description of Results

The variation of the intensity of the 100 superlattice peak with temperature for all the samples are shown in Figures IV-10 to IV-16 in increasing order of cobalt concentration. In each case, the intensity is large at low temperatures and decreases continuously with increasing temperature up to a certain temperature above which it remains constant. This behaviour is quantitatively what is expected for a critical phase transition (see Section I-1). The temperature at which the intensity becomes constant with increasing temperature is the transition temperature T_c. There is a rounding of T_c in all the samples. The magnitude of this rounding increases as the alloy composition becomes further from the stoichiometric 50% composition. It is likely that this effect is due to microscopic inhomogeneities in the specimens, since, as will be demonstrated later, T_c varies rapidly with composition for alloys far from stoichiometry. Inspection of the graphs shows no anomaly in any of the samples at about 550°C in contrast to some authors (S. Kaya et al 1943, H. Asano et al 1967) who have reported such an anomaly in specific heat versus tempera-

Table IV-1. Data for FeCo, 34.6 at. % Cobalt

Heating or cooling	Temperature (C)	Count/2 minutes
H	703.0	779± 6
C	723.3	776± 5
C	715.5	780± 5
H	632.6	1395±12
H	637.9	1350±12
H	646.0	1267±10
H	650.8	1184±11
H	655.6	1096±10
H	659.5	1024±10
H	666.1	919±10
H	676.1	829± 8
H	706.9	781± 9
C	701.7	792±10
C	695.7	801± 6
C	685.5	807±10
C	677.4	841±10
C	671.9	833± 9
C	668.1	903±10
C	662.1	1000±10
C	658.1	1078±10
C	648.1	1240±11
C	641.0	1343±12
C	620.0	1541±12
H	600.0	1737±19
C	587.9	1793±19
H	630.0	1436±17

Table IV-2. Data for FeCo, 47.5 at.% cobalt

Heating or cooling	Temperature (C)	Count/2 minutes
H	631.7	1888±18
H	675.2	1566±16
C	737.1	771±11
C	727.6	802±12
H	735.9	776±10
C	731.9	761±11
C	728.6	769±11
C	723.8	884±12
C	717.5	1042±11
C	720.0	959±13
C	713.6	1105±14
C	709.1	1169±14
C	704.1	1254±15
C	701.2	1287±15
C	695.0	1384±15
C	691.4	1412±15
C	679.5	1523±16
C	656.9	1718±17
C	660.0	1692±17
C	642.1	1836±18
C	636.7	1864±18
C	623.4	1915±18
C	604.5	2015±18
C	592.4	2089±19
C	570.5	2130±16
C	533.9	2228±12

Table IV-3. Data for FeCo, 50.2 at. % cobalt

Heating or Cooling	Temperature (C)	Count/2 minutes
H	680.2	133.7±1.7
H	710.1	106.8±1.1
H	713.9	101.3±1.3
H	716.1	99.3±1.3
H	719.0	97.5±1.2
H	722.1	89.5±1.1
H	725.0	85.4±1.0
H	750.2	82.1±1.4
C	734.9	82.5±1.0
C	726.2	84.2±1.0
C	723.1	88.7±1.1
C	717.2	99.5±1.2
C	713.0	106.4±1.2
C	704.8	112.9±1.5
C	700.0	119.4±1.2
C	659.9	148.8±1.7
C	628.0	160.3±2.6
C	519.6	199.7±3.7
H	695.1	123.8±1.5
H	728.1	83.5±1.0
H	729.8	82.9±1.1
C	724.5	84.2±1.1
C	720.3	93.7±1.0
C	707.5	111.5±1.3
C	589.7	175.7±1.7

Table IV-4. Data for FeCo, 59.9 at. % cobalt

Heating or Cooling	Temperature (C)	Count/2 minutes
H	600.5	1604±13
H	634.8	1345±10
H	665.7	1007±10
H	698.8	837± 8
C	724.8	812±10
C	718.3	820±10
H	735.7	809±10
C	731.2	812±10
C	711.4	827±10
C	703.3	832±10
C	697.1	839±10
C	686.1	855±10
C	676.9	849±10
C	674.5	870±10
C	670.7	893±11
C	666.7	976±11
C	660.2	1063±12
C	653.6	1139±12
C	649.3	1182±12
C	644.5	1251±13
H	656.7	1112±12
C	640.2	1290±13
C	635.5	1345±13
C	631.2	1366±13
C	625.2	1442±13
C	621.0	1469±14
C	612.1	1514±14
C	605.7	1580±14
C	592.1	1661±14
C	576.4	1759±15

ture curves.

Below about 450°C the intensity of the superlattice peak ceased to vary appreciably with temperature; this is presumed to have happened because diffusion becomes too slow at these temperatures to bring the specimen into equilibrium during the course of the measurements (D. W. Clegg and R. A. Buckley 1973). At temperatures just below T_c, the superlattice peak appeared to change intensity to its new equilibrium value immediately as the temperature was changed. This suggests that the relaxation time of the alloy near T_c is smaller than the time - about one minute - required for the specimen to come to thermal equilibrium.

The intensity measured above T_c at the superlattice position is not connected with the ordering process - although just above T_c, there may be some contribution to the intensity from critical scattering (see section II-6) - but it is due primarily to incoherent scattering from the cobalt in the alloy, with lesser contributions from inelastic scattering, scattering by the furnace and general neutron background. Since these processes take place both below and above T_c and have very little dependence on temperature, they contribute a similar amount to the intensity measured below T_c as to that above T_c. This intensity, called background intensity, was subtracted from the measured superlattice peak intensity in order to obtain the intensity that was due to the ordering phenomena.

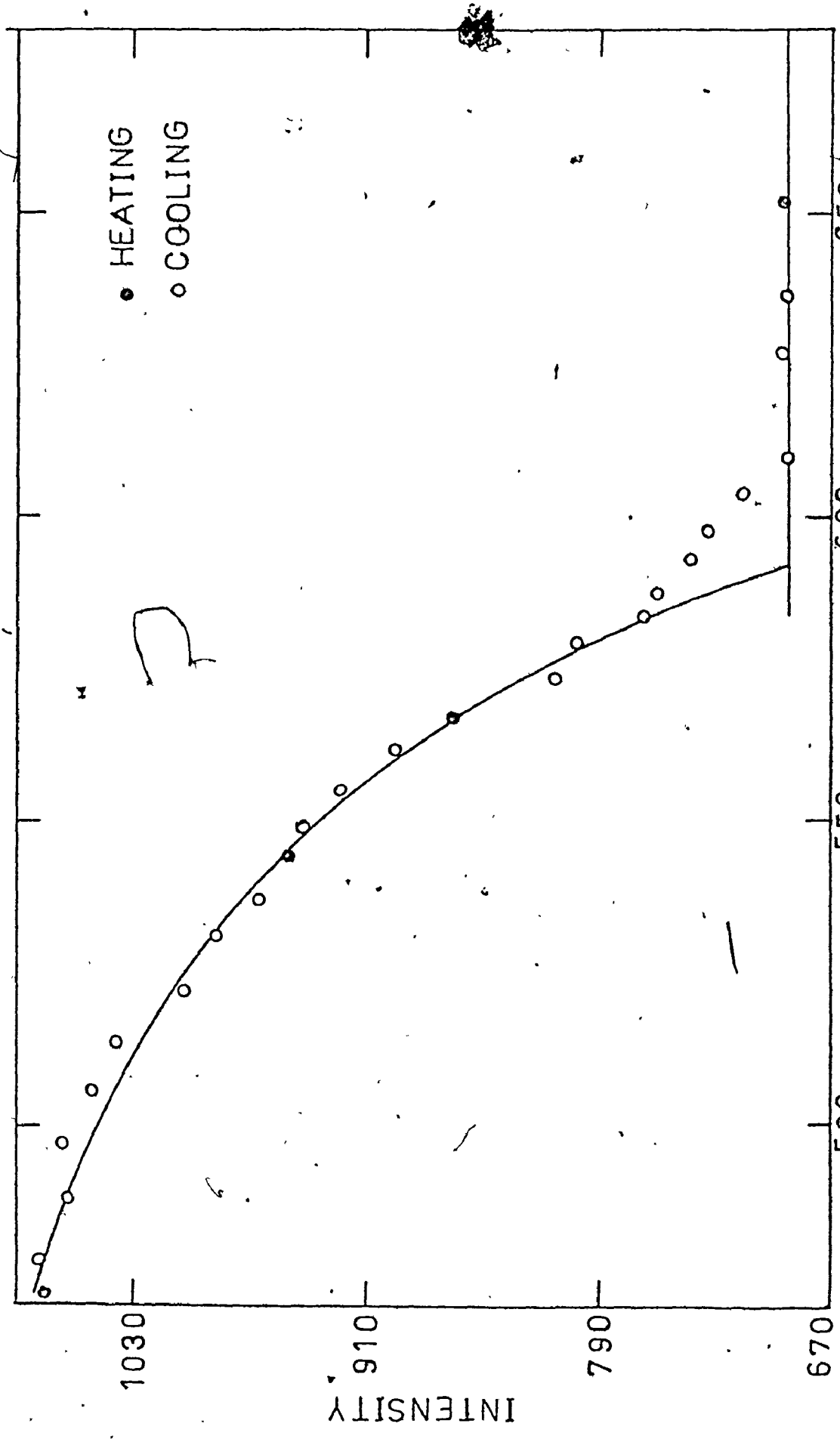

Fig. IV-10. Temperature dependence of the (100) superlattice peak intensity in FeCo 29.6 at.% cobalt.

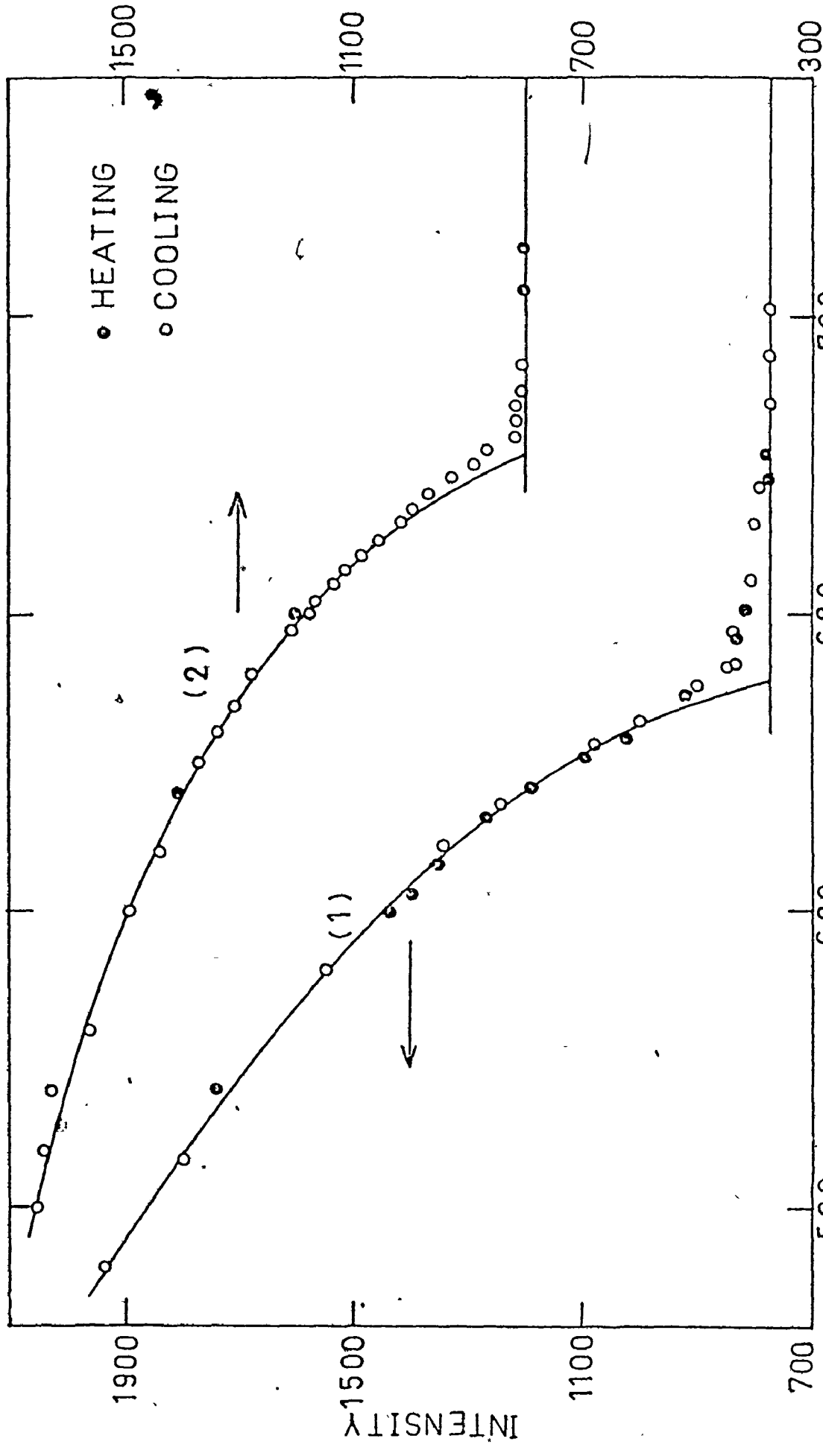

Fig. IV-11. Temperature dependence of the (100) superlattice peak intensity in FeCo 34.6 at.% cobalt (1) and 40.0 at.% cobalt (2).

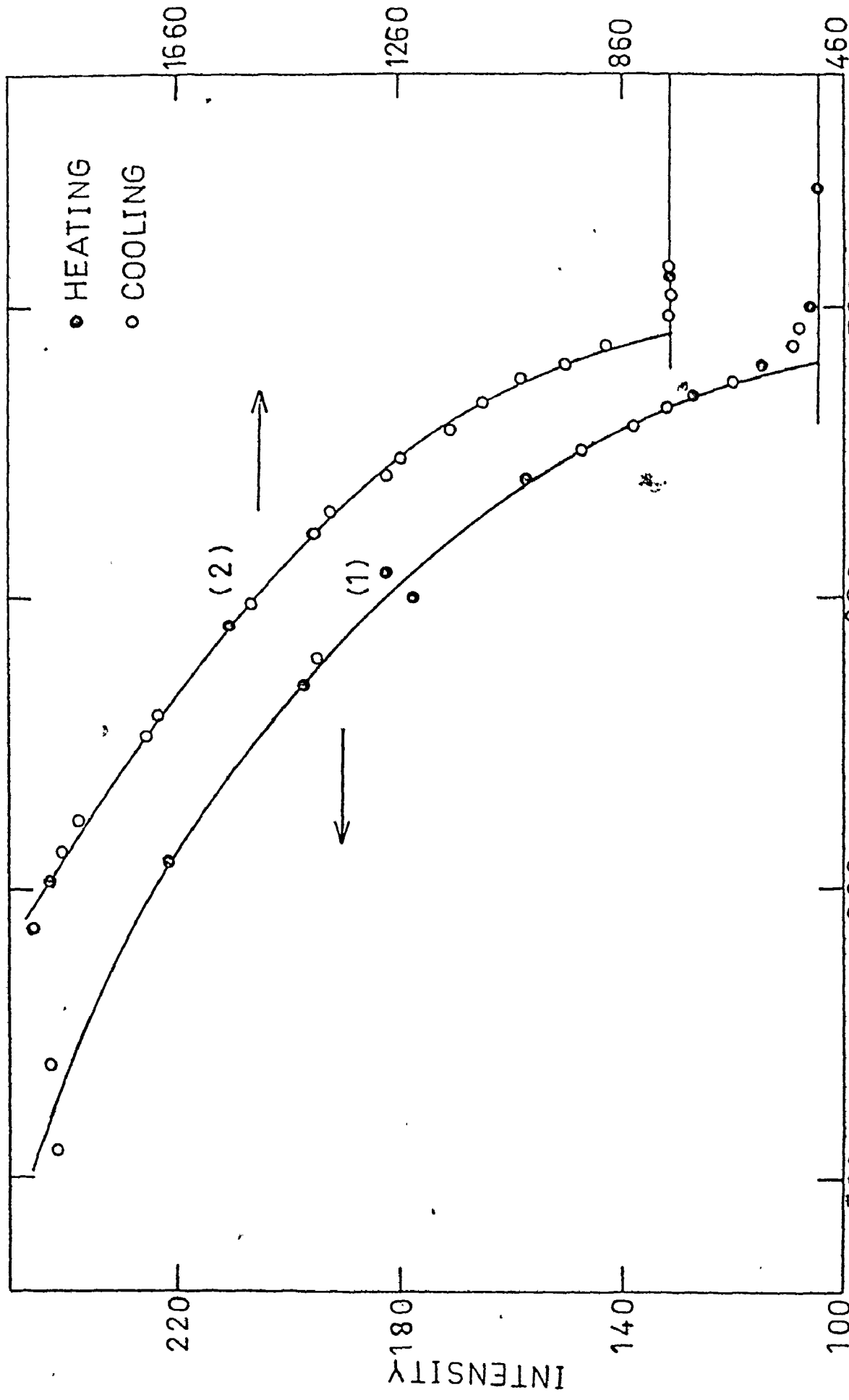

Fig. IV-12. Temperature dependence of the (100) superlattice peak intensity in FeCo 45.1 at.% cobalt (1) and 47.5 at.% cobalt (2).

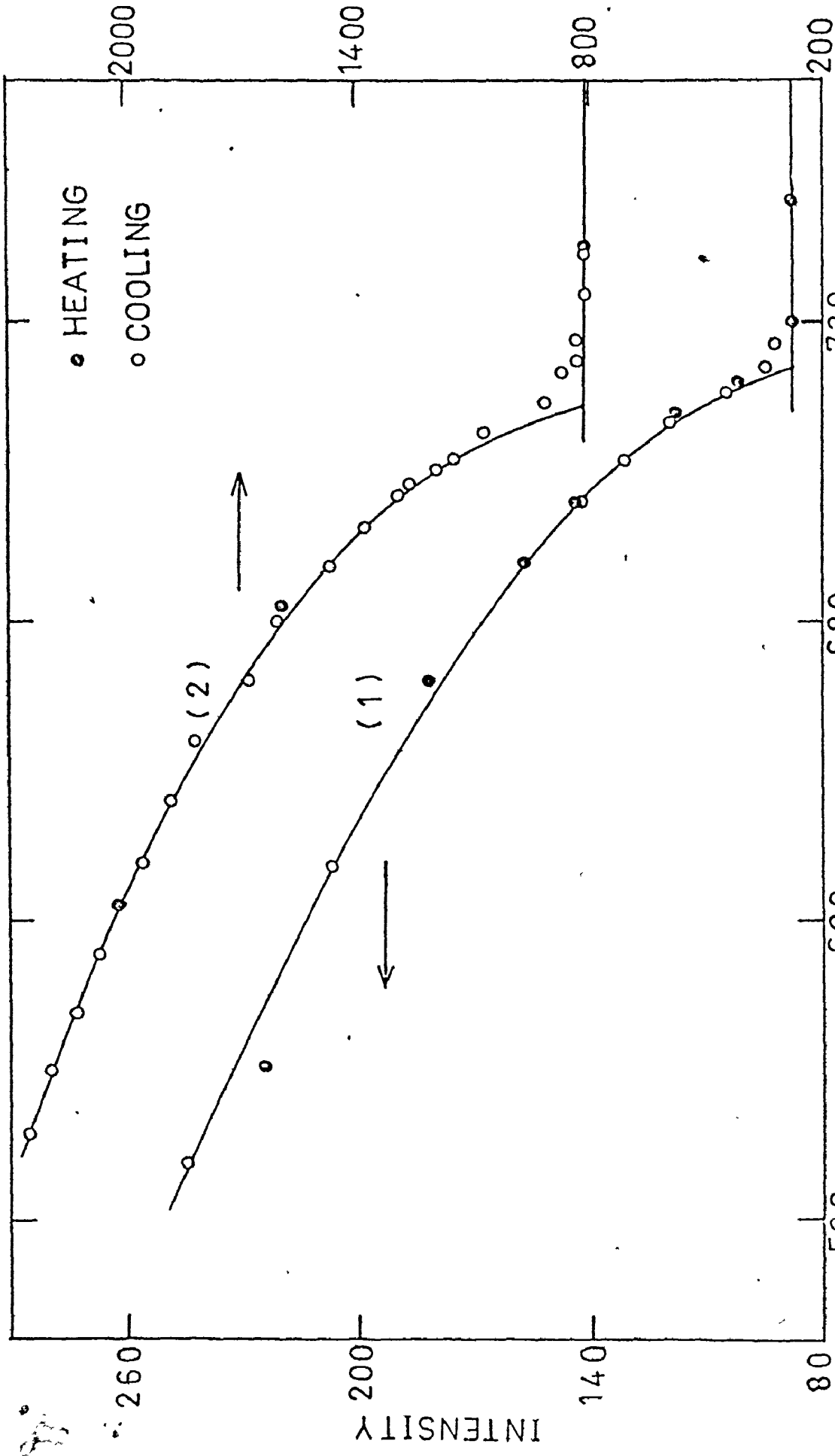

Fig. IV-13. Temperature dependence of the (100) superlattice peak intensity in FeCo superlattice peak intensity in FeCo 49.4 at.% cobalt (1) and 52.2 at.% cobalt (2).

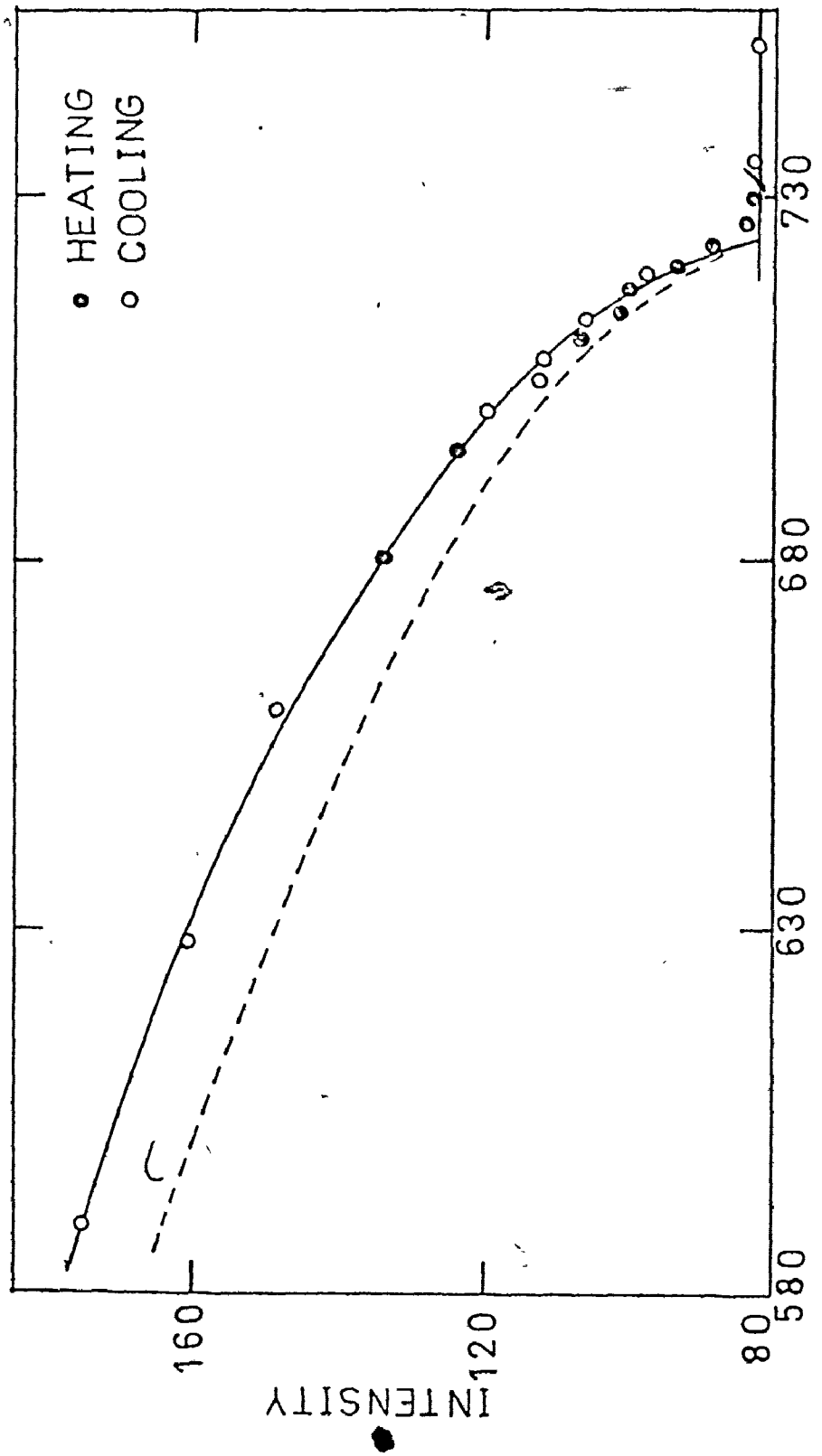

Fig. IV-14. Temperature dependence of the (100) superlattice peak intensity in FeCo 50.2 at.% cobalt. The solid points and open circles are our data. The dashed curve gives the calculated variation of intensity with temperature for a simple Ising model fitted to give the appropriate critical temperature. The solid line shows the calculated curve multiplied by 1.15.

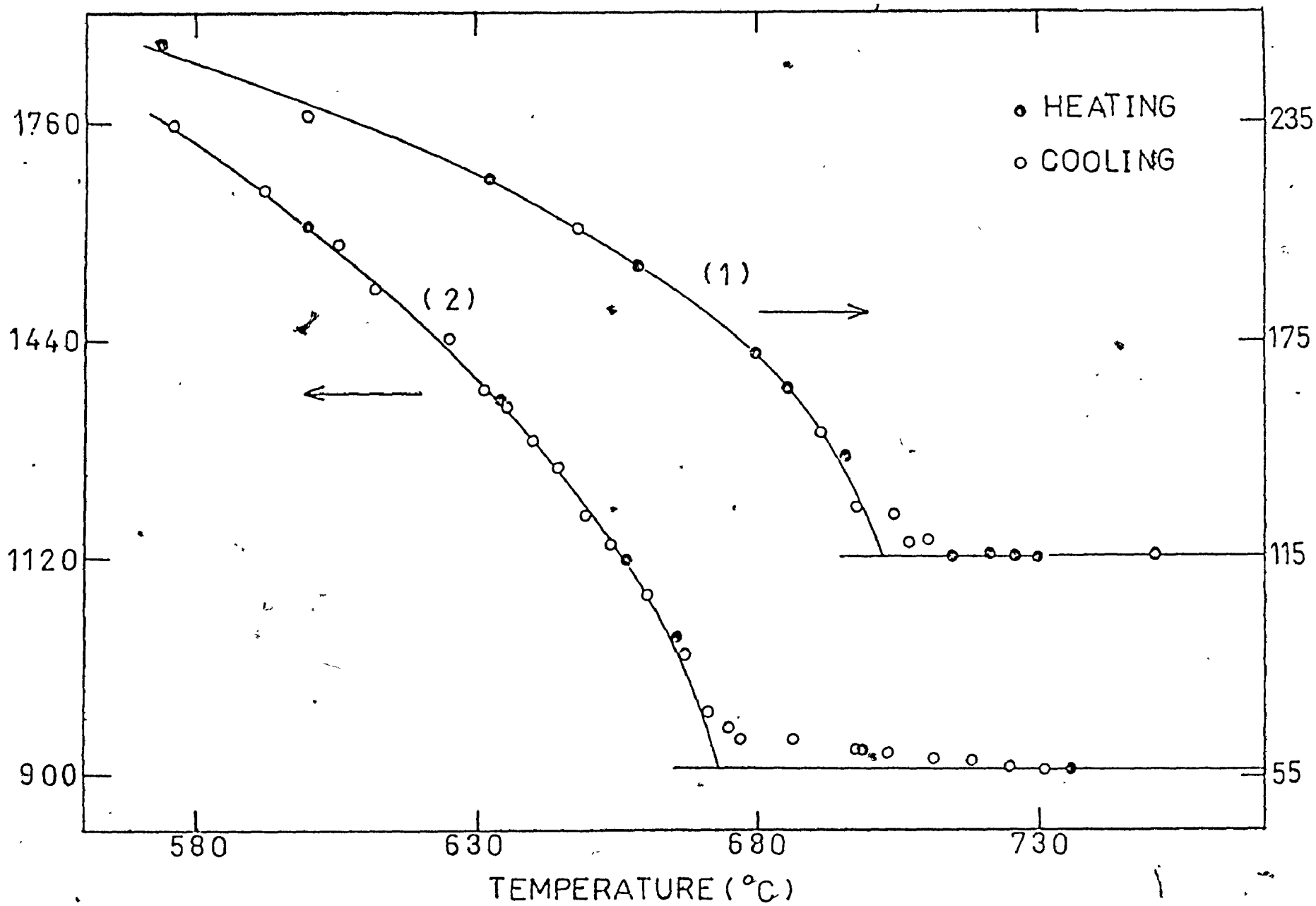

Fig. IV-15. Temperature dependence of the (100) superlattice peak intensity in FeCo 55.1 at.% cobalt (1) and 59.9 at.% cobalt (2).

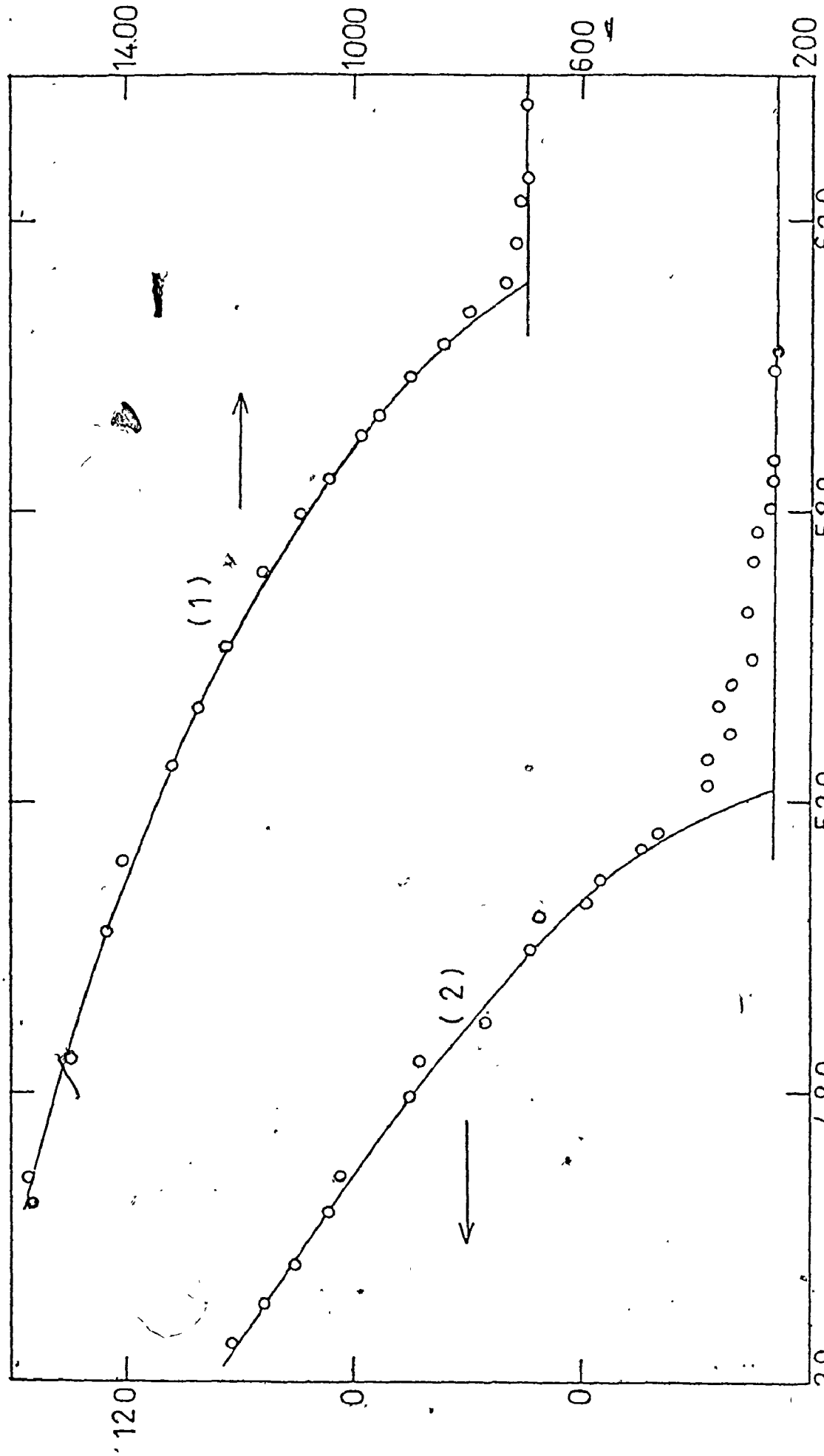

Fig. IV-16. Temperature dependence of the (100) superlattice peak intensity in FeCo 64.7 at.% cobalt (1) and 69.5 at.% cobalt (2).

IV-4. Critical Exponent β

The intensity of the superlattice peak, I, is (eq. II-38)

$$I \propto S^2[(b_{Fe}e^{-W_{Fe}} - b_{Co}e^{-W_{Co}})^2 + q^2(p_{Fe}e^{-W_{Fe}} - p_{Co}e^{-W_{Co}})^2],$$

where b and p are the nuclear and magnetic scattering lengths, q, W and S are respectively the magnetic interaction vector, the Debye-Waller factor, and the order parameter. Since the alloys remain ferromagnetic at temperatures well above the critical ordering temperatures, it is reasonable to neglect the temperature dependence of p over small ranges of temperature just below T_c. The Debye-Waller factors are near to unity - about 0.97 at T = 724°C - for the first superlattice peak, but they may make an important contribution to the intensity and its temperature dependence if the scattering lengths of the constituents are almost the same. This was demonstrated by Chipman and Walker (1971) for the interpretation of x-ray data from CuZn where the x-ray form factors are close to being equal. The effect is less important but still significant for the neutron data in CuZn because the scattering lengths are close to being equal with $(b_{Cu}-b_{Zn})/(b_{Cu}+b_{Zn}) = 0.14$. In FeCo the scattering lengths are much less similar with a corresponding factor of 0.55. This reduces substantially the influence of the Debye-Waller factor. Further, the physical properties of iron and cobalt are more similar than those

of copper and zinc, so one might expect their Debye-Waller factors to be more nearly equal. In view of these points we have neglected the temperature dependence of W near to T_c, so that the intensity of the superlattice line is taken to vary with temperature in the same way as the square of the order parameter near to T_c.

A log-log plot of the intensity versus the reduced temperature $(1-T/T_c)$ for the two most non-stoichiometric alloys, 29.6 and 69.5% cobalt is shown in Figure IV-17. Figure IV-18 shows similar plots for two alloys that are close to the equiatomic composition, 47.5 and 50.2 at. % cobalt. All the plots fit straight lines over a considerable range of reduced temperature. For these plots T_c was selected so as to make the graph most nearly linear at small values of reduced temperature. The fits are good to within about 10 and 15°K of the critical temperature for 29.6 and 69.5% cobalt respectively, while they are good to within about 2°K of the critical temperature for 47.5 and 50.2% cobalt, showing how there is a much larger amount of apparent rounding of T_c for the most non-stoichiometric alloys.

To estimate the errors in T_c and in the slope of the plots, similar plots were made with slightly different values of T_c. For the 50.2% cobalt alloy, plots for T_c = 999, 997, and 995°K gave linear fits to within 6, 2 and 5 K of their assumed critical temperatures with fitted slopes of 0.655, 0.615, and 0.545 respectively. The plot for T_c = 997°K is

shown in Figure IV-18, and those for T_c = 999 and 995°K are shown in Figure IV-19. The error in T_c and in the slope was arbitrarily defined as the difference between the best-fit values and the (interpolated) values where the departures from the linear plot commence twice as far from T_c as for the best fits. For the 50.2% alloy case quoted above this corresponds to an error in the slope of 0.02 on the high-temperature side and 0.04 on the low-temperature side.

The slopes in Figures IV-17 and IV-18 are 0.600, 0.605, 0.586 and 0.615 for the four compositions 29.6, 69.5, 47.5, and 50.2% cobalt respectively. Since the intensity is proportional to S^2, the critical index β is therefore 0.300, 0.303, 0.293 and 0.308 respectively for the four specimens. Values of β for the other specimens were obtained in a similar manner; and these are given in Table IV-5. It is apparent that there is no appreciable composition dependence of β and a weighted mean value of the results gives β = 0.303±0.004 assuming the errors are all independent.

The best theoretical estimate of the critical exponent β for an Ising model is 0.312±0.005 (D. S. Gaunt and M. F. Sykes 1973). As found in other experiments, the experimental values obtained for β are slightly lower than the theoretical estimate. In β brass, Norvell and Als-Nielsen (1970) find β = 0.304±0.007 and in Fe_3Al, Guttman et al (1969) find β = 0.307±0.011. Baker and Essam (1971) have suggested that lattice compressibility

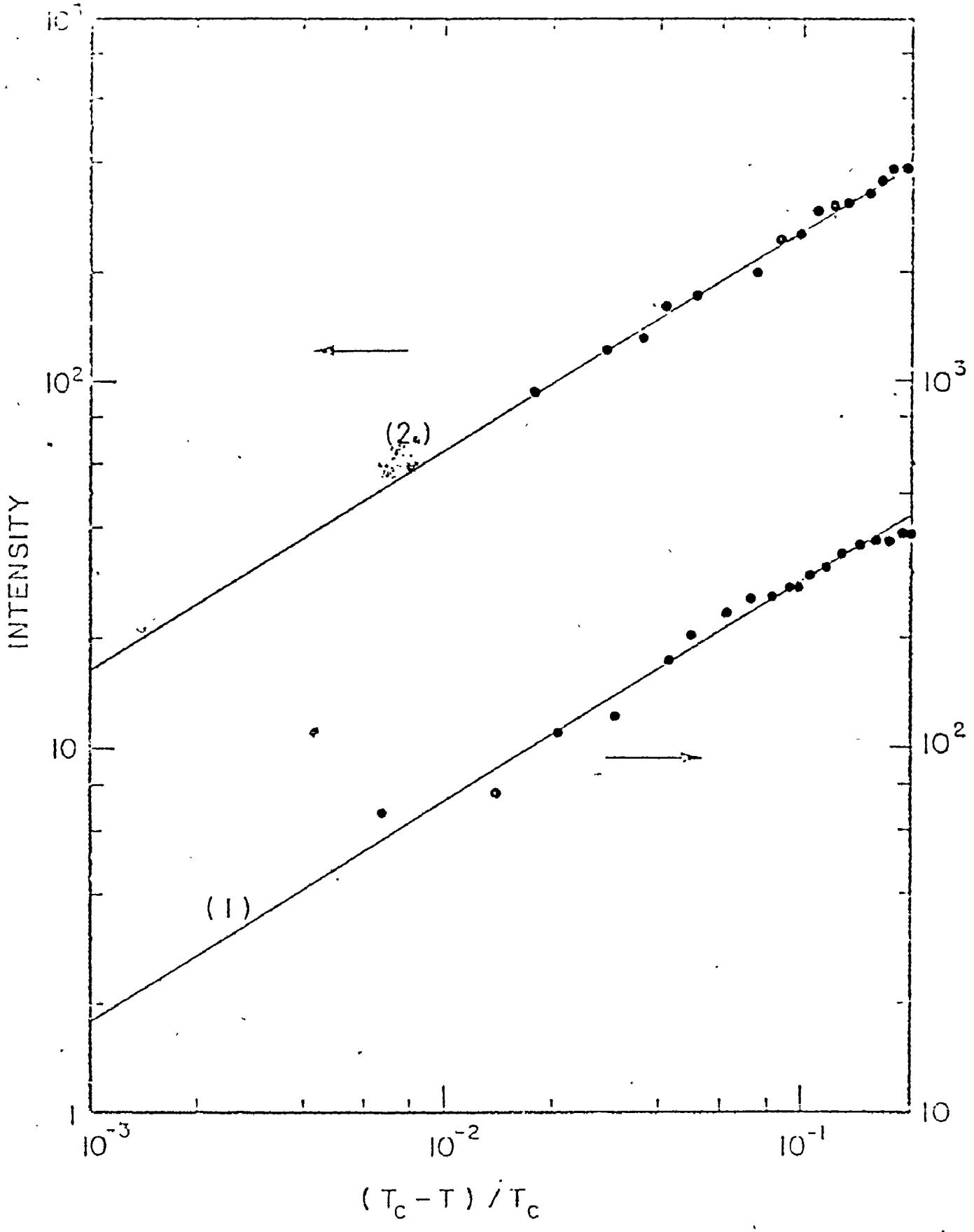

Fig. IV-17. Log-log plot of the (100) superlattice peak intensity against the reduced temperature in 29.6 at.% cobalt (1) and 69.5 at.% cobalt (2). The slopes of the lines are 0.600 0.605

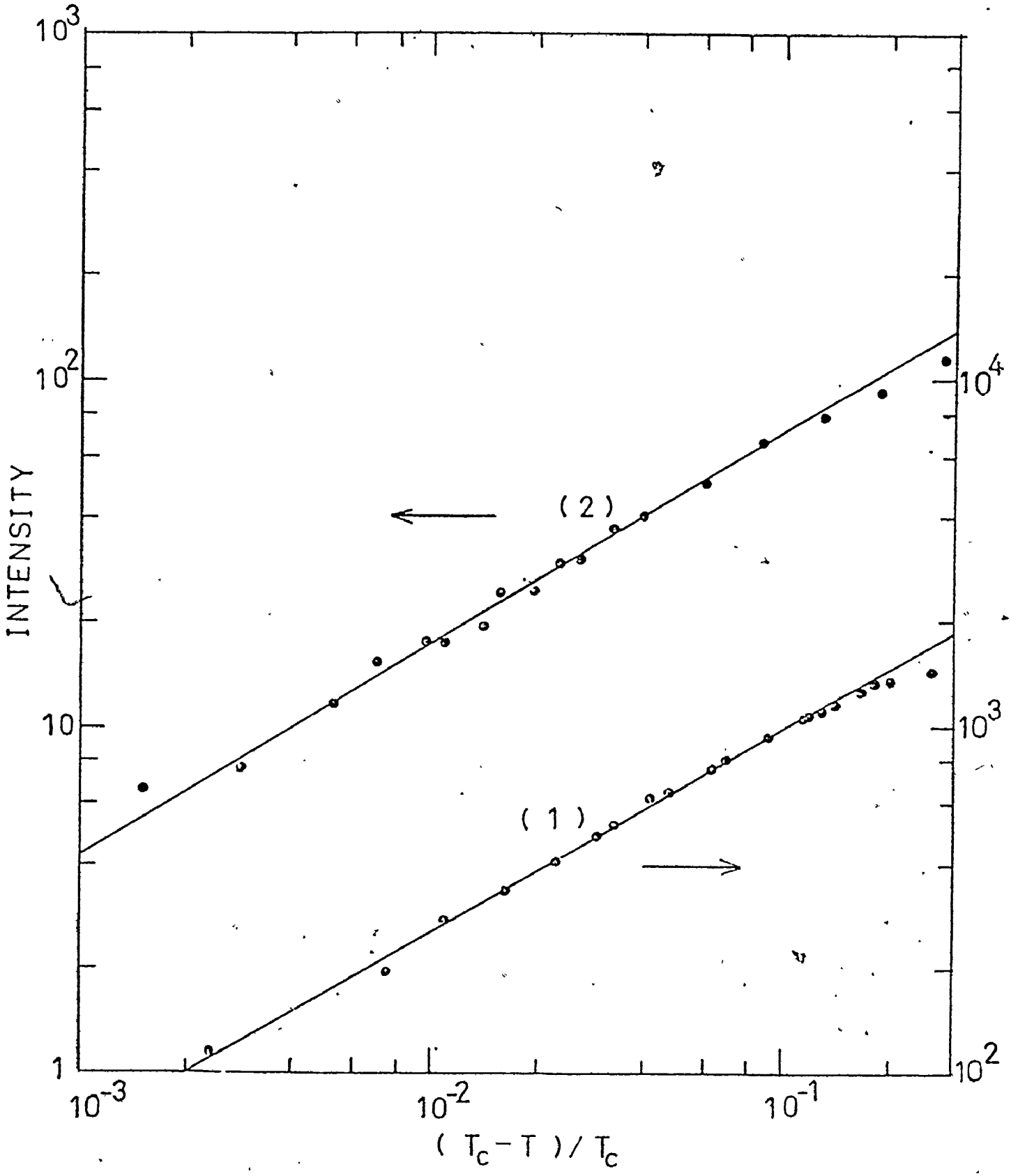

Fig. IV-18. Log-log plot of the (100) superlattice peak intensity against the reduced temperature in 47.5 at.% cobalt (1) and 50.2 at.% cobalt (2). The slopes of the lines are 0.585 and 0.615 respectively.

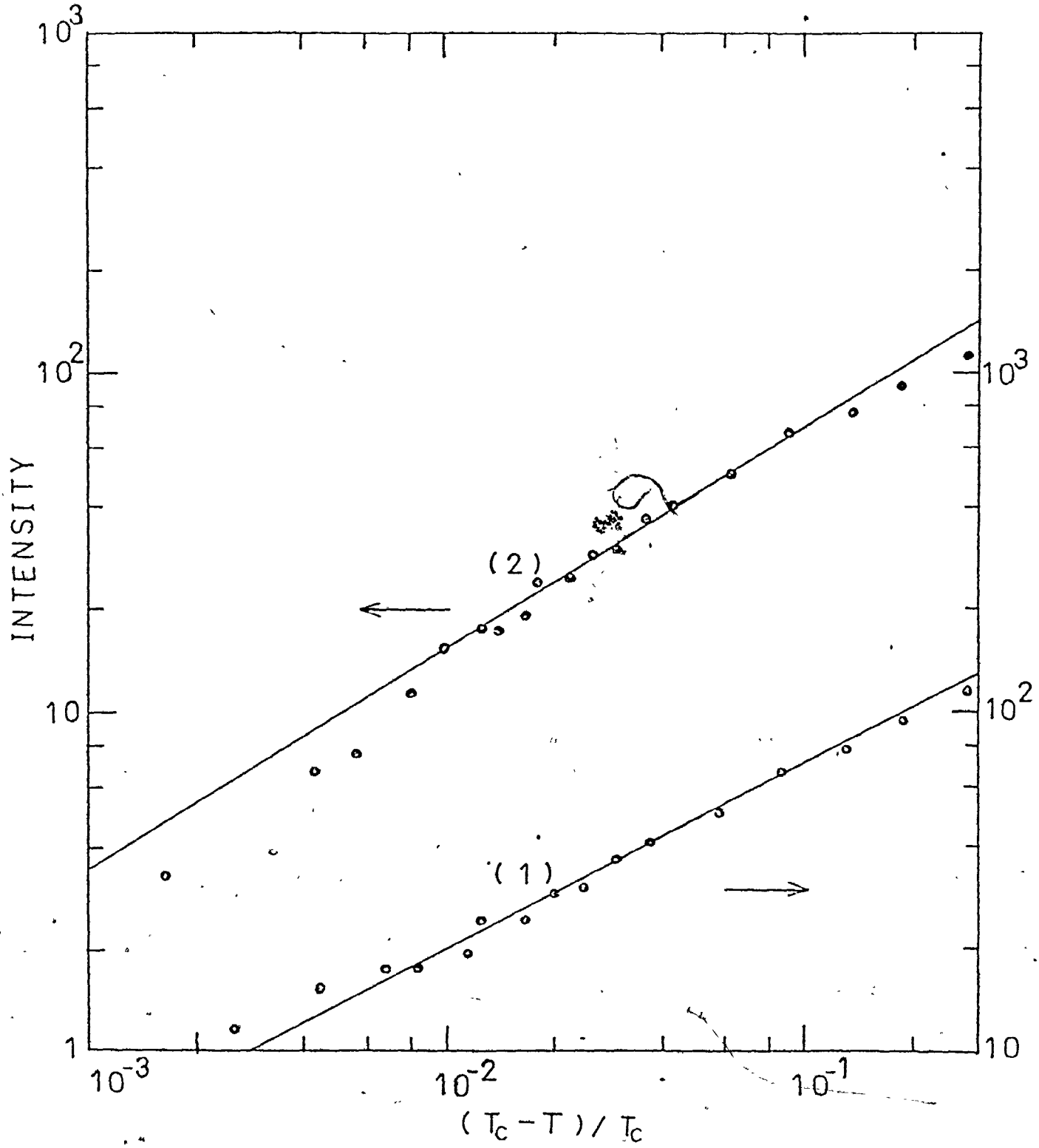

Fig. IV-19. Log-log plot of the (100) superlattice peak intensity against the reduced temperature in 50.2 at.% cobalt for two trial values of T_C. For T_C = 722 (1) the slope of the line is 0.545, and for T_C = 726 (2) the slope of the line is 0.655.

Table IV-5. The order-disorder critical temperature T_c and exponent β as measured in each specimen. The errors in the composition and transition temperature are of the order 0.3 and 2K respectively.

Composition (atomic % Co)	Transition Temperature T_c (°K)	Critical exponent β
29.6	865	0.300±0.014
34.6	942	0.315±0.014
40.0	980	0.300±0.011
45.1	993	0.302±0.011
47.5	998.5	0.293±0.008
49.4	995	0.295±0.010
50.2	997	0.308±0.014
52.2	989	0.300±0.010
55.1	975	0.308±0.007
59.9	946	0.319±0.018
64.7	892	0.321±0.018
69.5	805	0.303±0.018

may reduce the critical index slightly. Within the limits of error our values of β are compatible with experimental results for other alloy systems.

IV-5. Absolute Degree of Order

The absolute value of the degree of order in the iron-cobalt alloys could be calculated by comparing the intensity of the (100) and (111) superlattice peaks with the intensity of the (110) and (200) fundamental peaks provided that the values of b_{Fe}, b_{Co}, p_{Fe}, p_{Co}, W_{Fe} and W_{Co} are known. An attempt was made to determine this value for the equiatomic 50.2% cobalt composition. The values of p_{Fe} and p_{Co} were obtained from the data of Spooner, Lynn and Cable (1972), and the values of b_{Fe} and b_{Co} recommended by the Neutron Diffraction Commission (1969) were used. The Debye-Waller factors are not known; the value for pure iron was used for both iron and cobalt. This can only be an approximate procedure but since $\exp(-W_{Fe})$ is 0.97 at the critical temperature, the errors involved should not be more than about 3 percent.

The dashed line in Figure IV-14 shows the predicted variation of the intensity of the superlattice line with temperature for an Ising model. The calculation used the Padé approximant method described by Essam and Fisher (1963) so as to continue the low temperature series expansion for the order parameter up to T_c. There could be systematic errors in the dashed line of as much as 4% but, after allowing for this, it is

still apparent that our experiments indicate a value of the long range order that is significantly higher than predicted. Chipman and Walker (1971) reported a similar result for β-brass in the temperature range 0.65 T_c to 0.85 T_c; in the temperature range 0.8 T_c to 0.85 T_c where our results overlap theirs, there is substantial agreement between the two sets of measurements,

Uncertainty in our procedure arises because there is some doubt over the value of b_{Co}. We have used the value of 2.50±0.03 F given by Moon (1964), but recently Koester et al (1974) have reported a value of 2.78±0.04 F. Adoption of the higher value would increase the discrepancy between the experimental data and the theoretical predictions and make the absolute degree of order greater than 1.

In the above comparison of the measured and predicted variation of the superlattice peak intensity with temperature, it was assumed that the absolute value of the degree of order in the alloy has been properly calculated from the measured intensities (at room temperature). But the results obtained in the non-equiatomic alloys cast some doubts on this assumption. Unlike in the equiatomic alloy, the values of the degree of order at room temperature (maximum or absolute degree of order) calculated from the superlattice and fundamental peak intensities in non-equiatomic alloys are greater than expected (see section I(a)). Also in non-equiatomic alloys, the measured

and calculated ratios of the integrated intensities at room temperature of the fundamental peaks and of the superlattice peaks are inconsistent; the ratio of the intensity of the (110) peak to that of the (200) peak (both fundamental reflections), and of the (100) peak to that of (111) peak (both superlattice reflections) are inconsistent by about 10%. These could be due to errors in the values of the magnetic scattering lengths p_{Fe} and p_{Co} used, since their values have not been accurately determined for non-equiatomic alloys, or it could be due to some of the assumptions made in calculating the intensities, such as the assumption that there is no preferred orientation in the specimens. Because of these inconsistencies, there may be an uncertainty of about 10% in the above comparison of the measured and predicted variation of the superlattice peak intensity with temperature.

IV-6. Composition Dependence of Transition Temperature

The composition dependence of the transition temperature T_c is shown in Figure IV-20. There is a well defined maximum in T_c and it is quite clear that this occurs at a cobalt concentration which is less than the stoichiometric value of 50%. This shift is surprising as for a first guess one might expect the peak to be at the stoichiometric composition. In fact all models predict a peak at the stoichiometric composition.

A shift in this peak has also been observed in the specific heat data of Asano et al (1967). As shown in Figure IV-21, our results agree with those of Asano et al at compositions

away from the peak of the curve but not around the peak. A more recent specific heat measurement on the 50-50 alloy by Orehotsky et al (1974) gave a critical temperature of 995°K in good agreement with our value of 996±1°K and significantly lower than the value of 1009°K given by Asano et al (1967). We should also note that the specific heat data of Asano et al (1967) indicated an anomaly at around 820 K for equiatomic alloys; our measurements indicate that this effect is not connected with the order-disorder process. Whatever the source may be of the discrepancy in values of T_c, it is interesting to note that the measurements of Asano et al give a shift in the position of the peak by about the same amount as is given by our data.

Since it is assumed in the Ising model that the transition occurs at a constant volume - because the interaction energies can be expected to vary with composition if the lattice parameter changes - a better comparison of the observed composition dependence of T_c with the predictions based on the Ising model could be made by converting the values of the observed T_c's to values corresponding to constant lattice parameters. Yoon and Jeffery (1970) have made such correction by combining their data of the pressure dependence of T_c with the T_c's measured by Asano et al (1967) in the composition range 40-60 atomic percent cobalt. The resulting composition dependence of T_c is only slightly different and the asymmetry about the

stoichiometric composition remains as shown in Figure IV-21.

A calculation of the composition dependence of the critical temperature has been done by Bienenstock and Lewis (1967). They used the low temperature series expansion treatment of the Ising model and the Padé approximant techniques (see section II-5). From a least squares fit of their results for the b.c.c. lattice to an analytic expression that is quadratic in composition they obtain

$$\frac{T_c(c)}{T_c(0.5)} = [1 - 9.007(c-0.5)^2]^{0.739} .$$

T_c and c are respectively the critical temperature and atomic composition. The predicted variation is quite different from the observed variation as shown in Figure IV-22 assuming $T_c(0.5) = 997°K$. Figure IV-22 also shows the predicted variation of Mościński and Rycerz (1977) assuming $T_c(0.5) = 997°K$. They used Monte Carlo techniques to calculate the composition dependence of the critical temperature for a binary b.c.c. system. As shown in the figure, the predicted variation is different from the observed variation and similar to that of Bienenstock and Lewis. Since the observed composition dependnece of T_c is not symmetric about the 50:50 composition but symmetric about 47.5 at.% cobalt, we tried a least squares fitting to

$$[T_c(max)-T_c] = A[c-c(max)]^2$$

where $T_c(max)$ is the maximum T_c (998.5°K), and c(max) is the composition for which it was observed (47.5 at.% cobalt). As shown in Figure IV-23, the fit is only satisfactory for compositions far away from the equiatomic composition; the T_c's for compositions close to 50:50 all lie below the fit. However it is not too bad; much better data than before. The data was then least square fitted to an expression like that of Bienenstock and Lewis, viz.,

$$T_c/T_c(max) = [1-p(c-c(max))^2]^g .$$

The fit is satisfactory as shown in Figure IV-24. The values obtained for $T_c(max)$, c(max), p, and g are 997.4±1.6°K, 0.479±0.003, 10.8±1.6 and 0.31±0.06 respectively. The observed composition dependence of T_c is symmetric about c(max) = 0.479. It is in the spirit of the theory of critical phenomena to propose an exponent such as g to describe the variation of T_c with composition or with the square of the composition just like the critical index β describes the variation of the order parameter with temperature.

It has also been observed in β-brass that the composition dependence of T_c predicted by Bienenstock and Lewis does not agree with experimental results. Yoon and Bienenstock (1968) have shown that the Ising model with a single volume dependent ordering interaction is insufficient to describe the order-disorder transition in β-brass over the composition range in which it is observed.

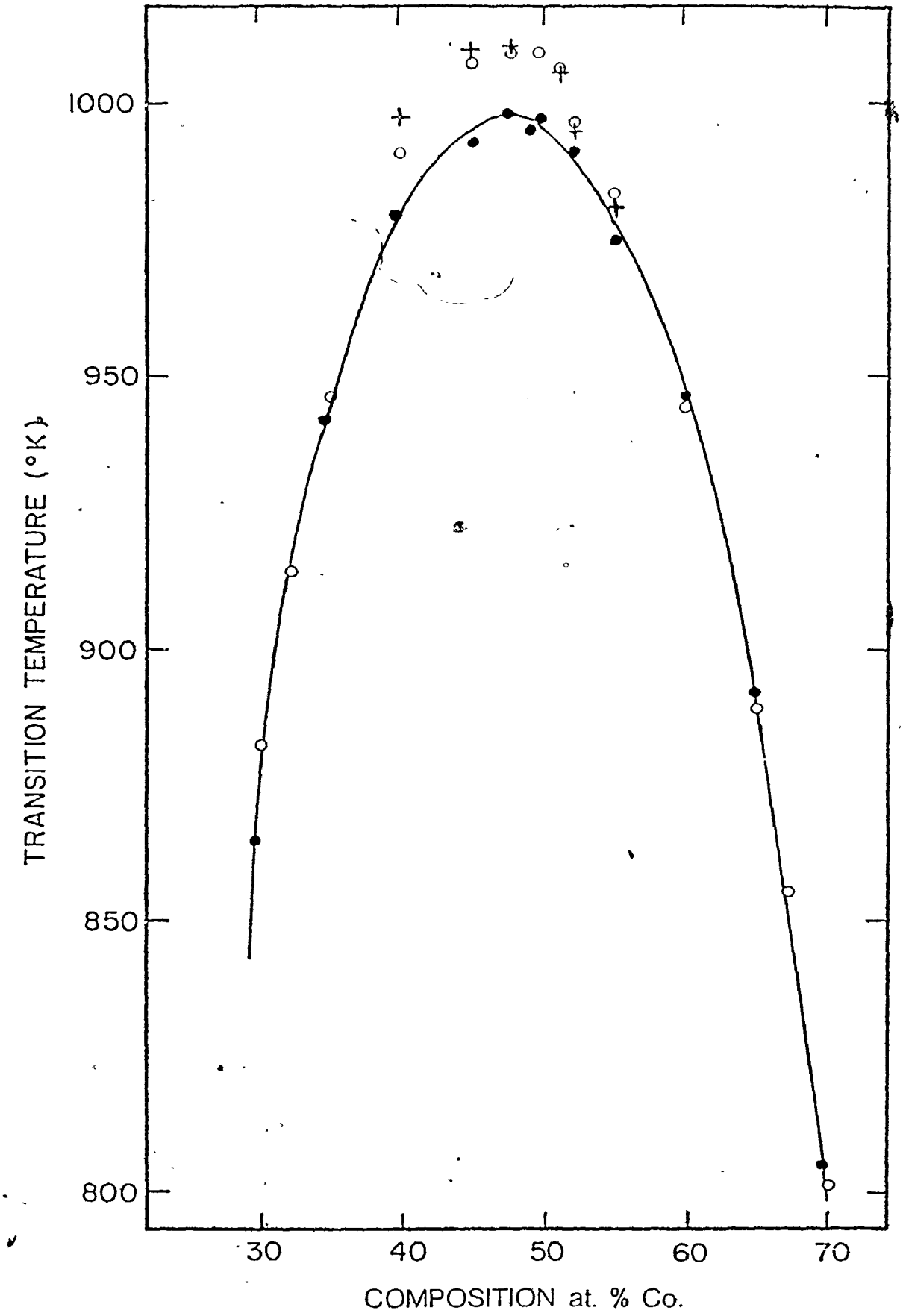

Fig. IV-21. The composition dependence of the transition temperature of FeCo. The solid points are our data. The open circles and plus signs are respectively the data of Asano et al (1967) and Yoon and Jeffrey (1970).

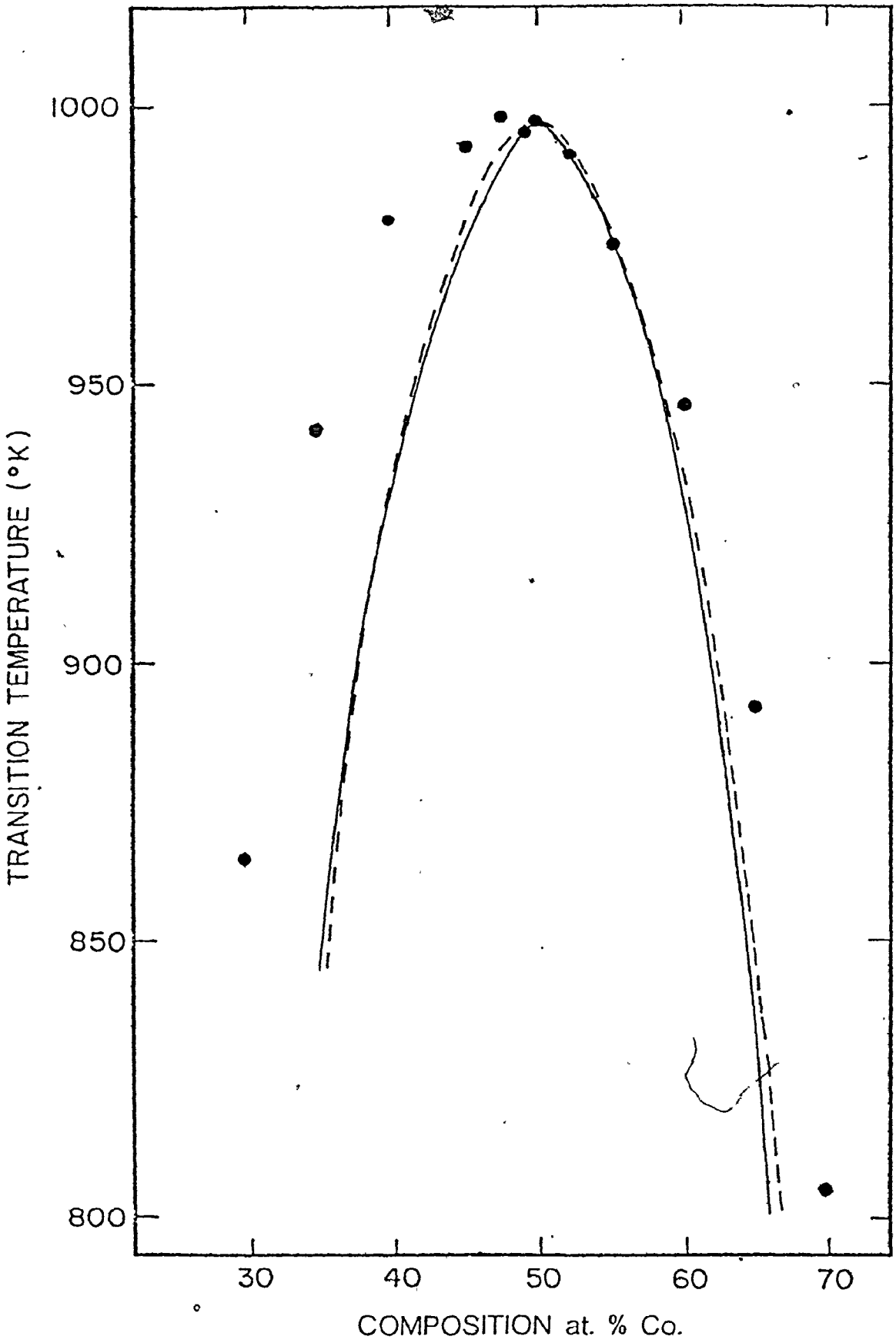

Fig. IV-22. The predicted variation of the transition temperature with composition for a binary b.c.c. system. The dashed curve is the prediction of Bienenstock and Lewis (1967) and the solid curve is that of Mościński and R 1) The are our on

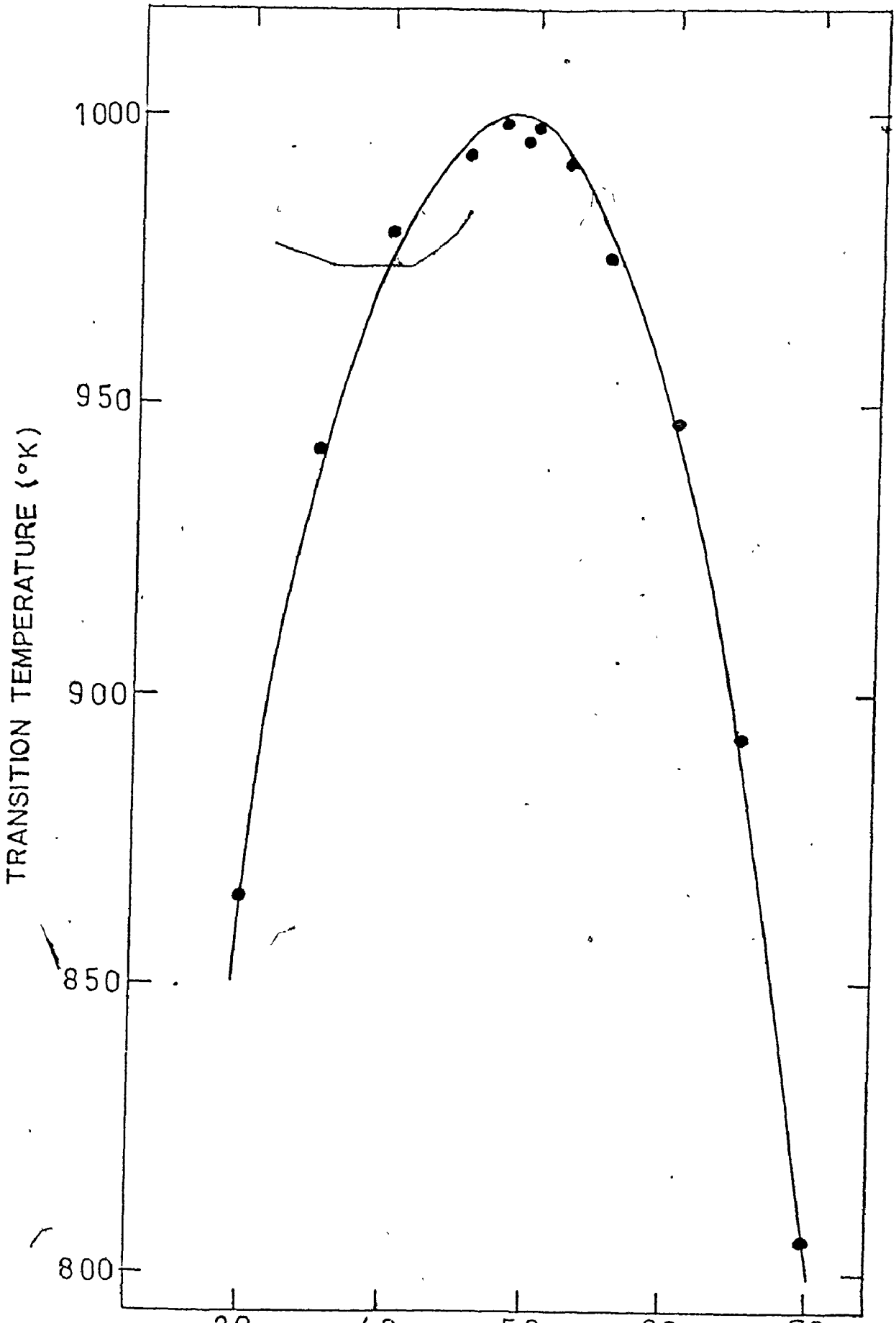
1000
950
900
850
800
TRANSITION TEMPERATURE (°K)
30
40
50
60
70
COMPOSITION at. % Co.

Fig. IV ... of

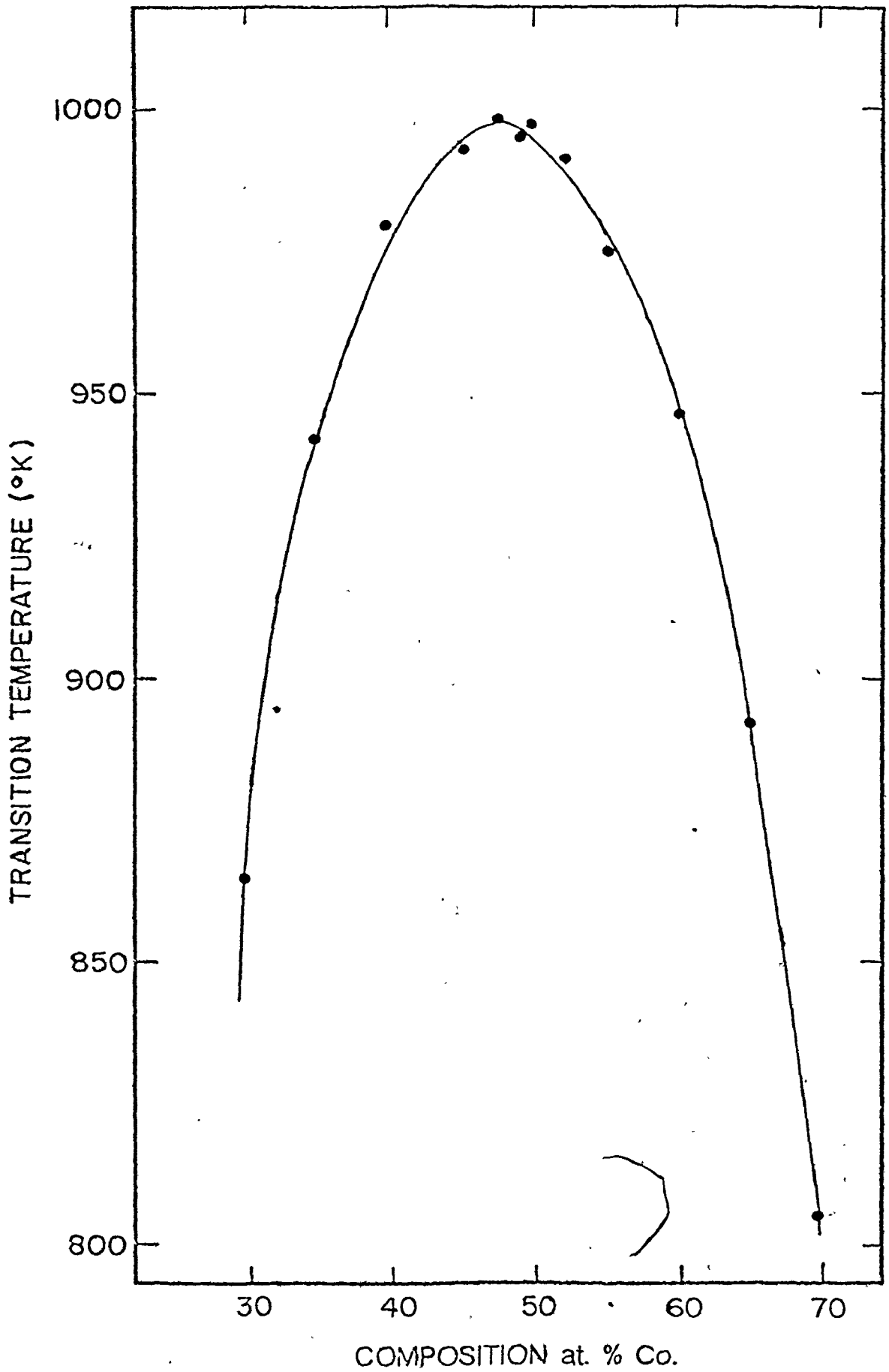

Fig. IV-24. The composition dependence of the transition temperature of FeCo. The solid points are our data and the curve is a non-linear least squares fitting of our a) an ex-

CHAPTER V

SUMMARY AND CONCLUSION

The order-disorder phase transition in iron-cobalt alloys has been investigated by neutron powder diffraction techniques for a composition range from 30 to 70 atomic percent cobalt. There appears to be a critical order-disorder phase transition throughout the composition range.

The alloys exhibit sharp superlattice peaks indicative of long range order. There was no anomaly in the intensity versus temperature curve in any of the samples at about 550°C in contrast to some authors (S. Kaya et al 1943, H. Asano et al 1967) who have reported such an anomaly in the specific heat versus temperature curve. The measurements were repeatable and there was no hysterisis effects in any of the intensity versus temperature curves.

Near T_c, the superlattice peak appeared to change intensity to its new equilibrium value immediately as the temperature was changed. One can therefore conclude that the relaxation time near T_c is smaller than one minute which is the time required for the specimen to come to thermal equilibrium.

The critical index β of the order parameter is, to within error, independent of composition; its weighted mean value is 0.303 ± 0.004. This value is comparable to the value

0.312±0.005 (D. S. Gaunt and M. F. Sykes 1973) predicted for an Ising model, and is comparable to the values 0.304±0.007 (Norvell and Als-Nielsen 1970) and 0.307±0.011 (Guttman et al 1969) obtained for β brass and Fe_3Al respectively.

The plot of the transition temperature against composition shows a peak at 47.9±0.3 atomic percent cobalt; this is unexpected since simple theories predict a peak at the stoichiometric 50 percent composition. As found in β brass, the composition dependence of T_c predicted by Bienenstock and Lewis (1967) on the basis of the Ising model, does not agree with our results. From a least squares fitting of our data to an expression like that of Bienenstock and Lewis, we obtained a value of 0.31±0.06 for the "exponent" g instead of 0.739 predicted by Bienenstock and Lewis.

It should be concluded that the Ising model with nearest neighbour interactions is insufficient to describe the order-disorder transition in iron-cobalt alloys.

CHAPTER VI

MAGNETISM AND SPIN WAVES

Spin waves are the results of microscopic interactions between the electrons of a magnetic system. These interactions in turn depend on the microscopic properties of the system. We shall therefore start the discussion of spin waves with a review of magnetism. In the first part of this chapter, a brief description of the types of magnetism is presented. The second and third parts are about the interactions which are responsible for magnetism, and the fourth part is about the elementary excitations or spin waves in a magnetic system. A detailed discussion of the magnetic structure of triangular antiferromagnets is presented in the fifth part and the properties of $CsMnBr_3$ which is an example of the triangular antiferromagnet is discussed in the last part of the chapter.

VI-1 Types of Magnetism

Magnetic systems are characterized by their response to an external magnetic field H. The response function is called the magnetic susceptibility (χ) and it is given by the ratio of the magnetisation M, which is defined as the average magnetic moment per unit volume to the applied field

($\chi = \partial M/\partial H$). Systems with a negative value of the susceptibility are called diamagnets while those having a positive value of the susceptibility are called paramagnets.

When cooled below a critical temperature, most paramagnets become either ferromagnets or antiferromagnets. Ferromagnets are materials where the magnetic moments at each site line up, on average, in the same direction even in the absence of a magnetic field. These materials are said to exhibit spontaneous magnetisation and the critical temperature is called the Curie temperature T_C. Antiferromagnets also exhibit spontaneous magnetisation at a critical temperature T_N called the Néel temperature but unlike the ferromagnet, the magnetic moments at each site do not line up in the same direction.

There is a variety of different types of magnetic materials within the above broad classification. They differ from one another by the different types of ordering of the magnetic moment of the atoms of the material. In simple antiferromagnets, the moments of the atoms are aligned in such a way that for every atom on a particular site, there is another atom with an antiparallel alignment of its moment. Such antiferromagnets can be considered as consisting of two sets of sublattices each of which has a non-zero mean magnetic moment, but the sum of the mean moments of the sub-

lattices is zero. The ordering in ferrimagnets is similar to that in simple antiferromagnets except for the fact that the magnetic moments on the sublattices are not equal. In triangular antiferromagnets, the magnetic moments of the atoms lie in the same plane but each moment points in a direction 120 degrees away from that of its neighbours. This structure will be discussed in more detail later. Helical and modulated structures have more complex ordering. Figure (VI-1) shows some different types of magnetic ordering.

VI-2 Exchange and Superexchange Interactions

Exchange interactions are the fundamental basis of ferromagnetism and antiferromagnetism. They are responsible for the correlation between the directions of the magnetic moments or spins of individual atoms and are directly associated with the proximity of the atoms in the crystal. The interaction is a quantum effect arising from indistinguishibility of identical particles. The exchange interaction H_{ex} of a magnetic crystal depends upon the orientation of the spins of its atoms and is written as (Heisenberg 1926, Dirac 1929)

$$H_{ex} = - \sum_{i \neq j} J_{ij}(\underline{r}_i - \underline{r}_j)\underline{S}_i \cdot \underline{S}_j \qquad (VI-1)$$

where S_i is the spin of atom i located at position vector r_i, and $J_{ij}(\underline{r}_i - \underline{r}_j)$ is the exchange integral between atoms i and j. This integral depends upon the distance between atoms i and j, usually falling off rapidly with increasing distance so that it is often sufficient to consider only nearest neigh-

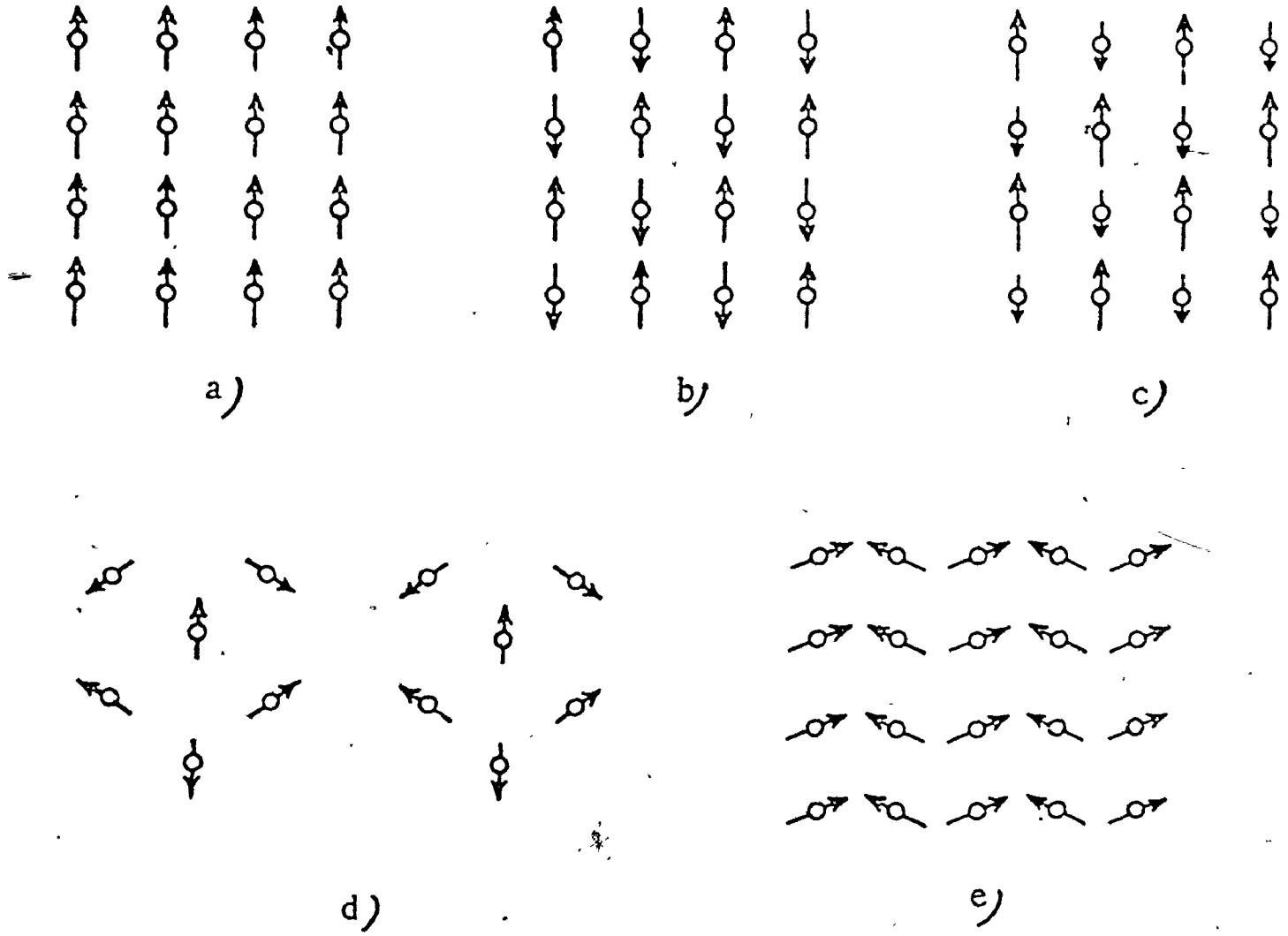

Fig. VI-1. Some different types of ordering in magnetic substances. (a) ferromagnetic, (b) antiferromagnetic, (c) ferrimagnetic, (d) triangular, and (e) weakly ferromagnetic.

bour exchange interactions in calculating the exchange energy of the crystal. If the exchange integral is positive, then the lowest energy state is that in which the spins are parallel, or ferromagnetic. But if the integral is negative, the lowest state of the interaction is that in which the spins are antiparallel or antiferromagnetic (Néel 1932).

The exchange interaction discussed above is called direct exchange because it is due to the overlap of wave-functions (or electronic charge distributions) of the electrons of neighbouring magnetic atoms. But in some materials that become antiferromagnetic at low temperatures such as MnO, the magnetic atoms are separated by one or more diamagnetic groups. Since it is believed that the exchange integral falls off rapidly with distance, the effect of direct exchange should be insignificant in such materials. The interaction responsible for magnetic ordering in such materials is called super-exchange. It is due to the fact that the magnetic cations have wave functions which are strongly admixed with anion wave functions due to covalent bonding. This mixing makes it possible for cations to couple indirectly (Kramers 1934). A more detailed explanation of super-exchange was put forward by Anderson (1959). His approach was to first construct the wave functions of magnetic ions surrounded by various diamagnetic anions, exclusive of the exchange effects

of the other magnetic ions, and then let the magnetic ions interact. He showed that the admixture of P wave functions into the magnetic wave function is the primary mechanism for superexchange. Thus covalent binding effects are responsible for superexchange in magnetic crystals.

VI-3 Anisotropic Interaction

The exchange interaction given by the Hamiltonian in eq. (VI-1) is isotropic. But in addition to this interaction, there may be anisotropic interactions present although they are often much less important compared with the isotropic interaction. These arise mainly from magnetic dipole-dipole interaction, spin-orbit coupling, and various crystalline fields. The effect of anisotropy on the magnetic structure is such as to orient the aligned moments along some crystallographic directions often called easy axes.

The type of anisotropy to be added to eq. (VI-1) depends on the properties of the magnetic system such as its magnetic structure and the electronic structure of the magnetic atom. For materials such as $CsMnBr_3$ where the magnetic moment arises from electronic spin and there is no net orbital angular momentum, the largest anisotropy term to be added to the Hamiltonian is the dipolar term H_{d-d} given by (White 1970)

$$H_{d-d} = \sum_{ij} D_{ij}[(\underline{S}_i \cdot \underline{S}_j) - 3(\underline{S}_i \cdot \underline{r}_{ij})(\underline{S}_j \cdot \underline{r}_{ij})/\underline{r}_{ij}^2] \quad \text{(VI-2)}$$

where

$$D_{ij} = g^2\mu_B^2/(2r_{ij}^3) \quad \text{and} \quad \underline{r}_{ij} = \underline{r}_j - \underline{r}_i \ .$$

The most important effects of dipolar couplings are long range. Hence it is essential that the summation in eq. (VI-2) be unrestricted rather than confined to nearest neighbours as is the case for the isotropic interaction (VI-1).

VI-4 Spin Waves

Spin waves are oscillations in the relative orientations of spins on a lattice. They are similar to the elementary excitations in an elastic solid. In an elastic solid we know that if any of its atoms is displaced from the equilibrium position, it oscillates with the normal modes of the crystal, and phonons are the quantization of these modes of vibration. Spin waves are the analogous normal modes for a magnetic material. They constitute a precession about the mean direction and their quantization leads to magnons.

The concept of spin waves was first introduced by Bloch (1930). To understand the origin of spin waves we can consider a ferromagnet at T=0. All the atomic magnetic moments then have the same direction which corresponds to minimum energy of the ferromagnet. If we deflect the magnetic moment of a particular atom and let go, the change of direction will not remain localized in the original atom, but owing to the presence of the exchange interaction, it will be propagated through the crystal in the form of waves. Spin waves can

propagate both in ferromagnets and in antiferromagnets.

Spin waves are characterized by a definite dependence of the frequency or energy (E) on the wave vector ($\underline{q}$). This dependence is called a 'dispersion relation'. The dispersion curves have always as many branches as different magnetic ions (sublattices) in the unit cell, though degenerate branches may occur in some cases. There is always an 'acoustical branch' whose energy goes to zero at $\underline{q} = 0$ when there is no anisotropy, the dispersion law being quadratic for ferro and ferrimagnets, and linear for antiferromagnets at small $\underline{q}$. The existence of a gap at $\underline{q} = 0$ is a consequence of anisotropy, so the study of the small $\underline{q}$-value region provides information about anisotropy. The presence of anisotropy also results in the removal of the degeneracy of the magnon branches in an antiferromagnet.

In calculating thermodynamic properties of a magnetic system such as the spontaneous magnetisation and the transition temperature, one needs to know the magnitude and sign of the exchange integral. This integral can not be calculated with any accuracy from first principles, but it could be determined accurately by comparing the predicted dispersion relations to the measured dispersion relation. One way of calculating the dispersion relation is to treat the spin as localized at lattice sites and solve the Hamiltonian given in eq. (VI-1) with the appropriate anisotropy term added. This

approach is suitable for insulating systems in which electrons may be considered as localized and it will be used in Chapter VII for calculating the dispersion relation in $CsMnBr_3$.

In solving the Hamiltonian (VI-1), we have to separate out the quantization axes because the fluctuations or oscillations in the spins leading to spin waves will take place relative to the corresponding quantization axes. In a simple ferromagnetic crystal, with the atoms occupying equivalent positions, there is only one magnetic sublattice and a single quantization axis. In crystals with a finite number of sublattices, the number of quantization axes should be no larger than the number of sublattices. In some cases, for example in helicoidal structures, the number of quantization axes may become infinite, since each spin may have a different orientation at each point of the crystal. Hence, in general, for each point occupied by a magnetic atom, we should introduce an individual axis of quantization directed along the average spin position, and with each point associate a local coordinate system so that the z-axis in this system coincides with the equilibrium spin direction at this point every time.

A more detailed discussion of magnetism and spin waves can be found in the books "Magnetic neutron diffraction" by Izyumov (1970), "Spin Waves" by Akhiezer, Bar'yakhtar and Peletminskii (1968), "Elements of theoretical magnetism"

by Krupicka and Sternsberk (1968), and "The theory of magnetism" by Mattis (1965), and in the reviews by Hennion (1972), and Keffer (1966).

VI-5 The Triangular Antiferromagnet

Triangular antiferromagnets have a simple hexagonal lattice array of magnetic atoms. The magnetic moments of the atoms in a plane are coplanar but the plane of the moments is not necessarily the same as the plane of the atoms. Each moment points in a direction 120 degrees away from that of its neighbours so that the moment directions form an equiangular triangle. There is a simple antiferromagnetic coupling between atoms on adjacent planes so that the magnetic moment of an atom in a plane points in a direction 180 degrees from that of its nearest neighbour on the adjacent plane as shown in Figure (VI-2).

The lattice vector of the unit cell that gives a stable triangular arrangement of magnetic moments was calculated by using the technique of Lyons and Kaplan (1960) for finding the low temperature structure of a Heisenberg system. Lyons and Kaplan showed that the low temperature structure has reciprocal lattice points at the minima of the Fourier transform of the exchange integral J(r). In the calculation we assumed antiferromagnetic coupling between neighbouring atoms and we also assumed that the exchange integral for interaction between nearest neighbour atoms which are on different

planes is antiferromagnetic. The magnitude of the exchange integral for interaction between an atom and a more distant neighbour was assumed to be much smaller than that for interaction between the atom and its nearest neighbour. With the antiferromagnetic interactions extended to fifth neighbours and assumed to fall off with increasing distance, the technique of Lyons and Kaplan showed that the same cell is stable for two neighbour interactions; this is the cell that gives rise to the triangular structure (Figure VI-2). Each of the six sublattices within the cell has a different quantization axis so that there are six quantization axes altogether. The cell naturally divides into two planes perpendicular to the c-axis with three sublattices per plane. A classical calculation of the energy of the cell shows that the equiangular triangular structure is stable for the Heisenberg Hamiltonian (eq. VI-1).

Anisotropic interactions determine the direction of the magnetic moments of the atoms with respect to crystal axes. They may also distort the triangular arrangements of magnetic moments in the plane of the moments so that the moment of an atom is no longer directed at precisely 120 degrees away from that of its neighbours but at a slightly different angle.

Single ion anisotropy of the form $-AS_z^2$, where A is a positive constant and S_z is the component of the spin along the crystal c-axis, has the effect of orienting the magnetic moment

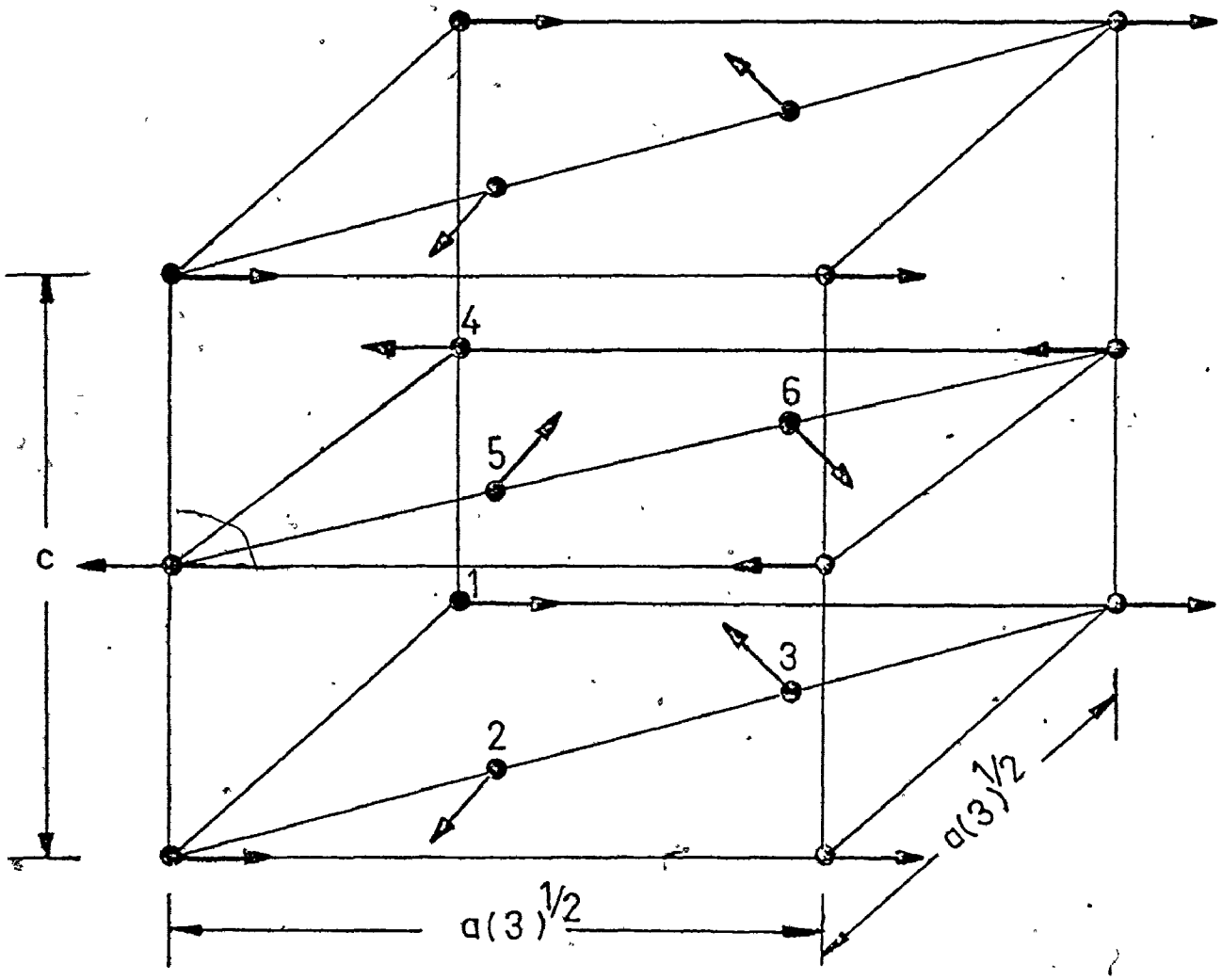

a = 7·56Å

c = 6·45Å

Fig. VI-2 Magnetic structure of $CsMnBr_3$.

into a plane which is perpendicular to that of the atoms. It also modifies the triangular structure in such a way that the moment directions no longer form an equiangular triangle, but form an isosceles triangle. Such effects have been observed in the triangular antiferromagnets $RbNiCl_3$ (Yelon and Cox 1972) and $CsNiCl_3$ (Sorgen, Cohen and Makovsky 1974).

The energy of a triangular antiferromagnet in which dipole-dipole interactions are the main source of anisotropy, is a minimum when the dipolar interactions confine the moments to the plane of the atoms. As we shall show in Chapter VII, the spin wave theory confirms this result and the theory also shows that the dipole-dipole interactions do not distort the equiangular triangular structure formed by the moment directions.

VI-6 Crystal and Magnetic Structure of $CsMnBr_3$

Cesium manganese tribromide is isomorphous with cesium nickel trichloride and is hexagonal with space group $P6_3/mmc$ (Goodyear and Kennedy 1972, Achiwa 1969). The lattice parameters of the hexagonal cell are a = 7.56 Å and c = 6.45 Å. A unit cell contains two cesium ions at $\frac{1}{3}\ \frac{2}{3}\ \frac{3}{4}$ and $\frac{2}{3}\ \frac{1}{3}\ \frac{1}{4}$, two manganese ions at 0 0 0 and 0 0 $\frac{1}{2}$, and six bromine ions at $x\ 2x\ \frac{1}{4}$, $-2x\ -x\ \frac{1}{4}$, $-x\ -2x\ \frac{3}{4}$, $2x\ x\ \frac{3}{4}$, $x\ -x\ \frac{1}{4}$, $-x\ x\ \frac{3}{4}$ where x = 0.1625. In the structure Cs ions and Br ions form a hexagonal closed-packed lattice and Mn ions occupy the octahedral interstices surrounded by six Br ions as shown in Figure (VI-3). There are chains of $MnBr_6$ octahedra along the c-axis with an

intrachain separation (3.2 Å).

$CsMnBr_3$ is chemically an insulating transition metal compound. Only the manganese atoms are magnetic and there is a coupling between the magnetic moments which leads to magnetic ordering at low temperatures. Neutron diffraction measurements have shown that there is a three dimensional ordering at $T_N = 8.3°K$ (Eibschütz et.al. 1972). Below T_N the Mn^{2+} magnetic moments are coupled antiferromagnetically along the chains but lie in the basal plane where they form a triangular array (section VI-1). There are six magnetic atoms and six sublattices in the magnetic unit cell, and the volume of the magnetic unit cell is three times larger than that of the chemical cell. Figure (VI-2) shows the magnetic unit cell of $CsMnBr_3$. In the basal plane, each Mn atom has six nearest neighbour Mn atoms which have moments along directions 120 degrees away from that of its own and which can be grouped into two sets; each set of three atoms are ferromagnetically aligned to each other in a direction 120 degrees away from that of the other set. Figure (VI-4) shows the equilibrium spin configuration in the basal plane of the crystal.

Two kinds of exchange interactions should be considered in this compound. One is the exchange interaction between the nearest neighbouring magnetic ions along the c-axis, and the other is the super-exchange interaction through the Mn-Br-Br-Mn path between linear chains (section VI-1). Since

the interchain separation is more than double the intrachain separation, the value of the exchange integral along the c-axis should be much greater than that in the basal plane.

The aim of this project is to develop spin wave theory in triangular antiferromagnets and to calculate numerically the spin wave dispersion relations in the triangular antiferromagnet $CsMnBr_3$. The spin wave theory is developed in Chapter VII, and the numerical calculation of the dispersion relations in $CsMnBr_3$ is presented in Chapter VIII.

We attempted to measure the spin wave dispersion relation in $CsMnBr_3$ but we ran into problems with the specimen. The specimen had a cylindrical shape and it was sealed in a glass container because it was hygroscopic. The presence of the glass container precluded alignment of the sample with x-rays. Instead we had to align the sample with a neutron beam.

During the early part of the alignment procedure, we discovered that the sample was not a single crystal but that it contained two crystals of about equal size which were misoriented from one another by about five degrees. The two crystals were present throughout the length of the sample and it was not possible to mask or remove one of them from the neutron beam. We thought it would be possible to make measurements on one of the crystals without interference from the other and so we aligned one of the crystals. The sample was placed inside a cryostat and we started to cool the sample

down to liquid helium temperature in order to observe the magnetic peaks and make measurements of the spin wave dispersion relations. Just below liquid nitrogen temperature, the sample shattered and, as a result, we could not continue with the experiment. Attempts to grow other crystals have not been successful as the samples shattered when cooled to room temperature.

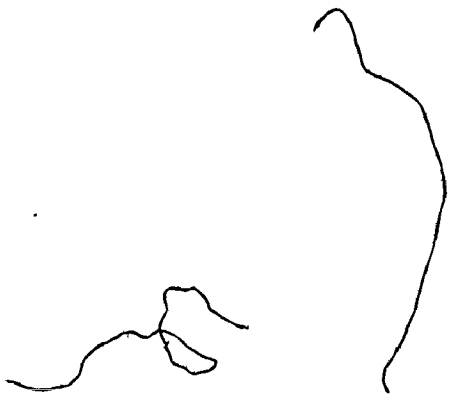

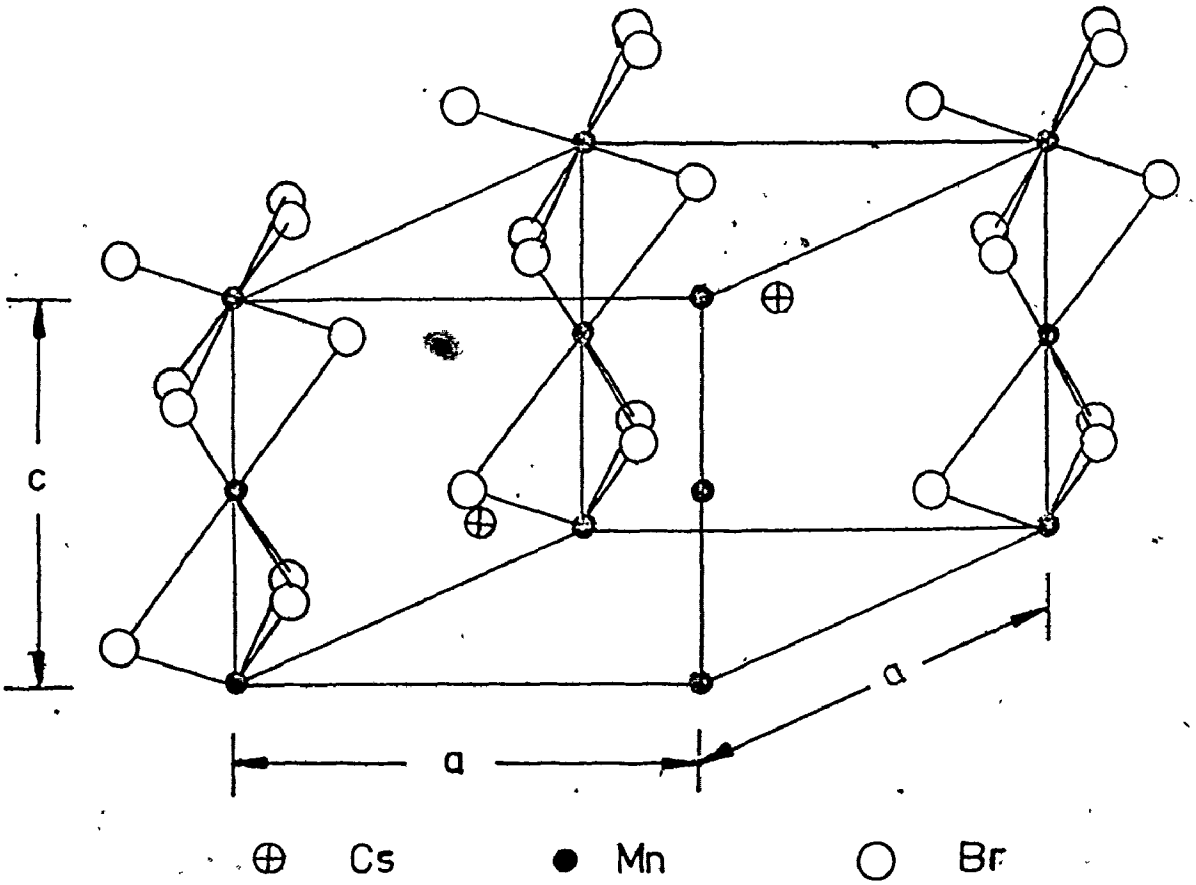

$a = 7{\cdot}56\,\mathring{A}$

$c = 6{\cdot}45\,\mathring{A}$

Fig. VI-3. Crystal structure of $CsMnBr_3$.

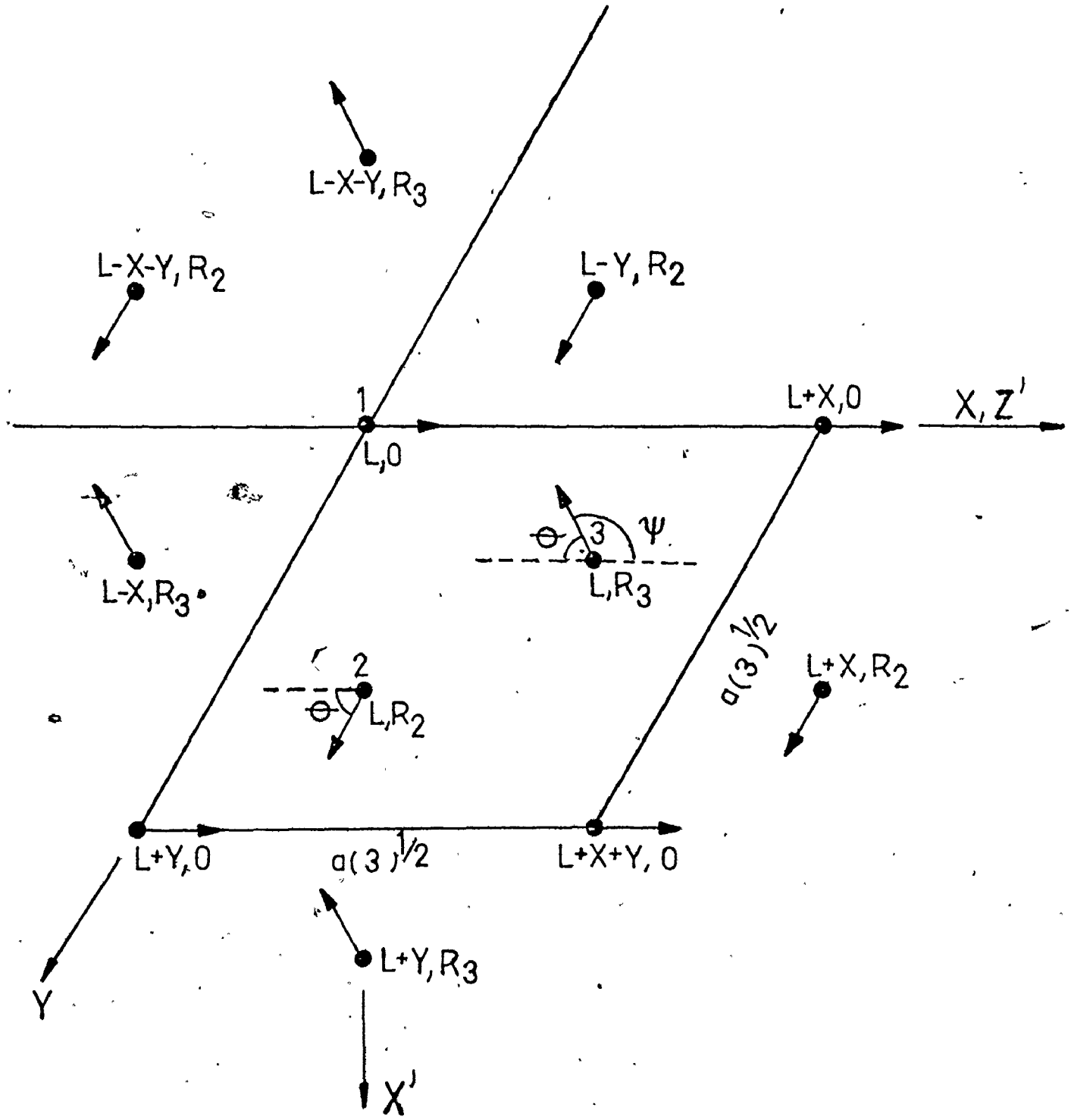

Fig. VI-4. configuration in the basal plane

CHAPTER VII

SPIN WAVE THEORY

The spectrum of all possible values of the energy of a quantum-mechanical system is determined by the eigenvalues of the Hamiltonian. For a magnetic crystal the magnetic moments of the atoms are coupled by the exchange interaction. The Hamiltonian of the magnetic system can be expressed in terms of spin operators, and at the moment there is no method of finding all its eigenvalues. However, for systems close to saturation, when only a small number of atomic spins deviates from complete order such as occurs at temperatures much lower than the magnetic ordering temperature, we may find the approximate energy spectrum of a magnetic crystal. States of a magnetic system corresponding to these levels are called spin waves.

In this chapter we shall first discuss spin waves in a simple antiferromagnet described only by the exchange Hamiltonian. The same basic concepts are used to develop the much more complicated theory of spin waves in triangular antiferromagnets. The theory for the triangular antiferromagnets is extended to the case where both exchange and dipole-dipole interactions are present.

VII-1 Spin Waves in a Simple Antiferromagnetic System

Consider a simple antiferromagnetic system having a magnetic Bravais lattice that can be divided into two sublattices L and P. The spins in one sublattice are all parallel to one another and antiparallel to the spins on the other sublattice (section VI-1). Let $\underline{L}$ and $\underline{P}$ be the vectors to an atom on the L and P sublattices from the origin and let $\underline{s}$ and $\underline{c}$ respectively be the vector joining atoms on the same sublattice and on different sublattices. The exchange constants for the interactions between sites on different sublattices, J_c, must be negative in magnitude for the antiferromagnetic structure to be stable. The exchange constants for interactions between atoms on the same sublattice is denoted by J_s. The Heisenberg exchange Hamiltonian can be written as (eq. VI-1)

$$H_{ex} = - \sum_{\underline{L},\underline{s}}^{N/2} J_s \underline{S}_L \cdot \underline{S}_{L+s} - \sum_{\underline{P}\underline{s}}^{N/2} J_s \underline{S}_P \cdot \underline{S}_{P+s} - 2 \sum_{\underline{L},\underline{c}}^{N/2} J_c \underline{S}_L \cdot \underline{S}_{L+c} \qquad \text{(VII-1)}$$

where N is the number of different magnetic atoms in the unit cell. The first two terms give the interaction within each sublattice while the third term gives the interaction between the two sublattices.

If we define S_x, S_y, and S_z as the three components of the spin operator for some particular atom along orthogonal directions x, y and z with z as the equilibrium direction of the spin, one can write

$$S^2 = (S_x)^2 + (S_y)^2 + (S_z)^2 \qquad \text{(VII-2)}$$

$$\underline{S}_i \cdot \underline{S}_j = S_i{}^x S_j{}^x + S_i{}^y S_j{}^y + S_i{}^z S_j{}^z \qquad \text{(VII-3)}$$

The spin ladder operators S^+ and S^- are defined as

$$S^+ = S_x + iS_y \quad ; \quad S^- = S_x - iS_y \,. \qquad \text{(VII-4)}$$

Using eq. (VII-3) and eq. (VII-4), eq. (VII-1) becomes

$$H_{ex} = - \sum_{\underline{Ls}} J_s [\tfrac{1}{2}(S^+_{\underline{L}} S^-_{\underline{L}+\underline{s}} + S^-_{\underline{L}} S^+_{\underline{L}+\underline{s}}) + S^z_{\underline{L}} S^z_{\underline{L}+\underline{s}}]$$

$$- \sum_{\underline{Ps}} J_s [\tfrac{1}{2}(S^+_{\underline{P}} S^-_{\underline{P}+\underline{s}} + S^-_{\underline{P}} S^+_{\underline{P}+\underline{s}}) + S^z_{\underline{P}} S^z_{\underline{P}+\underline{s}}]$$

$$- 2 \sum_{\underline{Lc}} J_c [\tfrac{1}{2}(S^+_{\underline{L}} S^-_{\underline{L}+\underline{c}} + S^-_{\underline{L}} S^+_{\underline{L}+\underline{c}}) + S^z_{\underline{L}} S^z_{\underline{L}+\underline{c}}] \,. \qquad \text{(VII-5)}$$

The next step is to express the spin operators in terms of boson creation operators a^+ and annihilation operators a, and thus make spin wave particles obey Bose statistics. There are two well known methods of doing this. One method is that of Holstein and Primakoff (1940) and the other method is that of Dyson (1956) and Maleev (1958).

The two methods of transformation are the same in the harmonic approximation (to be discussed later). Since our discussion in this chapter will be confined to the harmonic approximation, we shall follow only the Holstein-Primakoff formalism. In this approach, the spin operators are expressed

in terms of the boson operators as

$$S_j^+ = (2S)^{1/2} f_j a_j$$
$$S_j^- = (2S)^{1/2} a_j^+ f_j \qquad \text{(VII-6)}$$
$$S_j^z = S - a_j^+ a_j = S - n_j \ ;$$

where

$$f_j = \left(1 - \frac{a_j^+ a_j}{2S}\right)^{1/2} = \left(1 - \frac{n_j}{2S}\right)^{1/2}$$

and $n_j = a_j^+ a_j$ is the operator of the number of spin deviations. The boson operators a^+, and a obey the commutation relation

$$[a_i, a_j^+] = \delta_{ij}$$
$$[a_i, a_j] = [a_i^+, a_j^+] = 0 \ . \qquad \text{(VII-7)}$$

As $T \to 0$, that is at very low temperatures, the number of spin deviations is very small compared to the spin of the atom and we can expand the square root in eq. (VII-6) binomially in a power series of $a^+a/2S$ so that

$$f_L = 1 - a_L^+ a_L / 4S + \ldots \approx 1 \ .$$

This is the harmonic or linear approximation for spin waves. With this approximation, eq. (VII-6) becomes

$$S_j^+ = (2S)^{1/2} a_j$$
$$S_j^- = (2S)^{1/2} a_j^+ \qquad \text{(VII-8)}$$
$$S_j^z = S - a_j^+ a_j \, .$$

Writing eq. (VII-8) in terms of the two sublattices in our simple antiferromagnet, we have

$$S_L^z = S - a_L^+ a_L \, ; \quad S_P^z = -S + b_P^+ b_P$$
$$S_L^+ = (2S)^{1/2} a_L \, ; \quad S_P^+ = (2S)^{1/2} b_P^+ \qquad \text{(VII-9)}$$
$$S_L^- = (2S)^{1/2} a_L^+ \, ; \quad S_P^- = (2S)^{1/2} b_P \, .$$

By using eq. (VII-9), the Hamiltonian given by eq. (VII-5) becomes

$$H_{ex} = - \sum_{\underline{L}\underline{s}} J_s [S^2 - S(a_{\underline{L}}^+ a_{\underline{L}} + a_{\underline{L}+\underline{s}}^+ a_{\underline{L}+\underline{s}}) + S(a_{\underline{L}} a_{\underline{L}+\underline{s}}^+ + a_{\underline{L}}^+ a_{\underline{L}+\underline{s}})]$$
$$- \sum_{\underline{R}\underline{s}} J_s [S^2 - S(b_{\underline{P}}^+ b_{\underline{P}} + b_{\underline{P}+\underline{s}}^+ b_{\underline{P}+\underline{s}}) + S(b_{\underline{P}}^+ b_{\underline{P}+\underline{s}}^+ + b_{\underline{P}} b_{\underline{P}+\underline{s}}^+)]$$
$$-2 \sum_{\underline{L}\underline{c}} J_c [-S^2 + S(a_{\underline{L}}^+ a_{\underline{L}} + b_{\underline{L}+\underline{c}}^+ b_{\underline{L}+\underline{c}}) + S(a_{\underline{L}} b_{\underline{L}+\underline{c}} + a_{\underline{L}}^+ a_{\underline{L}+\underline{c}}^+)]$$

(VII-10)

where we have neglected fourth order terms in the expansion to be consistent with the linear approximation.

We now make a transformation from boson operators a_j^+, a_j to spin wave operators a_q, a_q^+ using the relationship,

$$a_{\underline{L}} = \left(\frac{2}{N}\right)^{1/2} \sum_{\underline{q}} e^{i\underline{q}\cdot\underline{L}} a_{\underline{q}}$$
and (VII-11)
$$b_{\underline{P}} = \left(\frac{2}{N}\right)^{1/2} \sum_{\underline{q}} e^{-i\underline{q}\cdot\underline{P}} b_{\underline{q}} \, ,$$

where $\underline{q}$ is the reduced wave vector and is confined to the first Brillouin zone. The spin wave operators obey similar commutation relations to those of the boson operators.

Using eq. (VII-11), eq. (VII-10) becomes

$$H_{ex} = NS^2[J_c(0)-J_s(0)]-2S \sum_{\underline{q}} [(J_c(0)-J_s(0)+J_s(\underline{q}) \times (a^+_{\underline{q}}a_{\underline{q}} + b^+_{b\underline{q}}b_{\underline{q}})] - 2S \sum_{\underline{q}} [J_c(\underline{q})(a_{\underline{q}}b_{\underline{q}} + a^+_{\underline{q}}b^+_{\underline{q}})] \quad \text{(VII-12)}$$

where

$$J_c(\underline{q}) = \sum_{\underline{c}} J_c \exp(i\underline{q}\cdot\underline{c}) \quad \text{(VII-13)}$$

$$J_s(\underline{q}) = \sum_{\underline{s}} J_s \exp(i\underline{q}\cdot\underline{s}) \ .$$

The first term in eq. (VII-12) is constant. It represents energies which don't change as the spins fluctuate. The second term is diagonal and represents the interactions within the individual sublattices and the third term is non-diagonal and represents the interactions between the two sublattices. Defining

$$E_o = NS^2(J_c(0)-J_s(0))$$

$$A_q = -2S(J_c(0)-J_s(0) + J_s(q)) \quad \text{(VII-14)}$$

$$B_q = -2SJ_c(q)$$

we have

$$H'_{ex} = H_{ex}-E_o = \sum_{\underline{q}} A_{\underline{q}}(a^+_{\underline{q}}a_{\underline{q}}+b^+_{\underline{q}}b_{\underline{q}}) + \sum_{\underline{q}} B_{\underline{q}}(a_{\underline{q}}b_{\underline{q}}+a^+_{\underline{q}}b^+_{\underline{q}}) \ . \quad \text{(VII-15)}$$

In dealing with an oscillating system in the harmonic approximation, the usual technique is to describe it in terms of some uncoupled oscillators or normal modes. This corresponds to a diagonalisation of the quadratic form (VII-14). We will use Bogoliubov's technique (1948) to diagonalize H'_{ex}. In this technique we transform H'_{ex} to a new set of Bose operators α_q and β_q which are obtained from linear combinations of a_q and b_q.

We define

$$\alpha_q = Ua_q + Vb_q^+$$
$$\beta_q = U'a_q^+ + V'b_q \qquad \text{(VII-16)}$$

and require that H'_{ex} can be written in the diagonal form

$$H'_{ex} = \sum_q (\lambda_{1q}\alpha_q^+\alpha_q + \lambda_{2q}\beta_q^+\beta_q) \qquad \text{(VII-17)}$$

where λ_{1q}, λ_{2q} are the spin wave energies. α_q and β_q must be boson operators and so must satisfy the commutation relations

$$[\alpha_q,\alpha_{q'}^+] = [\beta_q,\beta_{q'}^+] = \delta_{qq'}$$
and $$\qquad \text{(VII-18)}$$
$$[\alpha_q,\beta_{q'}] = [\alpha_q,\beta_{q'}^+] = 0 .$$

Using eq. (VII-15), we find

$$[\alpha_q,H'_{ex}] = U(A_q a_q + B_q b_q^+) + V(-A_q b_q^+ - B_q a_q) . \qquad \text{(VII-19)}$$

From eq. (VII-17), it is found that

$$[\alpha_{\underline{q}}, H'_{ex}] = \lambda_{1\underline{q}}(Ua_{\underline{q}} + Vb^{+}_{\underline{q}}) \quad . \qquad \text{(VII-20)}$$

Equating eq. (VII-19) to eq. (VII-20) we have

$$\begin{aligned} A_{\underline{q}}U - B_{\underline{q}}V &= \lambda_{1q}U \\ B_{\underline{q}}U - A_{\underline{q}}V &= \lambda_{1q}V \quad . \end{aligned} \qquad \text{(VII-21)}$$

In order to have non-trivial solutions for U and V, the determinant of the above set of equations must vanish. That is

$$\begin{bmatrix} A_q - \lambda_{1\underline{q}} & -B_{\underline{q}} \\ B_{\underline{q}} & -A_{\underline{q}} - \lambda_{1\underline{q}} \end{bmatrix} = 0 \quad . \qquad \text{(VII-22)}$$

We get

$$\lambda_{1\underline{q}} = \pm(A_q^2 - B_q^2)^{1/2} \qquad \text{(VI-23)}$$

as the two degenerate eigenvalues of the isotropic exchange Hamiltonian. As can be seen from eq. (VII-23), the condition for the stability of the model is

$$A_q \geq B_q \quad .$$

U and V are obtained by substituting λ_{1q} back into eq. (VII-21). This gives

$$V = \sinh\theta_{\underline{q}} \quad ; \quad U = \cosh\theta_{\underline{q}} \qquad \text{(VII-24)}$$

where

$$\sinh 2\theta_{\underline{q}} = \frac{B_{\underline{q}}}{\lambda_{1\underline{q}}} \quad , \quad \text{and} \quad \cosh 2\theta_{\underline{q}} = \frac{A_{\underline{q}}}{\lambda_{1\underline{q}}} \quad .$$

VII-2. Spin Wave in Triangular Antiferromagnets

We shall first develop the spin wave theory for this system using only the exchange Hamiltonian (eq. (VI-1)) and later on we will add the effects of dipole-dipole interactions to the Hamiltonian. Because of the possibility that the dipole-dipole interaction may distort the triangular arrangement of spins in the plane of the moments (section VI-5) we will use a parameter $\psi(=180-\theta)$ for the angle which each spin makes with its neighbour and calculate the value of ψ for which the structure is stable. The equiangular triangular structure corresponds to $\psi=120°$. Since the spin wave theory for the case in which the plane of the moments and the plane of the atoms are perpendicular to one another is similar to the theory for the case in which the two planes are parallel, we shall only discuss the spin wave theory for the latter case. However, the numerical results for the two cases will be discussed in Chapter VIII.

(a) The Isotropic Exchange Hamiltonian

As discussed in section VI-5, triangular antiferromagnets have a simple hexagonal lattice array of magnetic atoms. The magnetic moments of the atoms in a plane are coplanar; this is shown in Figures (VI-2) and (VI-4) for the case in which the plane of the moments is parallel to the plane of the atoms. There is a simple antiferromagnetic coup-

ling between atoms on adjacent planes while the directions of the moments of atoms on the same plane form a triangular structure. There are six sublattices in a unit cell and these could be grouped into two; three of them are in the basal plane located at C=0, where C is the dimension of the unit cell along the hexagonal Z axis, and the others are in the basal plane located at C = $\frac{1}{2}$ as shown in Figure (VI-2). A more detailed discussion of this structure has been given in section VI-5. We define the lattice translation vector as

$$\underline{L}_n = n_1\underline{a} + n_2\underline{b} + n_3\underline{c} \qquad \text{(VII-25)}$$

and the vector connecting the ith atom to the origin of a cell by

$$\underline{r}_i = m_i\underline{a} + m_i'\underline{b} + m_i''\underline{c} \qquad \text{(VII-26)}$$

where $\underline{a}$, $\underline{b}$ and $\underline{c}$ are the primitive crystal axes; n_1, n_2 and n_3 are integers and m_i, m_i', and m_i'' are the atomic coordinates of ith atom in the cell.

Let a cell have vector $\underline{L}$ and atoms 1, 2....6, have positions Lo, Lr_2, Lr_3, Lo $\frac{c}{2}$, Lr_2 $\frac{c}{2}$, and Lr_3 $\frac{c}{2}$ respectively, where

$$r_2 = \frac{1}{3}\underline{a} + \frac{2}{3}\underline{b} \quad , \quad r_3 = \frac{2}{3}\underline{a} + \frac{1}{3}\underline{b}$$
$$r_2\,\frac{c}{2} = \frac{1}{3}\underline{a} + \frac{2}{3}\underline{b} + \frac{1}{2}\underline{c} \quad , \quad r_3\,\frac{c}{2} = \frac{2}{3}\underline{a} + \frac{1}{3}\underline{b} + \frac{1}{2}\underline{c} \qquad \text{(VII-27)}$$

and 'o' denotes the fact that atom 1 is at the origin of the cell. There are six sublattices in the magnetic unit cell

and there are six quantization axes (section VI-5). Because of the geometry of the system, there are two types of exchange integrals; one along the c-axis (J_c) and the other in the basal plane (J_p) (section VI-5). If we denote by H_i, the Hamiltonian for the interaction between an atom on the ith sublattice and its neighbouring atoms, then the total Hamiltonian for the system is

$$H = H_1 + H_2 + \ldots H_6 \qquad \text{(VII-28)}$$

Using the labellings on figure (VI-4), and dropping the vector signs on S, L, and r_i for convenience, we have

$$\begin{aligned}
H_1 &= -\sum_L J_p[S_{Lo}\cdot(S_{Lr_2}+S_{Lr_3}+S_{L-y,r_2}+S_{L-y-x,r_2}+S_{L-y-x,r_3}+S_{L-x,r_3})] \\
&\quad -\sum_L J_c[S_{Lo}\cdot(S_{Lo\ c/2}+S_{L-z,o\ c/2})] \\
H_2 &= -\sum_L J_p[S_{L,r_2}\cdot(S_{Lr_3}+S_{Lo}+S_{L-x,r_3}+S_{L+y,o}+S_{L+y,r_3}+S_{L+x+y,o})] \\
&\quad -\sum_L J_c[S_{Lr_2}\cdot(S_{Lr_2\ c/2}+S_{L-z,r_2,c/2})] \\
H_3 &= -\sum_L J_p[S_{Lr_3}\cdot(S_{Lr_2}+S_{Lo}+S_{L-y,r_2}+S_{L+x,o}+S_{L+x,r_2}+S_{L+x+y,o})] \\
&\quad -\sum_L J_c[S_{Lr_3}\cdot(S_{Lr_3\ c/2}+S_{L-z,r_3\ c/2})] \\
H_4 &= -\sum_L J_p[S_{Lo\ c/2}\cdot(S_{Lr_2\ c/2}+S_{Lr_3\ c/2}+S_{L-y,r_2 c/2}+S_{L-y-x,r_2\ c/2}+ \\
&\qquad S_{L-y-x,r_3,c/2}+S_{L-x,r_3\ c/2})] \\
&\quad -\sum_L J_c[S_{Lo\ c/2}\cdot(S_{Lo}+S_{L+z,o})]
\end{aligned} \qquad \text{(VII-29)}$$

H_5 and H_6 are like H_2 and H_3 except for the fact that each of the r_i's are replaced by $r_i \frac{c}{2}$ and vice versa, and S_{L-Z} is replaced by S_{L+Z}. (This can be seen by comparing H_4 with H_1).

The expression multiplying J_p in eq. (VII-29) represent interactions between one sublattice and its neighbours in the same plane while those multiplying J_c represent interactions between one sublattice and its neighbours in the other basal plane.

In order to expand the products in eq. (VII-29), we have to assign a local coordinate system to each of the six atoms such that the spin of each atom has components x, y and z in its own coordinate system with its average spin directed along its z-axis (section VI-4 and figure VI-4).

We define crystal Cartesian axes, X', Y' and Z' such that the Y' and Z' axes are respectively along the Z and X axes of the hexagonal system as shown in figure VI-4. It is straight forward to relate the six spin coordinate systems (or local axes) to the crystal axes. If S_j^β denotes the β-component of the jth spin in its local coordinate system, then, in terms of the crystal Cartesian axes,

atom 1 has components

S_1^x along X', S_1^y along Y', and S_1^z along Z'

atom 2 has components

$(S_2^z \sin\theta - S_2^x \cos\theta)$ along X', S_2^y along Y', and

$(-S_2^z \cos\theta - S_2^x \sin\theta)$ along Z'

atom 3 has components (VII-30)

$$(-S_3^z \sin\theta - S_3^x \cos\theta) \text{ along } X', \quad S_3^y \text{ along } Y'$$

and

$$(-S_3^z \cos\theta + S_3^x \sin\theta) \text{ along } Z'$$

Using the spin ladder operators defined in eq. (VII-4) and the Holstein Primakoff transformations given by eq. (VII-6) and eq. (VII-9), eq. (VII-30) can be written as (S_i^α denotes the α component of spin of atom i with respect to the crystal Cartesian coordinate system),

For atom 1

$$\begin{aligned} S_{Lo}^X &= \frac{\sqrt{2s}}{2} \left(a_{Lo} + a_{Lo}^+\right), \\ S_{Lo}^Y &= \frac{\sqrt{2s}}{2i} \left(a_{Lo} - a_{Lo}^+\right) \\ S_{Lo}^Z &= S - a_{Lo}^+ a_{Lo} \end{aligned} \tag{VII-31}$$

For atom 2

$$\begin{aligned} S_{Lr_2}^X &= S \sin\theta - a_{Lr_2}^+ a_{Lr_2} \sin\theta - \frac{\cos\theta}{2} \sqrt{2S} \left(a_{Lr_2} + a_{Lr_2}^+\right) \\ S_{Lr_2}^Y &= \frac{\sqrt{2S}}{2i} \left(a_{Lr_2} - a_{Lr_2}^+\right) \\ S_{Lr_2}^Z &= -S \cos\theta + a_{Lr_2}^+ a_{Lr_2} \cos\theta - \frac{\sin\theta}{2} \sqrt{2S} \left(a_{Lr_2} + a_{Lr_2}^+\right) \end{aligned} \tag{VII-32}$$

For atom 3

$$\begin{aligned} S_{Lr_3}^X &= -S \sin\theta + a_{Lr_3}^+ a_{Lr_3} \sin\theta - \frac{\cos\theta}{2} \sqrt{2S} \left(a_{Lr_3} + a_{Lr_3}^+\right) \\ S_{Lr_3}^Y &= \frac{\sqrt{2S}}{2i} \left(a_{Lr_3} - a_{Lr_3}^+\right) \\ S_{Lr_3}^Z &= -S \cos\theta + a_{Lr_3}^+ a_{Lr_3} \cos\theta + \frac{\sin\theta}{2} \sqrt{2S} \left(a_{Lr_3} + a_{Lr_3}^+\right) \end{aligned} \tag{VII-33}$$

and for atoms 4 we have (with c/2 replaced by c and r_i c/2 written as r_{ic})

$$S^X_{Loc} = \frac{\sqrt{2S}}{2}\,(a^+_{Loc} + a_{Loc})$$

$$S^Y_{Loc} = \frac{\sqrt{2S}}{2i}\,(a^+_{Loc} - a_{Loc}) \qquad \text{(VII-34)}$$

$$S^Z_{Loc} = -S + a^+_{Loc}a_{Loc}$$

For atom 5

$$S^X_{Lr_{2c}} = -\,S\sin\theta + a^+_{Lr_{2c}}a_{Lr_{2c}}\sin\theta - \frac{\cos\theta}{2}\sqrt{2s}\,(a^+_{Lr_{2c}} + a_{Lr_{2c}})$$

$$S^Y_{Lr_{2c}} = \frac{\sqrt{2S}}{2i}\,(a^+_{Lr_{2c}} - a_{Lr_{2c}}) \qquad \text{(VII-35)}$$

$$S^Z_{Lr_{2c}} = S\cos\theta - a^+_{Lr_{2c}}a_{Lr_{2c}}\cos\theta - \frac{\sin\theta}{2}\sqrt{2S}\,(a^+_{Lr_{2c}} + a_{Lr_{2c}})$$

For atom 6

$$S^X_{Lr_{3c}} = S\sin\theta - a^+_{Lr_{3c}}a_{Lr_{3c}}\sin\theta - \frac{\cos\theta}{2}\sqrt{2S}\,(a^+_{Lr_{3c}} + a_{Lr_{3c}})$$

$$S^Y_{Lr_{3c}} = \frac{\sqrt{2S}}{2i}\,(a^+_{Lr_{3c}} - a_{Lr_{3c}}) \qquad \text{(VII-36)}$$

$$S^Z_{Lr_{3c}} = S\cos\theta - a^+_{Lr_{3c}}a_{Lr_{3c}}\cos\theta + \frac{\sin\theta}{2}\sqrt{2S}\,(a^+_{Lr_{3c}} + a_{Lr_{3c}})$$

There are four distinct products to be expanded in eq. (VII-29). These are $\underline{S}_{Po}\cdot\underline{S}_{Pr_2}$, $\underline{S}_{Po}\cdot\underline{S}_{Pr_3}$, $\underline{S}_{Pr_2}\cdot\underline{S}_{Pr_3}$ and $\underline{S}_{Pr}\cdot S_{Pr_c}$, where P identifies the cell vector. Other products can be readily derived using the fact that the Z-axis for axes 1, 2 and 3 are antiparallel to the Z axis for axes 4, 5 and 6 respectively. Using equations (VII-31) to (VII-36), we have

$$\underline{S}_{Lo}\cdot\underline{S}_{Lr_2} = -\frac{S\cos\theta}{2}\left[a_{Lo}a_{Lr_2}+a_{Lo}^{+}a_{Lr_2}+a_{Lo}^{+}a_{Lr_2}+a_{Lo}^{+}a_{Lr_2}^{+}\right]$$

$$-\frac{S}{2}\left[a_{Lo}a_{Lr_2}-a_{Lo}a_{Lr_2}^{+}-a_{Lo}^{+}a_{Lr_2}+a_{Lo}^{+}a_{Lr_2}^{+}\right]$$

$$-S^2\cos\theta + S\cos\theta\left(a_{Lo}^{+}a_{Lo} + a_{Lr_2}^{+}a_{Lr_2}\right)$$

$$= -S^2\cos\theta + \frac{S}{2}\cos\theta\left(2a_{Lo}^{+}a_{Lo} + 2a_{Lr_2}^{+}a_{Lr_2}\right)$$

$$+\frac{S}{2}(\cos\theta+1)\left[-a_{Lo}a_{Lr_2}-a_{Lo}^{+}a_{Lr_2}^{+}\right]+\frac{S}{2}(1-\cos\theta)\left(a_{Lo}a_{Lr_2}^{+}+a_{Lo}^{+}a_{Lr_2}\right)$$

(VII-37)

$$\underline{S}_{Lo}\cdot\underline{S}_{Lr_3} = -S\frac{\cos\theta}{2}\left[a_{Lo}a_{Lr_3}+a_{Lo}a_{Lr_3}^{+}+a_{Lo}^{+}a_{Lr_3}+a_{Lo}^{+}a_{Lr_3}^{+}\right]$$

$$-\frac{S}{2}\left[a_{Lo}a_{Lr_3}-a_{Lo}a_{Lr_3}^{+}-a_{Lo}^{+}a_{Lr_3}+a_{Lo}^{+}a_{Lr_3}^{+}\right]$$

$$-S^2\cos\theta + S\cos\theta\left(a_{Lo}^{+}a_{Lo}+a_{Lr_3}^{+}a_{Lr_3}\right)$$

$$= -S^2\cos\theta + \frac{S}{2}\cos\theta\left(2a_{Lo}^{+}a_{Lo}+2a_{Lr_3}^{+}a_{Lr_3}\right)$$

$$+\frac{S}{2}(1+\cos\theta)\left[-a_{Lo}a_{Lr_3}-a_{Lo}^{+}a_{Lr_3}^{+}\right]+\frac{S}{2}(1-\cos\theta)\left[a_{Lo}a_{Lr_3}^{+}+a_{Lo}^{+}a_{Lr_3}\right]$$

(VII-38)

$$\underline{S}_{Lr_2}\cdot\underline{S}_{Lr_3} = [-S^2\sin^2\theta+S\sin^2\theta(a^+_{Lr_2}a_{Lr_2}+a^+_{Lr_3}a_{Lr_3})$$
$$+\frac{S}{2}\cos^2\theta(a_{Lr_2}a_{Lr_3}+a_{Lr_2}a^+_{Lr_3}+a^+_{Lr_2}a_{Lr_3}+a^+_{Lr_2}a^+_{Lr_3})$$
$$+\frac{S}{2}(-a_{Lr_2}a_{Lr_3}+a_{Lr_2}a^+_{Lr_3}+a^+_{Lr_2}a_{Lr_3}-a^+_{Lr_2}a^+_{Lr_3})$$
$$+ S^2\cos^2\theta-S\cos^2\theta(a^+_{Lr_2}a_{Lr_2}+a^+_{Lr_3}a_{Lr_3})$$
$$+\frac{S\sin^2\theta}{2}(a_{Lr_2}a_{Lr_3}-a_{Lr_2}a^+_{Lr_3}-a^+_{Lr_2}a_{Lr_3}-a^+_{Lr_2}a^+_{Lr_3})$$
$$= -S^2(1-2\cos^2\theta)+\frac{S}{2}(1-2\cos^2\theta)(2a^+_{Lr_2}a_{Lr_2}+2a^+_{Lr_3}a_{Lr_3})$$
$$+S(1-\cos^2\theta)(-a_{Lr_2}a_{Lr_3}-a^+_{Lr_2}a^+_{Lr_3})+S\cos^2\theta(a_{Lr_2}a^+_{Lr_3}+a^+_{Lr_2}a_{Lr_3}) \quad \text{(VII-39)}$$

$$\underline{S}_{Lr_2}\cdot\underline{S}_{Lr_{2c}} = -S^2\sin^2\theta+S\sin^2\theta(a^+_{Lr_{2c}}a_{Lr_{2c}}+a^+_{Lr_2}a_{Lr_2})$$
$$+\frac{S\cos^2\theta}{2}(a_{Lr_2}a^+_{Lr_{2c}}+a_{Lr_2}a_{Lr_{2c}}+a^+_{Lr_2}a^+_{Lr2c}+a^+_{Lr_2}a_{Lr_{2c}})$$
$$+\frac{S}{2}(-a_{Lr_2}a^+_{Lr_{2c}}+a_{Lr_2}a_{Lr_{2c}}+a^+_{Lr_2}a^+_{Lr_{2c}}-a^+_{Lr_2}a_{Lr_{2c}})$$
$$-S^2\cos^2\theta+S\cos^2\theta(a^+_{Lr_{2c}}a_{Lr_{2c}}+a^+_{Lr_2}a_{Lr_2})$$
$$+\frac{S}{2}\sin^2\theta(a_{Lr_2}a^+_{Lr_{2c}}+a_{Lr_2}a_{Lr_{2c}}+a^+_{Lr_2}a^+_{Lr_{2c}}+a^+_{Lr_2}a_{Lr_{2c}})$$
$$= -S^2+S(a^+_{Lr_{2c}}a_{Lr_{2c}}+a^+_{Lr_2}a_{Lr_2})+S(a_{Lr_2}a_{Lr_{2c}}+a^+_{Lr_2}a^+_{Lr_{2c}}) \quad \text{(VII-40)}$$

In general,

$$\underline{S}_{Lr}\cdot\underline{S}_{Lrc} = -S^2+S(a^+_{Lrc}a_{Lrc}+a^+_{Lr}a_{Lr})+S(a_{Lr}a_{Lrc}+a^+_{Lr}a^+_{Lrc}) \quad \text{(VII-41)}$$

Products of the form $a^{+}_{Lr}a_{Lr}a^{+}_{Lr_i}a_{Lr_i}$ have been neglected in equations (VII-37) to (VII-41) for the reason discussed in section VII-1.

Substituting equation (VII-37) to (VII-41) into eq. (VII-29), the total Hamiltonian for the system becomes,

$$H=[-J_p\sum_{Li}^{3}\sum[[\ -12S^2\cos\theta-6S^2(1-2\cos^2\theta)+\frac{\sqrt{2S}}{2}S\sin\theta(3a_{Lo}+3a^{+}_{Lo}-a_{L_ir_2}-a^{+}_{L_ir}$$

$$+\frac{S}{2}\cos\theta(6a^{+}_{Lo}a_{Lo}+2a^{+}_{L_ir_2}a_{L_ir_2})+\frac{1}{2}S(1+\cos\theta)(-3a_{Lo}a_{L_ir_2}-3a^{+}_{Lo}a^{+}_{L_ir_2})$$

$$+\frac{1}{2}S(1-\cos\theta)(a_{Lo}a^{+}_{L_ir_2}+a^{+}_{Lo}a_{L_ir_2})$$

$$-\frac{\sqrt{2S}}{2}S\sin\theta(3a_{Lo}+3a^{+}_{Lo}-a_{k_ir_3}-a^{+}_{k_ir_3})+\frac{S}{2}\cos\theta(6a^{+}_{Lo}a_{Lo}+2a^{+}_{k_ir_3}a_{k_ir_3})$$

$$+\frac{1}{2}S(1+\cos\theta)(-3a_{Lo}a_{k_ir_3}-3a^{+}_{Lo}a^{+}_{k_ir_3})+\frac{S}{2}(1-\cos\theta)(a_{Lo}a^{+}_{k_ir_3}+a^{+}_{Lo}a_{k_ir_3})$$

$$+\sqrt{2S}\,S\cos\theta\sin\theta(3a_{Lr_2}+3a^{+}_{Lr_2}-a_{f_ir_3}-a^{+}_{f_ir_3})$$

$$+\frac{S}{2}(1-2\cos^2\theta)(6a^{+}_{Lr_2}a_{Lr_2}+2a^{+}_{f_ir_3}a_{f_ir_3})+S(1-\cos^2\theta)(-3a_{Lr_2}a_{f_ir_3}-$$

$$-3a^{+}_{Lr_2}a^{+}_{f_ir_3})$$

$$+S\cos^2\theta(a_{Lr_2}a^{+}_{f_ir_3}+a^{+}_{Lr_2}a_{Lf_ir_3})+\frac{\sqrt{2S}}{2}S\sin\theta(a_{h_io}+a^{+}_{h_io}-3a_{Lr_2}-3a^{+}_{Lr_2})$$

$$+\frac{S}{2}\cos\theta(2a^{+}_{h_io}a_{h_io}+6a_{Lr_2}a_{Lr_2})+\frac{1}{2}S(1+\cos\theta)(-3a_{h_io}a_{Lr_2}-3a^{+}_{h_io}a^{+}_{Lr_2})$$

$$+\frac{1}{2}S(1-\cos\theta)(a_{h_io}a^{+}_{Lr_2}+a^{+}_{h_io}a_{Lr_2})-\frac{\sqrt{2S}}{2}S\sin\theta(a_{T_io}+a^{+}_{T_io}-3a_{Lr_3}-3a^{+}_{Lr_3})$$

$$+\frac{S}{2}\cos\theta(2a^{+}_{T_io}a_{T_io}+6a^{+}_{Lr_3}a_{Lr_3})+\frac{S}{2}(1+\cos\theta)(-3a_{T_io}a_{Lr_3}-3a^{+}_{T_io}a^{+}_{Lr_3})$$

$$+\frac{S}{2}(1-\cos\theta)(a_{T_i o}a^{+}_{Lr_3}+a^{+}_{T_i o}a_{Lr_3})$$

$$+\sqrt{2S}\,S\cos\theta\sin\theta(a_{g_i r_2}+a^{+}_{g_i r_2}-3a_{Lr_3}-3a^{+}_{Lr_3})$$

$$+\frac{S}{2}(1-\cos^2\theta)(2a^{+}_{g_i r_2}a_{g_i r_2}+6a^{+}_{Lr_3}a_{Lr_3})+S(1-\cos^2\theta)(-3a_{g_i r_2}a_{Lr_3}-3a^{+}_{g_i r_2}a^{+}_{Lr_3})$$

$$+S\cos^2\theta(a_{g_i r_2}a^{+}_{Lr_3}+a^{+}_{g_i r_2}a_{Lr_3}))+(\text{all the above terms with o and r replaced by oc and rc respectively}).$$

$$-J_c\sum_{Li}^{3}\Big((-6S^2+S(a^{+}_{Lr_i}a_{Lr_i}+a^{+}_{Lr_i c}a_{Lr_i c}+a_{Lr_i}a_{Lr_i c}+a^{+}_{Lr_i}a^{+}_{Lr_i c})$$

$$+S(a^{+}_{xr_i}a_{xr_i}+a_{yr_i c}a_{yr_i c}+a_{xr_i c}+a_{xr_i}a_{yr_i c}+a^{+}_{xr_i}a^{+}_{yr_i c}))$$

$$+(\text{all above terms with x and y replaced by (L+z) and L respectively}))\Big] \qquad \text{(VII-42)}$$

where $x = L$, $y = (L-z)$, and $r_1 = 0$

$L_1 = k_1 = f_1 = h_1 = g_1 = T_1 = L$

$L_2 = g_2 = L-y$

$L_3 = k_3 = L-y-x$

$k_2 = f_2 = L-x$

$f_3 = h_3 = L+y$

$h_2 = T_2 = L+x+y$

$g_3 = T_3 = L+x$.

If the assumed magnetic structure is the ground state configuration of the system, the linear terms in eq. (VII-42) should add up to zero. This is the case when and only when $\theta = 0°$, $60°$ and $180°$. The cases $\theta = 0°$ and $\theta = 180°$ correspond to simple antiferromagnetic and ferromagnetic arrangements of spins. In this thesis discussion is limited to the solutions with $\theta = 60°$ corresponding to the triangular structure. This case implies that each spin is oriented in a direction 120° from its neighbours in the basal plane, i.e. the spins form an equiangular triangular structure. A classical calculation of the energy of the system when the spin makes an arbitrary angle with each other (in the basal plane) shows that the system has its minimum energy for the equiangular triangular structure for antiferromagnetic in-plane exchange interactions. This conclusion is the same as the one given by the condition that the linear terms in spin wave theory vanish, so it seems certain that the equiangular triangular structure is stable. As discussed in the introduction to this chapter, we shall continue to denote the angles between the spin direction with ψ although we know that the angle is 120° for Heisenberg interaction.

The next step is to Fourier transform eq. (VII-42) using analogous techniques as those used in section VII-1. The transformations are given by

$$a_{\underline{Lr}} = \left(\frac{6}{N}\right)^{1/2} \sum_{\underline{q}} e^{-i\underline{q}\cdot(\underline{r}+\underline{L})} a_{\underline{r}}(\underline{q}) \,, \quad a_{\underline{Lrc}} = \left(\frac{6}{N}\right)^{1/2} \sum_{\underline{q}} e^{+i\underline{q}\cdot(\underline{rc}+\underline{L})} a_{\underline{rc}}(\underline{q})$$

$$a^{+}_{Lr}=\left(\frac{6}{N}\right)^{1/2}\sum_{q} e^{iq\cdot(r+L)}a^{+}_{r}(q)\ ,\quad a^{+}_{Lrc}=\left(\frac{6}{N}\right)^{1/2}\sum_{q} e^{-iq\cdot(rc+L)}a^{+}_{rc}(q) \qquad \text{(VII-43)}$$

Eq. (VII-43) is substituted in eq. (VII-42) and the resulting Hamiltonian is symmetrized with q restricted to only positive values in the summation. We get

$$\begin{aligned}
H=&[2J_pNS^2(2\cos\theta+1-2\cos^2\theta)+2NJ_cS^2\\
&-(12SJ_p\cos\theta+2J_c^o)\sum_q[a_1^+(q)a_1(q)+a_1^+(-q)a_1(-q)+a_{1c}^+(q)a_{1c}(q)\\
&\qquad+a_{1c}^+(-q)a_{1c}(-q)]\\
&-(6SJ_p(\cos\theta+1-2\cos^2\theta)+2J_c^o)\sum_q[a_2^+(q)a_2(q)+a_2^+(-q)a_2(-q)\\
&\quad+a_3^+(q)a_3(q)+a_3^+(-q)a_3(-q)+a_{2c}^+(q)a_{2c}(q)+a_{2c}^+(-q)a_{2c}(-q)\\
&+a_{3c}^+(q)a_{3c}(q)+a_{3c}^+(-q)a_{3c}(-q)]\\
&+\frac{S}{2}J_p(1+\cos\theta)\sum_q[(a_1(q)a_2(-q)f+a_1(q)a_3(-q)f^*+a_2(q)a_1(-q)f^*+\\
&\qquad+a_3(q)a_1(-q)F\\
&+a_1(-q)a_2(q)f^*+a_1(-q)a_3(q)f+a_2(-q)a_1(q)f+a_3(-q)a_1(q)f^*\\
&+a_{1c}(q)a_{2c}(-q)f^*+a_{1c}(q)a_{3c}(-q)f+a_{2c}(q)a_{1c}(-q)f+a_{3c}(q)a_{1c}(-q)f^*\\
&+a_{1c}(-q)a_{2c}(q)f+a_{1c}(-q)a_{3c}(q)f^*+a_{2c}(-q)a_{1c}(q)f^*+a_{3c}(-q)a_{1c}(q)f)\\
&+\text{h.c.}]\\
&+SJ_p(1-\cos^2\theta)\sum_q[(a_2(q)a_3(-q)f+a_3(q)a_2(-q)f^*+a_2(-q)a_3(q)f^*\\
&+a_3(-q)a_2(q)f+a_{2c}(q)a_{3c}(-q)f^*+a_{3c}(q)a_{2c}(-q)f\\
&+a_{2c}(-q)a_{3c}(q)f+a_{3c}(-q)a_{2c}(q)f^*)+\text{h.c.}]
\end{aligned}$$

$$
\begin{aligned}
&- \frac{SJ_p}{2}(1-\cos\theta)\sum_q [(a_1^+(q)a_2(q)f^*+a_1^+(q)a_3(q)f+a_2^+(q)a_1(q)f+a_3^+(q)a_1(q)f^* \\
&+a_1^+(-q)a_2(-q)f+a_1^+(-q)a_3(-q)f^*+a_2^+(-q)a_1(-q)f^*+a_3^+(-q)a_1(-q)f \\
&+a_{1c}^+(q)a_{2c}(q)f+a_{1c}^+(q)a_{3c}(q)f^*+a_{2c}^+(q)a_{1c}(q)f^*+a_{3c}^+(q)a_{1c}(q)f \\
&+a_{1c}^+(-q)a_{2c}(-q)f^*+a_{1c}^+(-q)a_{3c}(-q)f+a_{2c}^+(-q)a_{1c}(-q)f+a_{3c}^+(-q)a_{1c}(-q)f^*) \\
&+ \text{h.c.}] \\
&- SJ_p\cos^2\theta \sum_q [(a_2^+(q)a_3(q)f^*+a_3^+(q)a_2(q)f+a_2^+(-q)a_3(-q)f+a_{3c}^+(-q)a_{2c}(-q)f^* \\
&+a_{2c}^+(q)a_{3c}(q)f+a_{3c}^+(q)a_{2c}(q)f^*+a_{2c}^+(-q)a_{3c}(-q)f^*+a_{3x}^+(-q)a_{2c}(-q)f \\
&+ \text{h.c.}] \\
&- 2\,J_c^o f_c \sum_q [(a_1(q)a_{1c}(q)+a_2(q)a_{2c}(q)+a_3(q)a_{3c}(q) \\
&+ a_1(-q)a_{1c}(-q)+a_2^+(-q)a_{2c}^+(-q)+a_3(-q)a_{3c}(-q) \\
&+ \text{h.c.}] \qquad \text{(VII-44)}
\end{aligned}
$$

where $J_c^o = 2SJ_c$, $f_c = \cos(\frac{cq_z}{2})$

$$f=[\cos(q_2r)+2\cos(\frac{q_2r}{2})\cos(\frac{\sqrt{3}q_1r}{2})+i[\sin(q_2r)-2\sin(\frac{q_2r}{2})\cos(\frac{\sqrt{3}q_1r}{2})]$$

f^* = hermitian conjugate of f

$q_1 = q_x\cos 30$

$q_2 = q_y+q_x\cos 60$

q_1, q_2 and q_3 are respectively the components of $\underline{q}$ along Z', X' and Y' axes (figure VI-4), and q_x, q_y and q_z are the components of $\underline{q}$ along the reciprocal lattice vectors (of the hexagonal system).

To diagonalize eq. (VII-44), we use a linear combination of the operators $a_i(q)$, $a_{ic}(q)$:

$$\alpha(q)=c_1a_1(q)+c_1'a_1^+(-q)+c_2a_2(q)+c_2'a_2^+(-q)+c_3a_3(q)$$
$$+ c_3'a_3^+(-q)+c_{1c}a_{1c}(-q)+c_{1c}'a_{1c}^+(q)+c_{2c}a_{2c}(-q)+c_{2c}'a_{2c}^+(q)$$
$$+ c_{3c}a_{3c}(-q)+c_{3c}'a_{3c}^+(q) . \qquad \text{(VII-45)}$$

We continue to follow procedures like those in section VII-1 and we obtain a matrix that gives the eigenvalues of the Hamiltonian. This matrix is shown on the next page; its elements are defined by the following equations

$$A = (-6SJ_p(\cos\theta+1-2\cos^2\theta)-2J_c^o)$$
$$A_k = (-12SJ_p\cos\theta-2J_c^o)$$

$$B = -SJ_p(1-\cos\theta)f$$
$$B_k = -2SJ_p\cos^2\theta f$$

$$C = -SJ_p(1-\cos\theta)f^*$$
$$C_k = -2SJ_p\cos^2\theta f^* \qquad \text{(VII-46)}$$

$$D = -SJ_p(1+\cos\theta)f$$
$$D_k = -2SJ_p(1-\cos^2\theta)f$$

$$E = -SJ_p(1+\cos\theta)f^*$$
$$E_K = -2SJ_p(1-\cos^2\theta)f^*$$

$$G = 2J_c^o f_c$$

A_k	O	B	D	C	E	O	G	O	O	O	O
O	$-A_k$	-D	-B	-E	-C	-G	O	O	O	O	O
C	E	A	O	B_k	D_k	O	O	O	G	O	O
-E	-C	O	-A	$-D_k$	$-B_k$	O	O	-G	O	O	O
B	D	C_k	E_k	A	O	O	O	O	O	O	G
-D	-B	$-E_k$	$-C_k$	O	-A	O	O	O	O	-G	O
O	G	O	O	O	O	A_k	O	B	D	C	E
-G	O	O	O	O	O	O	$-A_k$	-D	-B	-E	-C
O	O	O	G	O	O	C	E	A	O	B_k	D_k
O	O	-G	O	O	O	-E	-C	O	-A	$-D_k$	$-B_k$
O	O	O	O	O	G	B	D	C_k	E_k	A	O
O	O	O	O	-G	O	-D	-B	$-E_k$	$-C_k$	O	-A

The matrix can be solved numerically for any given wave vector $\underline{q}$ if the exchange constants are specified. Such numerical solutions will be discussed in Chapter VIII.

(b) The Effects of the Dipole-Dipole Interactions

Expressions were derived for the spin wave energies in the previous section using only an isotropic exchange Hamiltonian. In actual materials, there are small anisotropic interactions in addition to the isotropic interactions. These arise mainly from magnetic dipole-dipole interaction and from spin-orbit coupling. In Mn^{2+} ions spin-orbit couplings are not important and magnetic dipole-dipole interactions are the most likely source of anisotropy (Section VI-5). The effects of dipole-dipole interactions on the spin wave dispersion relations will be discussed in this section.

The total Hamiltonian H_T is given by

$$H_T = H + H_{d-d} \qquad \text{(VII-47)}$$

where H is the isotropic Hamiltonian given by eq. (VII-42), and H_{d-d} represents the dipole-dipole interactions. The dipole interactions are given by (section VI-3)

$$H_{d-d} = \frac{g^2\mu_B^2}{2} \sum_{ij} \frac{1}{r_{ij}^5} [\underline{r}_{ij}^2 (\underline{S}_i \cdot \underline{S}_j) - 3(\underline{S}_i \cdot \underline{r}_{ij})(\underline{S}_j \cdot \underline{r}_{ij})] \qquad \text{(VII-48)}$$

where $\underline{r}_{ij} = \underline{r}_j - \underline{r}_i$ and $\underline{r}_i$ and $\underline{S}_i$ are respectively the position vector and spin of atom i.

In calculating the dipolar interactions, we have to know the orientation of the spins with respect to each other and with respect to the crystallographic axes. This is in contrast to the exchange terms where if every spin in the lattice is rotated through any given angle, the energy is unchanged. We do not know the orientation of the spins relative to the crystallographic axes, but since the spins form a triangular structure in the basal plane, it is reasonable to believe that one of the spins will be aligned along the easy axis in the basal plane. We will therefore assume that the spin of the atom at the origin is aligned along the hexagonal x-axis as shown in figure (VI-4).

If we define α and β as the x, y or z directions for a set of cartesian axes, and if we represent the position vector of a cell by $\underline{R}$, eq. (VII-48) can be written as

$$H_{d-d} = \sum_{\underline{R}\underline{R}'} \sum_{\alpha\beta} \frac{1}{r^5} \left(S_i^\alpha S_j^\beta \delta_{\alpha\beta}(r^2 - 3(r^\alpha)^2) - 3S_i^\alpha S_j^\beta (1-\delta_{\alpha\beta}) r^\alpha r^\beta\right) \quad \text{(VII-49)}$$

where $\underline{r} = \underline{r}_{ij} = \underline{R}-\underline{R}' + \underline{r}_i - \underline{r}_j$.

There are six magnetic atoms in the magnetic unit cell and we therefore have to calculate H_{d-d} for 36 sets of interactions! Symmetry reduces this number to 21, but this is still a large number and we shall only discuss explicitly the calculation for two of these terms. We choose the terms connecting atoms 2 and 3, and atoms 2 and 5.

Denoting the dipolar interaction between atoms at sites 2 and 3 by $H_{d-d}^{2,3}$ and using equations (VII-32) and (VII-33)

(with $\underline{R}$ identifying the position vector of a cell rather than $\underline{L}$), in eq. (VII-49) we have

$$H_{d-d}^{2,3} = m \sum_{R} \sum_{R'} \frac{1}{r^5}[(r^2-3(r^x)^2)(-S^2\sin^2\theta+S(a_3^+(R')a_3(R')\sin^2\theta$$
$$+a_2^+(R)a_2(R)\sin^2\theta)$$
$$+\frac{S\cos^2\theta}{2}(a_2^+(R)a_3(R')+a_2(R)a_3^+(R')+a_2^+(R)a_3(R')+a_2^+(R)a_3^+(R')))$$
$$+(r^2-3(r^y)^2)(\frac{S}{2}(-a_2(R)a_3(R')+a_2(R)a_3^+(R')+a_2^+(R)a_3(R')$$
$$-a_2^+(R)a_3^+(R')))$$
$$+(r^2-3(r^z)^2)[S^2\cos^2\theta+S(-a_3^+(R')a_3(R')\cos^2\theta-a_2^+(R)a_2(R)\cos^2\theta)$$
$$+\frac{S\sin^2\theta}{2}(-a_2(R)a_3(R')-a_2(R)a_3^+(R')-a_2^+(R)a_3(R')-a_2^+(R)a_3^+(R'))]$$
$$-3r^xr^y[\frac{S\cos\theta}{2i}(-a_2(R)a_3(R')+a_2(R)a_3^+(R')-a_2^+(R)a_3(R')+a_2^+(R)a_3^+(R'))]$$
$$-3r^yr^x[\frac{S\cos\theta}{2i}(-a_2(R)a_3(R')-a_2(R)a_3^+(R')+a_2^+(R)a_3(R')+a_2^+(R)a_3^+(R'))]$$
$$-3r^xr^z[-S^2\sin\theta\cos\theta+[a_3^+(R')a_3(R')+a_2^+(R)a_2(R)]S\sin\theta\cos\theta$$
$$+\frac{S\sin\theta\cos\theta}{2}(-a_2(R)a_3(R')-a_2(R)a_3^+(R')-a_2^+(R)a_3(R')-a_2^+(R)a_3^+(R')))$$
$$-3r^zr^x[S^2\cos\theta\sin\theta+(-a_3^+(R')a_3(R')-a_2^+(R)a_2(R))S\cos\theta\sin\theta$$
$$+\frac{S\sin\theta\cos\theta}{2}(a_2(R)a_3(R')+a_2(R)a_3^+(R')+a_2^+(R)a_3(R')+a_2^+(R)a_3^+(R'))$$
$$-3r^yr^z(\frac{S\sin\theta}{2i})(a_2(R)a_3(R')+a_2(R)a_3^+(R')-a_2^+(R)a_3(R')-a_2^+(R)a_3^+(R'))$$
$$-3r^zr^y(\frac{S\sin\theta}{2i})(-a_2(R)a_3(R')+a_2(R)a_3^+(R')-a_2^+(R)a_3(R')+a_2^+(R)a_3^+(R'))]$$

where $m = g^2\mu_B^2/2$, and we have dropped third and fourth order terms in the operators as discussed in the last section.

In order to fourier transform the operators in eq. (VII-50), we use the following transformations:

$$a_i(\underline{R}) = (\frac{6}{N})^{1/2} \sum_{\underline{q}} e^{-i\underline{q}\cdot(\underline{R}+\underline{r}_i)} a_i(\underline{q}), a_i^+(\underline{R}) = (\frac{6}{N})^{1/2} \sum_{\underline{q}} e^{i\underline{q}\cdot(\underline{R}+\underline{r}_i)} a_i^+(q)$$

and for later use, we define

$$a_{ic}(R) = (\frac{6}{N})^{1/2} \sum_{\underline{q}} e^{i\underline{q}\cdot(\underline{R}+\underline{r}_i)} a_{ic}(\underline{q}), a_{ic}^+(R) = (\frac{6}{N})^{1/2} \sum_{\underline{q}} e^{-i\underline{q}\cdot(\underline{R}+\underline{r}_i)} a_{ic}^+(\underline{q}) \quad \text{(VII-51)}$$

Setting aside for the time being, the terms linear in the magnon operators in eq. (VII-50), and fourier transforming the quadratic terms in the equation, we have, with the sum over q restricted to over positive q,

$$\begin{aligned} H_{d-d}^{2,3} = \text{constant} + ms \sum_{q} [& (a_2^+(q)a_2(q) + a_2^+(-q)a_2(-q))f_{8,1}^{(0)} \\ & + (a_3^+(q)a_3(q) + a_3^+(-q)a_3(-q))f_{8,2}^{(0)} \\ & + a_2(q)a_3(-q)f_{8,3}(q) + a_2(-q)a_3(q)f_{8,3}(-q) \\ & + a_2^+(q)a_3(q)f_{8,4}(q) + a_2^+(-q)a_3(-q)f_{8,4}(-q) \\ & + a_2(q)a_3^+(q)f_{8,5}(q) + a_2(-q)a_3^+(-q)f_{8,5}(-q) \\ & + a_2^+(q)a_3^+(-q)f_{8,6}(q) + a_2^+(-q)a_3^+(q)f_{8,6}(-q)] \end{aligned} \quad \text{(VII-52)}$$

where

$$f_{8,2}(q)=\sum_R \frac{1}{r^5}\left[\sin^2\theta(r^2-3(r^x)^2)-\cos^2\theta(r^2-3(r^z)^2)\right]e^{i\underline{q}\cdot\underline{r}}$$

$$f_{8,4}(q)=\sum_R \frac{1}{r^5}\left[\frac{\cos^2\theta}{2}(r^2-3(r^x)^2)+\frac{1}{2}(r^2-3(r^y)^2)-\frac{\sin^2\theta}{2}(r^2-3(r^z)^2)\right.$$
$$\left.+\frac{6\sin\theta}{2i}r^y r^z\right]e^{i\underline{q}\cdot\underline{r}}$$

$$f_{8,6}(q)=\sum_R \frac{1}{r^5}\left[\frac{\cos^2\theta}{2}(r^2-3(r^x)^2)+\frac{1}{2}(r^2-3(r^y)^2)-\frac{\sin^2}{2}(r^2-3(r^z)^2)\right.$$
$$\left.-\frac{6\cos\theta}{2i}r^y r^z\right]e^{i\underline{q}\cdot\underline{r}}$$

$f_{8,1}(q)$, $f_{8,3}(q)$, $f_{8,5}(q)$ are complex conjugate of $f_{8,2}(q)$, $f_{8,6}(q)$, and $f_{8,4}(q)$ respectively.

For the dipolar interaction between atoms 2 and 5, we substitute equations (VII-32) and (VII-35) in eq. (VII-49), and use eq. (VII-51) to obtain (for the quadratic terms),

$$\begin{aligned}H_{d-d}^{2,2c} = \text{constant} + ms\sum_q\ & [(a_2^+(q)a_2(q)+a_2^+(-q)a_2(-q))f_{10,1}(o)\\ &+(a_{2c}^+(q)a_{2c}(q)+a_{2c}^+(-q)a_{2c}(-q))f_{10,2}(o)\\ &+a_2(q)a_{2c}(q)f_{10,3}(q)+a_2(-q)a_{2c}(-q)f_{10,3}(-q)\\ &+a_2^+(q)a_{2c}(-q)f_{10,4}(q)+a_2^+(-q)a_{2c}(q)f_{10,4}(-q)\\ &+a_2(q)a_{2c}^+(-q)f_{10,5}(q)+a_2(-q)a_{2c}^+(q)f_{10,5}(-q)\\ &+a_2^+(q)a_{2c}^+(q)f_{10,6}(q)+a_2^+(-q)a_{2c}^+(-q)f_{10,6}(-q)]\end{aligned}$$

(VII-53)

where

$$f_{10,1}(q)=\sum_R \frac{1}{r^5}[\sin^2\theta(r^2-3(r^x)^2+\cos^2\theta(r^2-3(r^z)^2)+6\sin\theta\cos\theta r^x r^z]e^{i\underline{q}\cdot\underline{r}}$$

$$f_{10,4}(q)=\sum_R \frac{1}{r^5}[\frac{\cos^2\theta}{2}(r^2-3(r^x)^2)-\frac{1}{2}(r^2-3(r^y)^2)+\frac{\sin^2\theta}{2}(r^2-3(r^z)^2)$$

$$-\frac{6}{2i}\cos\theta r^x r^y-\frac{6}{2}\cos\theta\sin\theta r^z r^x-\frac{6}{2i}\sin\theta r^y r^z]e^{i\underline{q}\cdot\underline{r}}$$

$$f_{10,6}(q)=\sum_R \frac{1}{r^5}[\frac{\cos^2\theta}{2}(r^2-3(r^x)^2)+\frac{1}{2}(r^2-3(r^y)^2)+\frac{\sin^2\theta}{2}(r^2-3(r^z)^2)$$

$$-\frac{6}{2}\cos\theta\sin\theta r^z r^x]e^{i\underline{q}\cdot\underline{r}}$$

$f_{10,2}(q)$, $f_{10,3}(q)$, $f_{10,5}(q)$ are respectively the complex conjugate of $f_{10,1}(q)$, $f_{10,6}(q)$ and $f_{10,4}(q)$.

The other 19 dipolar interactions are calculated in a similar fashion to the above calculations. The Total Hamiltonian is then given by

$$H_T = H + \sum_{k=1}^{36} H_{d-d}^k \qquad \text{(VII-54)}$$

with the linear terms in the operators included in both the isotropic Hamiltonian H, and the dipole-dipole interaction H_{d-d}.

As discussed in the previous section, the linear terms in eq. (VII-54) should add up to zero for a stable structure. These terms only add up to zero when θ = 0°, 60° and 180°. As before the cases θ=0° and θ=180° are not considered while the case θ=60° corresponds to the triangular structure which is the subject under discussion. The fact that the dipolar terms do not affect the value of θ shows that the equiangular triangular

structure is not changed by dipolar interactions.

With the linear terms in eq. (VII-54) set equal to zero, the Hamiltonian is diagonalized by the linear combination of operators given in eq. (VII-45). The resulting matrix which gives the spin wave energies is shown on page 161, where A, A_k, B, B_k, C, C_k, D, D_k, E, E_k, and G are as defined in eq. (VII-46), and $\theta = 60°$. j and m in $f_{j,m}(q)$ and r_j specify respectively which of the 21 interactions and 6 quadratic operators is being referred to (see equations (VII-52) and (VII-53)). For j = 1 to 6, 7 to 11, 12 to 15, 16 to 18, 19 to 20, and 21, the interactions are respectively between atom 1 and atom 1^* to 6, atom 2 and atoms 2^* to 6, atom 3 and atoms 3^* to 6, atom 4 and atom 4^* to 6, atom 5 and atom 5^* to 6, and atom 6 and atom 6^*. (The stars on atoms 1, 2, ... 6 indicate that the atom is located at R' while the atom with which it interacts is located at R.)

We have used the following definitions in the matrix:

$$A_1(q) = A_k + f_{2,1}(o) + f_{3,1}(o) + f_{1,2}(o) + f_{4,1}(o) + f_{5,1}(o) + f_{6,1}(o) + \frac{1}{2} f_{1,4}(q) + \frac{1}{2} f^*_{1,4}(q)$$

$$A_3(q) = A + f_{2,2}(o) + f_{8,1}(o) + f_{7,2}(o) + f_{9,1}(q) + f_{10,1}(o) + f_{11,1}(o) + \frac{1}{2} f_{7,4}(q) + \frac{1}{2} f^*_{7,4}(q)$$

$$A_5(q) = A + f_{3,2}(o) + f_{8,2}(o) + f_{12,2}(o) + f_{13,1}(o) + f_{14,1}(o)$$
$$+ f_{15,1}(o) + \frac{1}{2} f_{12,4}(q) + \frac{1}{2} f^*_{12,4}(q)$$

$$A_7(-q) = A_k + f_{18,1}(o) + f_{17,1}(o) + f_{16,2}(o) + f_{4,2}(o) + f_{9,2}(o)$$
$$+ f_{13,2}(o) + \frac{1}{2} f_{16,4}(-q) + \frac{1}{2} f^*_{16,4}(-q)$$

$$A_9(-q) = A + f_{17,2}(o) + f_{20,1}(o) + f_{19,2}(o) + f_{5,2}(o) + f_{10,2}(o)$$
$$+ f_{14,2}(o) + \frac{1}{2} f_{19,4}(-q) + \frac{1}{2} f^*_{19,4}(-q)$$

$$A_{11}(-q) = A + f_{18,2}(o) + f_{20,2}(o) + f_{21,2}(o) + f_{6,2}(o) + f_{11,2}(o)$$
$$+ f_{15,2}(o) + \frac{1}{2} f_{21,4}(-q) + \frac{1}{2} f^*_{21,4}(-q)$$

Defining

$$D^{\alpha\beta} = \sum_R \frac{1}{r_i^5} [3r^\alpha r^\beta - r^2 \delta_{\alpha\beta}] \exp(i\underline{q}\cdot\underline{r}_i) \qquad \text{(VII-55)}$$

where α and β represent any of the three cartesian coordinates x, y, z, we have, with $T = g^2\mu_B^2 S/2$, (F and f are used interchangeably)

$$F_{1,1}(o) = F_{1,2}(o) = -F_{4,1}(o) = 2TD^{zz}$$

$$F_{1,4}(q) = F_{4,6}(q) = T[-D^{xx} - D^{yy}]$$

$$F_{1,6}(q) = F_{4,4}(q) = T(-D^{xx} + D^{yy} - 2iD^{xy}]$$

$$F_{2,1}(o) = F_{2,2}(o) = -F_{5,2}(o) = -F_{9,2}(o) = 2T[-D^{zz}\cos\theta + D^{zx}\sin\theta]$$

$$F_{2,4}(q) = f_{5,6}(q) = F^h_{9,6}(q) = T[D^{xx}\cos\theta - D^{yy} + (1+\cos\theta)iD^{xy}$$
$$+ \sin\theta D^{xz} + i\sin\theta D^{yz}]$$

$$F_{2,6}(q) = F'_{5,4}(q) = F''_{9,4}(q) = T[D^{xx}\cos\theta + D^{yy} + (\cos\theta-1)iD^{xy} + \sin\theta D^{xz} + i\sin\theta D^{yz}]$$

$$F_{3,1}(o) = F_{3,2}(o) = -F'_{6,2}(o) = -f''_{13,2}(o) = 2T[-D^{zz}\cos\theta - D^{zx}\sin\theta]$$

$$F'_{3,4}(q) = F''_{6,6}(q) = F^{h}_{13,6}(q) = T[D^{xx}\cos\theta - D^{yy} + (1+\cos\theta)iD^{xy} - D^{xz}\sin\theta - i\sin\theta D^{yz}]$$

$$F_{3,6}(q) = F'_{6,4}(q) = F''_{13,4} = T[D^{xx}\cos\theta + D^{yy} + (\cos\theta-1)iD^{xy} - D^{xz}\sin\theta - i\sin\theta D^{yz}]$$

$$F_{7,1}(o) = F_{7,2}(o) = -f'_{10,1}(o) = 2T[D^{xx}\sin^2\theta + D^{zz}\cos^2\theta - 2\cos\theta\sin\theta D^{xz}]$$

$$F_{7,4}(q) = f'_{10,6}(q) = T[-D^{xx}\cos^2\theta - D^{yy} - D^{zz}\sin^2\theta - 2\cos\theta\sin\theta D^{zx}]$$

$$F_{7,6}(q) = f'_{10,4} = T[-D^{xx}\cos^2\theta + D^{yy} - D^{zz}\sin^2\theta + 2i\cos\theta D^{xy} - 2\cos\theta\sin\theta D^{zx} + 2i\sin\theta D^{yz}]$$

$$F_{8,1}(o) = F_{8,2}(o) = -F'_{14,2}(o) = -f''_{11,2}(o) = 2T[-D^{xx}\sin^2\theta + D^{zz}\cos^2\theta]$$

$$F'_{8,4}(q) = F''_{11,6}(q) = F^{h}_{14,6}(q) = T[-D^{xx}\cos^2\theta - D^{yy} + D^{zz}\sin^2\theta - 2i\sin\theta D^{zy}]$$

$$F_{8,6}(q) = F'_{11,4}(q) = F''_{14,14}(q) = T[-D^{xx}\cos^2\theta + D^{yy} + D^{zz}\sin^2\theta - 2i\cos\theta D^{xy}]$$

$$F_{12,1}(o) = F_{12,2}(o) = -F'_{15,1}(o) = 2T[D^{xx}\sin^2\theta + D^{zz}\cos^2\theta + 2\sin\theta\cos\theta D^{xz}]$$

$$F_{12,4}(q) = F'_{15,6}(q) = T[-D^{xx}\cos^2\theta - D^{yy} - D^{zz}\sin^2\theta + 2\cos\theta\sin\theta D^{zx}]$$

$$F_{12,6} = F'_{15,4}(q) = T[-D^{xx}\cos^2\theta + D^{yy} - D^{zz}\sin^2\theta + 2i\cos\theta D^{xy} + 2\cos\theta\sin\theta D^{zx} - 2i\sin\theta D^{yz}]$$

and for k = 2, 4, and 6, we have

$$F_{16,k}(q) = F^{*}_{1,k}(q) \quad , \quad F_{17,k}(q) = F^{*}_{2,k}(q) \quad , \quad F_{18,k}(q) = F^{*}_{3,k}(q)$$

$$F_{19,k}(q) = F^{*}_{7,k}(q) \quad , \quad F_{20,k}(q) = F^{*}_{8,k}(q) \quad , \quad F_{21,k}(q) = F^{*}_{12,k}(q)$$

The primes on $F'_{j,k}(q)$ means that $D^{\alpha\beta}$ should be evaluated using the appropriate lattice vector $\underline{r}_j$, and the superscript h means that the hermitian conjugate of the terms multiplying $D^{\alpha\beta}$ should be taken. For $CsMnBr_3$, with S = 5/2,

$$T/\text{volume of unit cell} = 0.0000678 \text{ THz} .$$

The numerical calculations of the dipole sums (eq. (VII-55)), can be performed using the Ewald technique. It is based on eq. (30-31) of 'Dynamical Theory of Crystal Lattices' by Born and Huang (1954). The technique involves doing the sums to near atoms directly, whereas the sums for atoms at more than a certain distance are done in reciprocal space. The computer program for calculating these sums was written by Dr. E. R. Cowley of Brock University.

It is apparent that the effects of the dipole-dipole interactions on the spin wave spectrum of $CsMnBr_3$ are complicated, and their contributions to the spin wave energies are wave vector dependent. These effects will be discussed in chapter VIII.

$A_1(q)$	$-\frac{1}{2}F^*_{1,6}(q)$ $-\frac{1}{2}F^*_{1,6}(-q)$	$F^*_{2,4}(q)$ $+B$	$-F^*_{2,6}(q)$ $+D$	$F^*_{3,4}(q)$ $+C$	$-F^*_{3,6}(q)$ $+E$	$F^*_{4,4}(q)$	$-F^*_{4,6}(q)$ $+G$	$F^*_{5,4}(q)$	$-F^*_{5,6}(q)$	$F^*_{6,4}(q)$	$-F^*_{6,6}(q)$
$\frac{1}{2}F_{1,6}(q)$ $+\frac{1}{2}F_{1,6}(-q)$	$-A_1(-q)$	$F_{2,6}(-q)$ $-D$	$-F_{2,4}(-q)$ $-B$	$F_{3,6}(-q)$ $-E$	$-F_{3,4}(-q)$ $-C$	$F_{4,6}(-q)$ $-G$	$-F_{4,4}(-q)$	$F_{5,6}(-q)$	$-F_{5,4}(-q)$	$F_{6,6}(-q)$	$-F_{6,4}(-q)$
$F_{2,4}(q)$ $+C$	$-F^*_{2,6}(-q)$ $+E$	$A_3(q)$	$-\frac{1}{2}F^*_{7,6}(q)$ $-\frac{1}{2}F^*_{7,6}(-q)$	$F^*_{8,4}(q)$ $+B_k$	$-F^*_{8,6}(q)$ $+D_k$	$F^*_{9,4}(q)$	$-F^*_{9,6}(q)$	$F^*_{10,4}(q)$	$-F^*_{10,6}(q)$ $+G$	$F^*_{11,4}(q)$	$-F^*_{11,6}(q)$
$F_{2,6}(q)$ $-E$	$-F^*_{2,4}(-q)$ $-C$	$\frac{1}{2}F_{7,6}(q)$ $\frac{1}{2}F_{7,6}(-q)$	$-A_3(-q)$	$F_{8,6}(-q)$ $-D_k$	$-F_{8,4}(-q)$ $-B_k$	$F_{9,6}(-q)$	$-F_{9,4}(-q)$	$F_{10,6}(-q)$ $-G$	$-F_{10,4}(-q)$	$F_{11,6}(-q)$	$-F_{11,4}(-q)$
$F_{3,4}(q)$ $+B$	$-F^*_{3,6}(-q)$ $+D$	$F_{8,4}(q)$ $+C_k$	$-F^*_{8,6}(-q)$ $+E_k$	$A_5(q)$	$-\frac{1}{2}F^*_{12,6}(q)$ $-\frac{1}{2}F^*_{12,6}(-q)$	$F^*_{13,4}(q)$	$-F^*_{13,6}(q)$	$F^*_{14,4}(q)$	$-F^*_{14,6}(q)$	$F^*_{15,4}(q)$	$-F^*_{15,6}(q)$ $+G$
$F_{3,6}(q)$ $-D$	$-F^*_{3,4}(-q)$ $-B$	$F_{8,6}(q)$ $-E_k$	$-F^*_{8,4}(-q)$ $-C_k$	$\frac{1}{2}F_{12,6}(q)$ $+\frac{1}{2}F_{12,6}(-q)$	$-A_5(-q)$	$F_{13,6}(-q)$	$-F_{13,4}(-q)$	$F_{14,6}(-q)$	$-F_{14,4}(-q)$	$F_{15,6}(-q)$ $-G$	$-F_{15,4}(-q)$
$F_{4,4}(q)$	$-F^*_{4,6}(-q)$ $+G$	$F_{9,4}(q)$	$-F^*_{9,6}(-q)$	$F_{13,4}(q)$	$-F^*_{13,6}(-q)$	$A_7(-q)$	$-\frac{1}{2}F^*_{16,6}(q)$ $-\frac{1}{2}F^*_{16,6}(-q)$	$F^*_{17,4}(-q)$ $+B$	$-F^*_{17,6}(-q)$ $+D$	$F^*_{18,4}(-q)$ $+C$	$-F^*_{18,6}(-q)$ $+E$
$F_{4,6}(q)$ $-G$	$-F^*_{4,4}(-q)$	$F_{9,6}(q)$	$-F^*_{9,4}(-q)$	$F_{13,6}(q)$	$-F^*_{13,4}(-q)$	$\frac{1}{2}F_{16,6}(q)$ $+\frac{1}{2}F_{16,6}(-q)$	$-A_7(q)$	$F_{17,6}(q)$ $-D$	$-F_{17,4}(q)$ $-B$	$F_{18,6}(q)$ $-E$	$-F_{18,4}(q)$ $-C$
$F_{5,4}(q)$	$-F^*_{5,6}(-q)$	$F_{10,4}(q)$	$-F^*_{10,6}(-q)$ $+G$	$F_{14,4}(q)$	$-F^*_{14,6}(-q)$	$F_{17,4}(-q)$ $+C$	$-F^*_{17,6}(q)$ $+E$	$A_9(-q)$	$-\frac{1}{2}F^*_{19,6}(q)$ $-\frac{1}{2}F^*_{19,6}(-q)$	$F^*_{20,4}(-q)$ $+B_k$	$-F^*_{20,6}(-q)$ $+D_k$
$F_{5,6}(q)$	$-F^*_{5,4}(-q)$	$F_{10,6}(q)$ $-G$	$-F^*_{10,4}(-q)$	$F_{14,6}(q)$	$-F^*_{14,4}(-q)$	$F_{17,6}(-q)$ $-E$	$-F^*_{17,4}(q)$ $-C$	$\frac{1}{2}F_{19,6}(q)$ $+\frac{1}{2}F_{19,6}(-q)$	$-A_9(q)$	$F_{20,6}(q)$ $-D_k$	$-F_{20,4}(q)$ $-B_k$
$F_{6,4}(q)$	$-F^*_{6,6}(-q)$	$F_{11,4}(q)$	$-F^*_{11,6}(-q)$	$F_{15,4}(q)$	$-F^*_{15,6}(-q)$ $+G$	$F_{18,4}(-q)$ $+B$	$-F^*_{18,6}(q)$ $+D$	$F_{20,4}(-q)$ $+C_k$	$-F^*_{20,6}(q)$ $+E_k$	$A_{11}(-q)$	$-\frac{1}{2}F^*_{21,6}(q)$ $-\frac{1}{2}F^*_{21,6}(-q)$
$F_{6,6}(q)$	$-F^*_{6,4}(-q)$	$F_{11,6}(q)$	$-F^*_{11,4}(-q)$	$F_{15,6}(q)$ $-G$	$-F^*_{15,4}(-q)$	$F_{18,6}(-q)$ $-D$	$-F^*_{18,4}(q)$ $-B$	$F_{20,6}(-q)$ $-E_k$	$-F^*_{20,4}(q)$ $-C_k$	$\frac{1}{2}F_{21,6}(q)$ $+\frac{1}{2}F_{21,6}(-q)$	$-A_{11}(q)$

CHAPTER VIII

NUMERICAL RESULTS AND DISCUSSION

The numerical results of the spin wave theory developed in chapter VII for triangular antiferromagnets will be discussed in this chapter. The two cases in which the plane of the moments is parallel, and perpendicular to the plane of the atoms will be considered. The discussion includes the effect of changes in the ratio of the exchange integrals (J_p to J_c) on the spin wave energies. The results obtained should be representative of what would be obtained in any triangular antiferromagnet having dipolar anisotropy; application is made especially to the case of $CsMnBr_3$.

VIII-1 Isotropic Interactions

In order to calculate numerically the dispersion relation from the exchange Hamiltonian (VII-44), the values of the exchange integral along the crystal c-axis (J_c) and in the basal plane (J_p) should be known. For the $CsMnBr_3$ system, Eibschütz et al. (1972) found $|J_c| = 9.6°K$ from magnetic susceptibility measurements, but the value of J_p is not known. In order to estimate the value of J_p, we will use the Green's function estimates of Oguchi (1964). Oguchi's calculation was performed for a loose-packed ensemble of chains, each chain having four nearest-neighbour chains. Thus the ratio of interchain to intrachain exchange interactions in Oguchi's

calculation is $2|J_p/J_c|$. In $CsMnBr_3$ the chains (section VI-6) are close packed with each chain having six nearest-neighbour chains. In the ordered phase, the ordering is not the simple up-down two sublattice antiferromagnet as assumed by Oguchi and the resulting effective interchain field is only half its "saturation" value. Thus in $CsMnBr_3$ the ratio of interchain to intrachain interactions in the ordered phase as defined by Oguchi is $|3J_p/2J_c|$. Oguchi gives

$$kT_N = 4JS(S+1)/3I(\eta) \quad . \qquad \text{(VII-1)}$$

where η is $\frac{1}{2}|3J_p/2J_c|$ and $I(\eta)$ as a function of η is tabulated. Putting $T_N = 8.3°K$, and $|J_c| = 9.6°K$ we find $I(\eta) \approx 13.49$ and $\eta \approx 0.002$. Thus for $CsMnBr_3$ the ratio of interchain to intrachain interaction is $|3J_p/2J_c| \approx 0.004$, implying that $|J_p| \approx 2.56\times10^{-2}$ °K. The signs of J_c and J_p must be negative to give the triangular structure, as was demonstrated in section VI-5. The value of J_p derived above will probably not be very reliable owing to the large value of the ratio of J_c to J_p. However it serves as a useful starting point for numerical studies.

With these values of J_c and J_p, the 12×12 matrix corresponding to the isotropic Hamiltonian (VII-44) (page 150) was solved numerically for different values of the wave vector along two high symmetry directions. For a given wave vector, the eigenvalues which give the spin wave energies are real;

they occur in pairs $\pm \omega(q)$, where ω is the frequency for the wave vector q. There are six such pairs for each wave vector. Figure (VIII-1) shows the calculated dispersion curves along the (ε00) direction in the Brillouin zone where ε is the dimensionless reduced wave vector $3aq_x/4\pi$. There are six branches to the dispersion curve as expected and they are non-degenerate at high values of the wave vector. Three of the branches have zero energy at zero wave vector. The maximum frequency of the spin wave at the zone boundary ($\varepsilon = 0.5$) is 0.206 THz.

Figure (VIII-2) shows the dispersion curve along the (00ε) direction ($\varepsilon = cq_z/2\pi$). There are six branches to the dispersion curves. At low q, one of the branches is doubly degenerate while another one is triply degenerate and goes to zero at $q = 0$. At the zone boundary one of the branches has four fold degeneracy while the other branch has two fold degeneracy. The maximum frequency of the spin wave is 2.012 THz at the zone boundary. This is much larger than the value 0.206 THz obtained at the zone boundary for spin wave propagating along the (ε00) direction and reflects the fact that there is a much stronger coupling of magnetic moments along the crystal c-axis (or in the chain) compared with those in the basal plane (or between chains).

The above results are also obtained in the case when the plane of the moments is perpendicular to the plane of the atoms. This is because the Heizenberg Hamiltonian is unaffected when every spin in the lattice is rotated through any

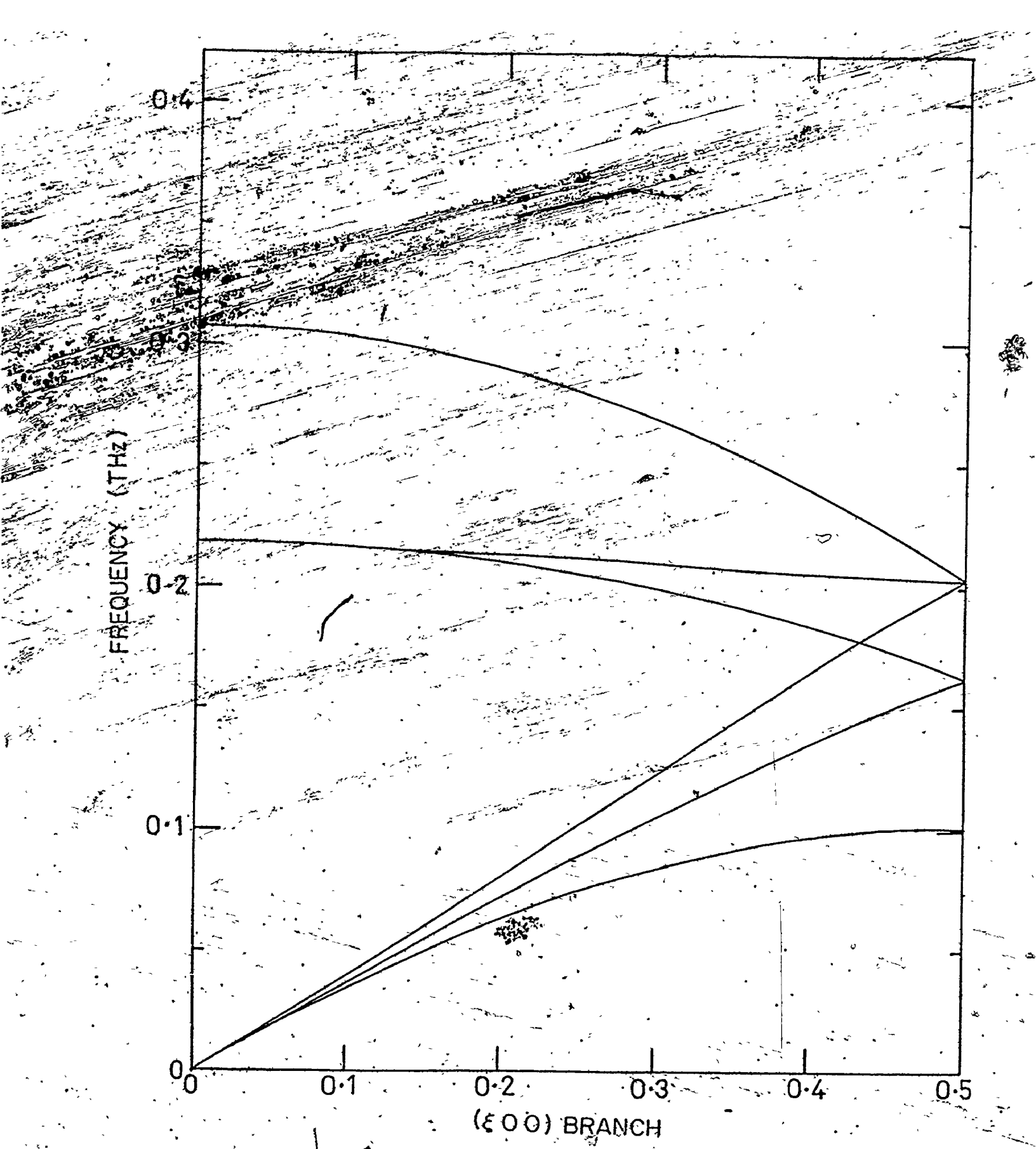

Fig. VIII-1. Calculated spin wave dispersion curves of $CsMnBr_3$ along the (ε00) direction. The calculation considered only isotropic interactions.

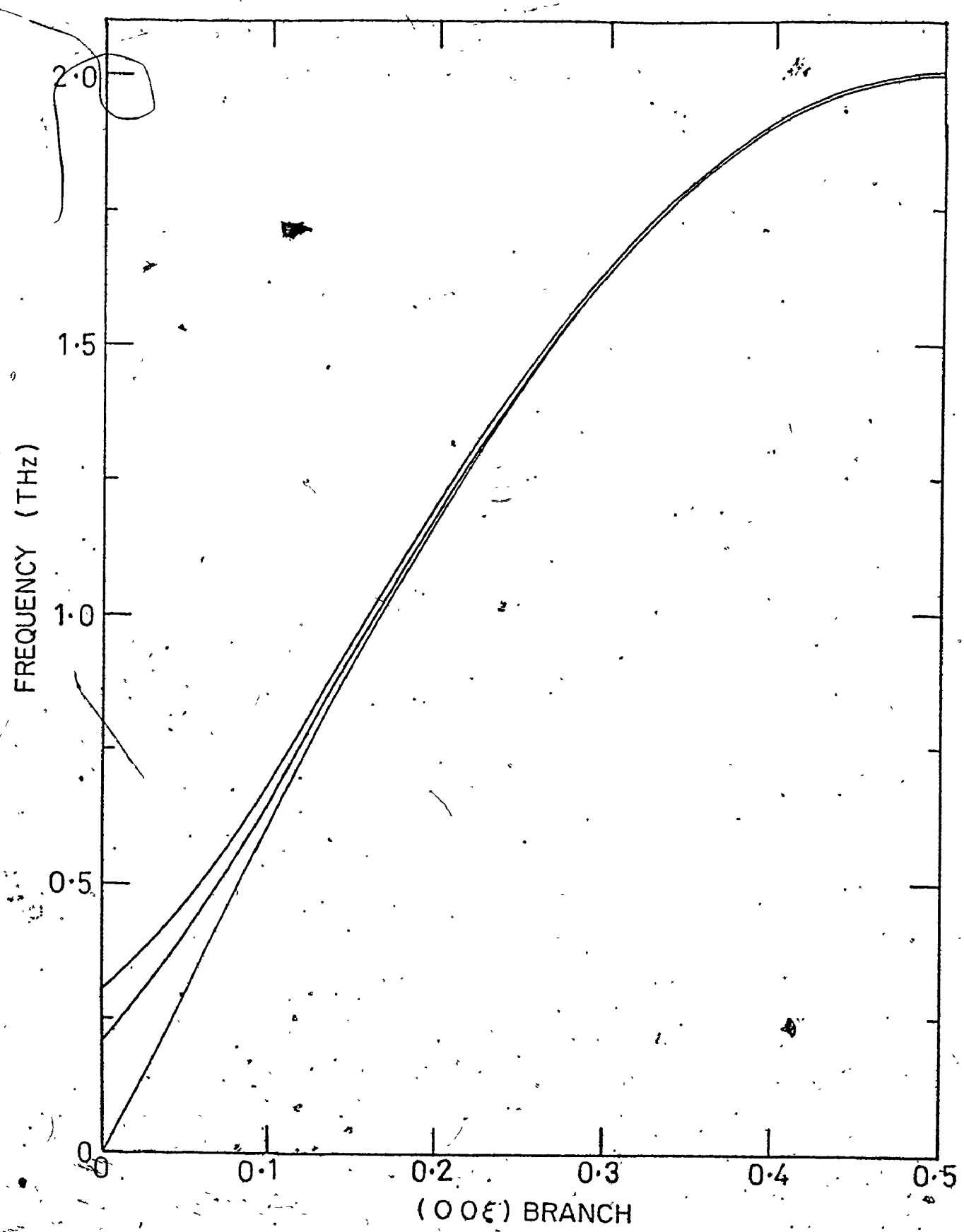

Fig. VIII-2. Calculated spin wave dispersion curves of $CsMnBr_3$ along the (00ε) direction. The calculation considered only isotropic interactions.

given angle.

VIII-2 The Effects of Dipole-Dipole Interactions on the Spin Wave Dispersion Relations

The matrix corresponding to the Hamiltonian (VII-47) for the case in which both isotropic and dipole-diple interactions are present, can be solved numerically for any wave vector by using the values of J_c and J_p calculated in the previous section. These values were used in solving the matrix on page 161 which is for the case in which the dipolar interactions confine the moments to the plane of the atoms. These values were also used in solving the matrix for the other case in which the plane of the moments is perpendicular to that of the atoms. The matrices were solved for different values of the wave vector along the symmetry directions considered in section (VIII-1).

In the case in which the plane of the moments is perpendicular to the plane of the atoms, the eigenvalues of the matrix, which are the spin wave energies, are imaginary. This indicates that the structure is not stable and shows that the dipole-dipole interactions will not orient the moments into a plane which is perpendicular to the plane of the atoms.

In the other case in which the plane of the moments is parallel to that of the atoms, the eigenvalues of the matrix are real and appear in pairs $\pm\omega(q)$ as obtained for isotropic interactions (section VIII-1). The fact that the spin wave energies are real shows that the structure is stable

and it confirms the earlier observation (section VI-5) that dipole-dipole interactions confine the moments to the plane of the atoms. There are six branches to the dispersion curves along the symmetry directions. Along the (ε00) direction (Figure VIII-3), only one branch goes to zero at q = 0 compared with three branches in the case of isotropic interactions. Two of the branches are doubly degenerate at low q but all the branches are non-degenerate at high q as was the case for the isotropic interactions. At the zone boundary, the maximum spin wave frequency is 0.356 THz which is larger than the value of 0.206 THz obtained for the isotropic interactions. The interactions J_p within the plane are sufficiently weak that dipolar interactions are of comparable magnitude to the exchange interactions. This raises doubts about the validity of our estimate of J_p in the previous section where dipole-dipole interactions were neglected. A good determination of J_p can only be made from further experimental work; for instance a determination of the spin wave dispersion relations by neutron diffraction.

Along the (00ε) direction (figure VIII-4), only one branch goes to zero at q = 0 compared with three branches in the case of isotropic interactions. At low q, two of the branches are doubly degenerate while at the zone boundary one branch has four fold degeneracy and another branch has two fold degeneracy as obtained for the isotropic interactions.

The maximum frequency of the spin wave at the zone boundary is 2.021 THz which is again much larger than that of waves propagating along the (ε00) direction. Because of the stronger exchange in this direction, the dipolar forces have much less effect on the spin wave energies than in the (ε00) direction.

The effects of the dipole-dipole interactions on the spin wave dispersion curves are particularly important at low values of the wave vector where the interactions remove some of the degeneracies in the dispersion curves. At q=0, the effect of the dipolar interactions is to make two of the branches that have zero frequency in the isotropic interaction limit, have non-zero frequencies.

Since the spin wave energy depends on the exchange integrals J_p and J_c, the ratio of the two exchange integrals will affect the frequency of the spin waves. We have therefore calculated the maximum frequencies of spin waves propagating along the (ε00) and (00ε) directions at q = 0, and at the zone boundary for different ratios of J_p/J_c with J_c fixed. As shown in Table (VIII-1) and Figure (VIII-5), the maximum frequency (at the zone boundary) of the spin wave propagating along the (00ε) direction is always much larger than that of propagation along (ε00) direction for all values of J_p less than J_c. At small values of J_p/J_c ($\sim$ 0.1), the maximum frequencies along the two symmetry directions are relatively large. This maximum frequency decreases with decreasing value of J_p/J_c along the two directions, with the decrease being further along the (ε00) direction up to

about $J_p/J_c \approx 5\times10^{-4}$ where the frequencies along the two directions become almost constant with further decrease in the ratio of J_p to J_c. The fact that the maximum frequencies of spin waves propagating along the (00ε) direction are much larger than those propagating along the (ε00) direction, is a reflection of the much stronger coupling of magnetic moments along the crystal c-axis (in the chains) compared with that in the perpendicular direction (between the chains).

The spin wave dispersion relations in the triangular antiferromagnets $CsNiCl_3$ and $RbNiCl_3$ have been calculated by Sorgen et.al. (1974). The calculation considered a single ion anisotropy along the crystal c axis so that the plane of the moments is perpendicular to that of the atoms. Their results have similar features with ours; there are six branches to the dispersion relations along the symmetry directions and the energies of spin waves propagating along the crystal c-axis are much larger than those propagating in the perpendicular direction. No experimental measurements of the spin wave dispersion relations are available for $CsNiCl_3$ or $RbNiCl_3$.

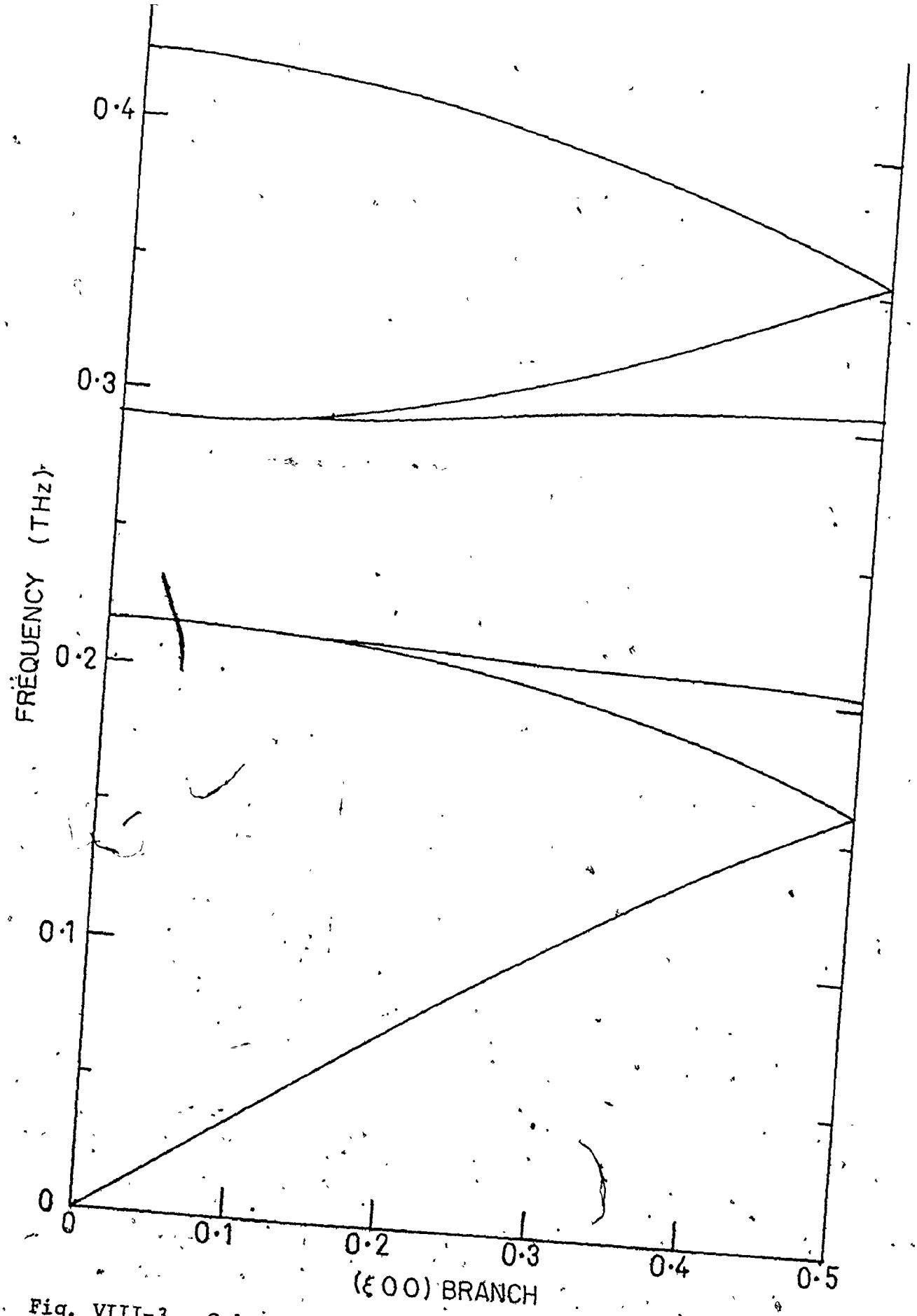

Fig. VIII-3. Calculated spin wave dispersion curves of $CsMnBr_3$ along the (ε00) direction. The calculation con-

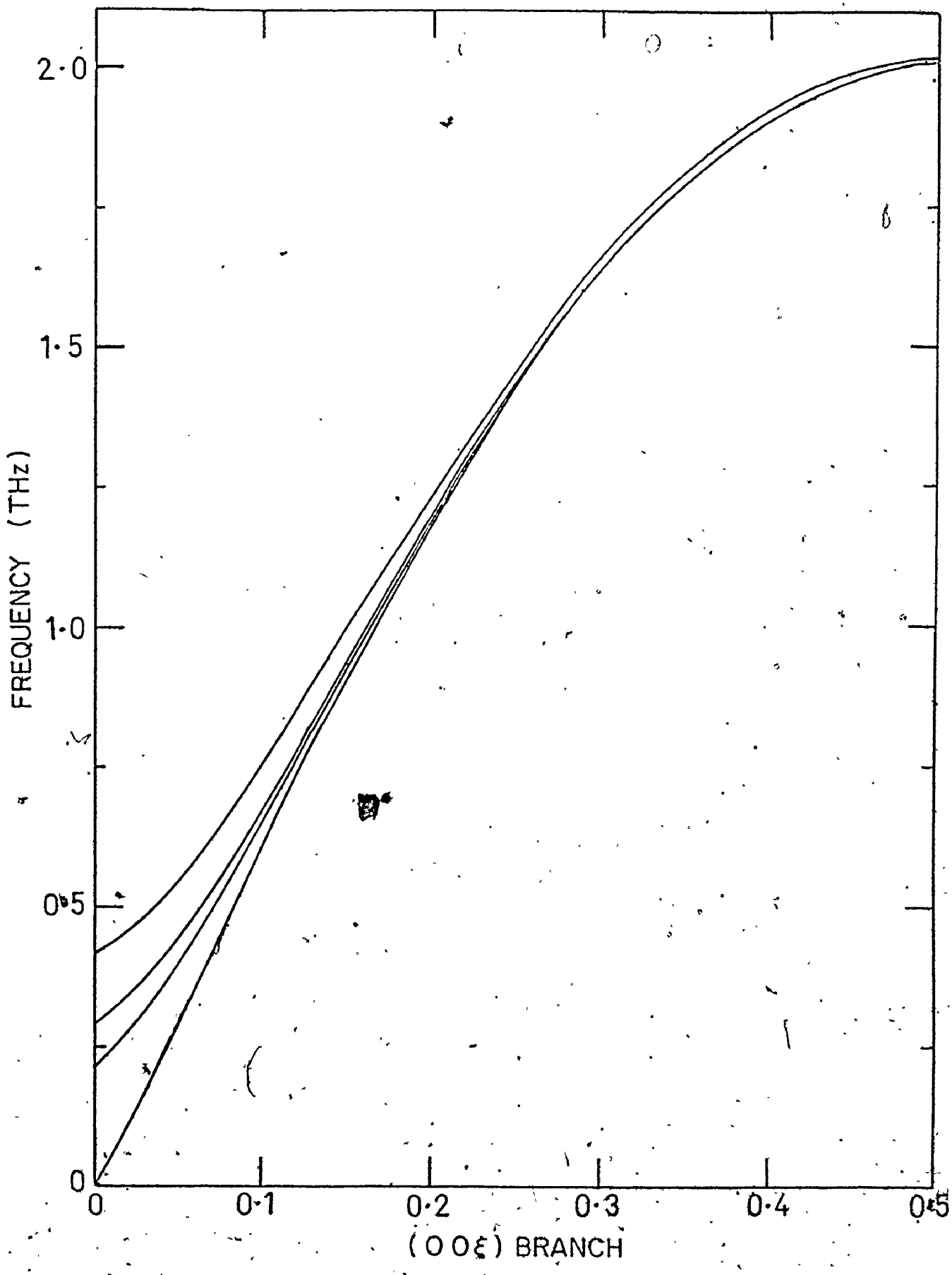

Fig. VIII-4. Calculated spin wave dispersion curves of $CsMnBr_3$ along the (00ε) direction. The calculation considered both isotropic and dipole-dipole interactions.

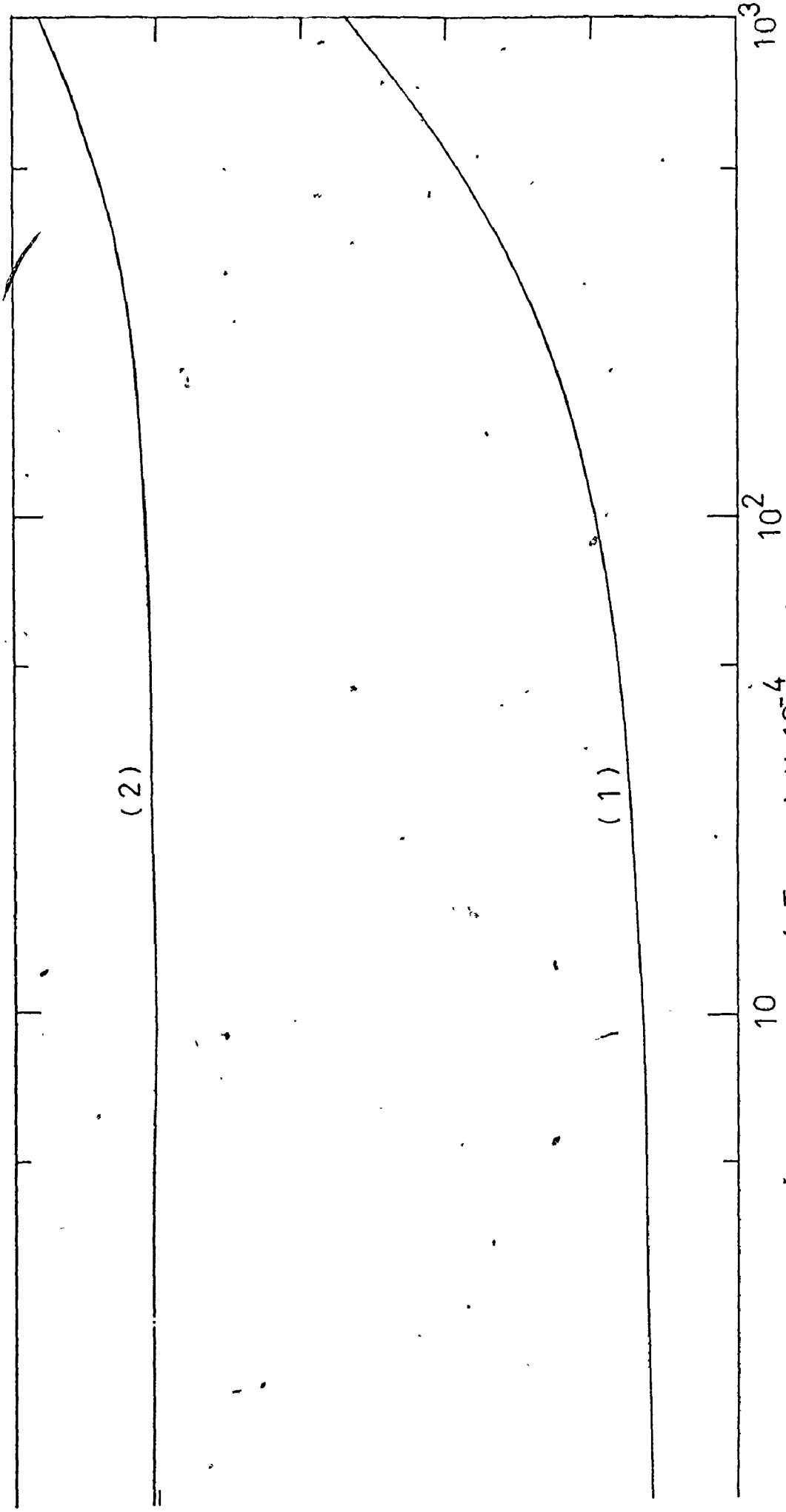

Fig. VIII-5. Semi-log plot of the maximum spin wave frequency at the zone boundary against the ratio of the exchange integrals (J_p/J_c) with J_c set equal to -0.20 THz. Curves (1) and (2) are respectively for spin waves propagating along (100) and (001) directions.

Table (VIII-1). Calculated spin wave frequencies at q = 0 and at the zone boundary for different ratios of the exchange integrals J_p/J_c with J_c fixed. Figures in parentheses show the number of degeneracies

$(J_p/J_c)\times10^{-3}$	Non-zero frequencies (THz) q = 0			Maximum frequency (THz)	
				(0.5 0 0)	(0 0 0.5)
100.00	0.30(2)	1.34(2)	1.92	1.34	2.42
50.00	0.30(2)	0.95(2)	1.38	0.96	2.22
10.00	0.29(2)	0.42(2)	0.67	0.50	2.05
5.00	0.29(2)	0.30(2)	0.52	0.41	2.03
1.00	0.13(2)	0.29(2)	0.35	0.32	2.01
0.50	0.09(2)	0.29(2)	0.32	0.30	2.01
0.10	0.04(2)	0.29(2)	0.30	0.29	2.01

CHAPTER IX

CONCLUSION

This is the conclusion of the discussion on spin waves in triangular antiferromagnets. The stability of the triangular antiferromagnet has been investigated and a spin wave theory has been developed for triangular antiferromagnets. The theory is applicable to any triangular antiferromagnet in which dipole-dipole interaction is the main source of anisotropy.

The unit cell that gives a stable triangular structure has six sublattices and each sublattice has its own quantization axis which is different from those of the others. A classical calculation of the energy shows that the equiangular triangular structure is stable for the Heisenberg Hamiltonian. It was observed in the spin wave theory for the triangular antiferromagnet described by the Heisenberg Hamiltonian that the terms linear in the magnon operators add up to zero only when the moment directions form an equiangular triangle or when there is a simple antiferromagnetic or ferromagnetic alignment of moments. It was also observed that these conditions under which the linear terms in the magnon operators add up to zero is unaffected by the addition of dipole-dipole interactions to the isotropic interactions. The cases of simple antiferromagnetic or ferromagnetic alignment of magnetic moments are not of interest in the discussion of spin waves in triangular antiferromagnets. Since a necessary

condition for the stability of a structure is that the linear terms in the magnon operators should add up to zero, it follows that the spin wave theory also shows that the equiangular triangular structure is stable. The fact that the linear terms still add up to zero for the equiangular triangular structure in the presence of dipolar interactions implies that the dipolar interactions, in contrast to single ion anisotropy (Yelon and Cox 1972), do not distort the equiangular triangular structure formed by the moment directions.

A classical calculation of the energy of the triangular antiferromagnet in which dipolar interactions are the source of anisotropy shows that the dipolar interactions confine the moments to the plane of the atoms and leave the triangular structure stable. This result is confirmed by the spin wave theory; the spin wave energies become imaginary when the moments are rotated out of the plane of the atoms.

Using approximate values of the exchange constants along directions parallel and perpendicular to the crystal c-axis, a numerical calculation of the spin wave dispersion relations in triangular antiferromagnets was carried out. There are six branches in the dispersion relations along the symmetry directions ($\varepsilon 00$) and (00ε). The effects of dipole-dipole interactions are more appreciable along the ($\varepsilon 00$) direction because the interactions J_p (estimated) within the plane are sufficiently weak that dipolar interactions are of comparable magnitude to the exchange interactions. Along the

(ε00) direction, the dipole-dipole interactions remove most of the degeneracies in the dispersion relations. The maximum energy of the spin wave propagating along the (ε00) direction increased by about 30% when dipolar interactions are included in the Hamiltonian. Because of the stronger exchange in the (00ε) direction, the dipolar forces have much less effect on the spin wave energy than in the (ε00) direction. The effects of the dipole-dipole interactions on the spin wave dispersion relations along the (00ε) direction are mainly apparent at low values of the wave vector where it removes some of the degeneracies in the dispersion relations. At zero value of the wave vector, some of the branches that have zero frequencies in the isotropic interaction limit, have non zero frequencies when dipole-dipole interactions were included. The spin wave energies are much larger for propagation along the crystal c-axis than for propagation along directions perpendicular to the crystal c-axis; this reflects the fact that there is a much stronger coupling of magnetic moments along the crystal c-axis compared with along the perpendicular direction.

BIBLIOGRAPHY

Achiwa, N., J. Phys. Soc. Japan 27, 561 (1969).

Akhiezer, A. I., Bar'Yakhtar, V. G. and Peletminskii, S. V., "Spin Waves", North-Holland Publishing Co. (1968).

Anderson, P.W., Phys. Rev. 115, 2 (1959).

Asano, H., Bando, Y., Nakanishi, N. and Kachi, S., Trans. Japan Inst. Metals, 8, 180 (1967).

Bacon, G. E., "Neutron Diffraction", 3rd. ed. Oxford (1975).

Baker, G. A., Jr. and Essam, J. W., J. Chem. Phys. 55, 861 (1971).

Bienenstock, A. and Lewis, J., Phys. Rev. 160, 393 (1967).

Bloch, F., Z. Phys. 61, 206 (1930).

Bogoliubov, N. and Tyablikov, S., Zhur. Eksperim. Teor. Fiz. 19, 251 (1948).

Born, M. and Huang, K., "Dynamical Theory of Crystal Lattices", Oxford University Press (1954).

Brockhouse, B. N., deWit, G. A., Hallman, E.D. and Rowe, J.M. Proceedings of the Symposium on Inelastic Scattering of Neutrons, IAEA, 259 (1968).

Chipman, D. R. and Walker, C. B., Phys. Rev. Lett. 26, 233 (1971).

Clegg, D. W. and Buckley, R. A., Metal Sci. J. 7, 48 (1973).

Collins, M. F. and Forsyth, J. B., Phil. Mag. 8, 401 (1963).

Collins, M. F. and Oyedele, J. A., Proceedings of the Conference on Neutron Scattering, Oak Ridge, 418 (1976).

Dirac, P. A. M., Proc. Roy. Soc. A123, 714 (1929).

Domb, C. and Green, M. S.,"Phase Transitions and Critical Phenomena" (5 volumes), Academic Press (1972-1976).

Dyson, F. J., Phys. Rev. 162, 1217 (1956).

Eibschütz, M., Sherwood, R. C., Hsu, F. S. L. and Cox, D. E., Proc. AIP Conf. on Magnetism and Magnetic Materials, 684 (1972).

Ellis, W. C. and Greiner, E. S., Trans. ASM, 29, 415 (1941).

Essam, J. W. and Fisher, M. E., J. Chem. Phys. 38, 802 (1963).

Fisher, M. E., Rep. Prog. Phys. 30, 615 (1967).

Gaunt, D. S. and Sykes, M. F., J. Phys. A 6, 1517 (1973).

Goodyear, J. and Kennedy, D. J., Acta. Cryst. B 28, 1640 (1972).

Guttman, L., Solid State Physics 3, 145 (1956).

Guttman, L., Schnyders, H. C. and Arai, G. J., Phys. Rev. Lett. 22, 517 (1969).

Heisenberg, W., Z. Phys. 38, 411 (1926).

Hennion, B. and Moussa, F., Ann. Phys. 233 (1972).

Holstein, F. and Primakoff, H., Phys. Rev. 58, 1908 (1940).

Izyumov, Yu.A. and Ozerov, R. P., "Magnetic Neutron Diffraction", Plenum Press (1970).

Kaya, S. and Sato, H., Proc. Phys. Math. Soc. Japan 25, 261 (1943).

Keffer, F., Handbuch Der Physik, XVIII/2, 1 (1966).

Koester, L., Knopf, K. and Waschowski, W., Z. Physik, 271, 201 (1974).

Kramers, H. A., Physica 1, 182 (1934).

Krivoglaz, M. A. and Smirnov, A. A., "The Theory of Order-Disorder in Alloys", American Elsevier Publ. Co. (1965).

Krupica, S. and Sternberg, J., "Elements of Theoretical Magnetism", CRC Press (1968).

Lyashenko, B. G., Litvin, D. F., and Abov, Yu.B., Sov. Phys-Cryst 6, 443 (1962).

Lyons, D. H., and Kaplan, T. A., Phys. Rev. 120, 1580 (1960).

Maleev, S. V., Sov. Phys.-JETP 6, 776 (1958).

Mattis, D. C., "The Theory of Magnetism", Harper and Rowe Publishers (1965).

Moon, R. M., Phys. Rev. 136, A195 (1964).

Mościński, J. and Rycerz, Z., Comp. Phys. Comm. 13, 9 (1977).

Néel, L., Ann. de Phys. 17, 64 (1932).

Neutron Diffraction Commission, Acta Cryst. A25, 391 (1969).

Norvell, J. C. and Als-Nielsen, J., Phys. Rev. B2, 277 (1970).

Oguchi, T., Phys. Rev. 133, A1098 (1964).

Onsager, L., Phys. Rev. 65, 117 (1944).

Orehotsky, J. and Schröder, K., J. Phys. F: Metal Phys. 4, 196 (1974).

Oyedele, J. A. and Collins, M. F., Phys. Rev. B 16, 3208 (1977).

Pearson, W. B., "A Handbook of Lattice Spacings and Structures of Metals and Alloys", Pergamon Press (1967).

Shull, C. G. and Seigel, S., Phys. Rev. 75, 1008 (1949).

Sorgen, A., Cohen, E. and Makovsky, J., Phys. Rev. B10, 4643 (1974).

Spooner, S., Lynn, J. W. and Cable, J. W., Proceedings of the Conference on Magnetism and Magnetic Materials, 1415 (1972).

Stanley, H. E., "Introduction to Phase Transitions and Critical Phenomena", Oxford University Press (1971).

Vogel, A. L., "A Test Book of Quantitative Inorganic Analysis", Longmans (1961).

White, R. M., "Quantum Theory of Magnetism", McGraw-Hill (1970).

Yelon, W. B. and Cox, D. E., Phys. Rev. B6, 204 (1972).

Yoon, D. and Bienenstock, A., Phys. Rev. 170, 631 (1968).

Yoon, D. and Jeffery, R., Phys. Chem. Solids, 31, 2635 (1970).